



**SYNTHESIS AND PERFORMANCE EVALUATION OF
NANOCOMPOSITE CERAMIC-SODALITE MEMBRANES FOR
PRE-COMBUSTION CO₂ CAPTURE**

Olawale Oloye

A dissertation submitted to the Faculty of Engineering and the Built Environment,
University of the Witwatersrand, Johannesburg, in fulfillment of the requirements for
the degree of Master of Science in Engineering.

Supervisor: Prof M.O. Daramola

9 February, 2017

DECLARATION

I, Olawale Oloye, declare that this dissertation is solely the fruit of my own unaided work. It is being submitted for the degree of Master of Science in Engineering at the University of the Witwatersrand, Johannesburg, South Africa. It has not been submitted before for any degree or examination in any other University.



Olawale Oloye

9th Day of February, 2017

ABSTRACT

Global climate change and other environmental disasters have been attributed to continuous anthropogenic carbon dioxide (CO₂) emission into the atmosphere. Today, researchers are constantly seeking measures to reduce anthropogenic CO₂ emission. Traditionally, absorption technology with use of monoethanolamine (MEA) is used for separating / capturing of anthropogenic CO₂. However, the use of MEA is associated with numerous shortcomings, including inefficient energy usage, high operating and capital cost, amine degradation, solvent loss and excessive equipment corrosion. Alternatively, zeolite based membrane systems are promising technique that prove handy and useful than the traditional processes (absorption with monoethanolamine). However, zeolitic membranes with zeolite coating on the supports (i.e. thin-film supported zeolite membranes) are susceptible to abrasion and thermal shock at elevated temperatures due to temperature mismatch between the supports and the membranes, making them to lose selectivity at early stages. On the contrary, nanocomposite architecture membranes, synthesized via pore-plugging hydrothermal route, are more thermally stable and membrane defects are controlled. Nanocomposite zeolite (sodalite) membranes have been proposed for gas separations, most importantly in the separation of H₂/CO₂, a major component in pre-combustion carbon capture. In addition, sodalite, a porous crystalline zeolite made up of cubic array of β-cages as primary building block having cage aperture in the range of 0.26 and 0.29 nm, is a potential candidate for the separation/purification of light molecules such as hydrogen which has a cage aperture of 0.27 nm under certain process conditions.

In this work, nanocomposite architecture hydroxy sodalite membrane with sodalite crystals embedded within α-alumina tubes were successfully synthesized using the pore-plugging hydrothermal synthesis technique and characterized using techniques such as scanning electron microscopy (SEM) and X-ray diffraction (XRD). The morphology of the synthesized membranes shows that sodalite crystals were indeed grown within the porous structures of the support. Furthermore, Basic Desorption Quality Test (BDQT) and gas separation measurement were conducted to evaluate the

quality of the as-synthesized membrane in industrial gas separation applications. The effects of operating variables such as pressure at 1.1 bar, 2.0 bar and 3.0 bar. Also, the effects of temperature were conducted on the nanocomposite membrane at 373 K, 423 K and 473 K. Finally, the gases permeation results were fitted with the well-known Maxwell-Stefan model.

Results indicated that, the nanocomposite sodalite / ceramic membrane is a potential candidate for removal of H₂ from H₂/CO₂ mixture. The gas permeation measurement from the one-stage nanocomposite membrane shows that the membrane displayed H₂ and CO₂ permeance of $3.9 \times 10^{-7} \text{ mol.s}^{-1}.\text{m}^{-2}.\text{Pa}^{-1}$ and $8.4 \times 10^{-8} \text{ mol.s}^{-1}.\text{m}^{-2}.\text{Pa}^{-1}$, respectively. However, the morphology of two-stage nanocomposite membrane shows that the support was more plugged with sodalite crystals and the permeance of H₂ and CO₂ were $7.4 \times 10^{-8} \text{ mol.s}^{-1}.\text{m}^{-2}.\text{Pa}^{-1}$ and $1.1 \times 10^{-8} \text{ mol.s}^{-1}.\text{m}^{-2}.\text{Pa}^{-1}$, respectively. Consequently, the H₂/CO₂ ideal selectivity for the one-stage nanocomposite membrane improved from 4.6 to 6.5 in the two-stage nanocomposite membrane.

In conclusion, the two-stage synthesized membrane shows better improvement. The porous support was well plugged and separation performance was evaluated. However, occluded organic matters present in the cages of hydroxy sodalite could have adverse effect on the gas permeation performance of the membrane. It is expected that an organic-free sodalite supported membrane (such as silica sodalite supported membrane) could out-perform the hydroxy sodalite supported membrane reported in this work in term of membrane flux because there will be enough pore space for gas permeation.

DEDICATION

This work is dedicated to the Alpha and Omega, the giver of Life, Knowledge, Wisdom and Understanding. I do pray that the source of wisdom and understanding in completing this academic research will not cease. Also, knowledge acquired through the period of this research work will be fully utilized to change the world into a better place for the future generation.

ACKNOWLEDGEMENTS

First and foremost, I would like to give all glory to Almighty God for the successful completion of this project.

I love to acknowledge the financial support from EnPe-NORAD grant for CO₂ capture project.

Boundless appreciation goes to Dr. (Mrs.) Aransiola for her endless support and belief in me.

Special and sincere thanks to my project supervisor and host at the University of the Witwatersrand, in person of Professor M. O. Daramola for his outstanding moral and financial supports.

Finally, I want to thank my parent (Mr & Mrs Rotimi Oloye), my darling wife (Mrs Opeyemi Oloye) and siblings (Ayodeji, Temitope and Oreoluwa) for their love and support throughout the entire research tenure.

God bless you all.

PUBLICATIONS AND PRESENTATIONS

Journal Publications

1. Daramola, M. O., **Oloye, O.**, Yaya, A., 2016. Nanocomposite sodalite/ceramic membrane for pre-combustion CO₂ capture: Synthesis and morphological characterization. *Int. J. Coal Sci. Technol.* 1-7.
2. Sekoai, T. P., Awosusi, A. A., Yoro, O. K., Singo, M., **Oloye, O.**, Ayeni, O. A., Bodunrin, M. O., Daramola, M. O., 2016. Microbial Cell Immobilization in Biohydrogen Production: A short overview. *Critical Reviews in Biotechnology* (manuscript under review).
3. **Oloye, O.**, Daramola, M. O., 2016. Performance Evaluation of Supported Nanocomposite Hydroxy Sodalite Membranes for Pre-Combustion Carbon Dioxide Capture (manuscript in preparation).
4. Kgaphola, K., **Oloye, O.**, Daramola, M. O., Sigalas, I., Deng, Z., 2016. Membrane Materials for CO₂ Capture: a short overview (manuscript in preparation).

Conference Proceedings

5. **Oloye, O.**, Daramola, M. O., 2016. Synthesis, Characterization of Supported Nanocomposite Hydroxy Sodalite Membranes for Hydrogen Purification. Unpublished paper at: International Conference on Environment, Materials and Green Technology, Vaal University of Technology, South Africa, 25th November, 2016.
6. **Oloye, O.**, Daramola, M. O., 2016. Nanocomposite sodalite/ceramic membrane for pre-combustion CO₂ capture: Single gas permeation measurement. In: *Proceedings of the Thirty-Third Annual Pittsburgh Coal Conference*, Cape Town, South Africa, 8th – 12th August, 2016.
7. **Oloye, O.**, Daramola, M. O., 2015. Synthesis, Characterization and Performance Evaluation of a Nanocomposite Ceramic - Sodalite Membrane for Pre-Combustion CO₂ Capture. Unpublished paper at: 6th National Student Colloquium, University of the Witwatersrand, South Africa, 30th June, 2015.

TABLE OF CONTENTS

DECLARATION	ii
ABSTRACT	iii
DEDICATION	v
ACKNOWLEDGEMENTS	vi
PUBLICATIONS AND PRESENTATIONS	vii
TABLE OF CONTENTS	viii
LIST OF FIGURES	xii
NOMENCLATURE.....	xvi
1 Introduction	2
1.1 Motivation	2
1.2 Problem statement	5
1.3 Research questions	7
1.4 Research aim and objectives	8
1.5 Expected outcomes	8
1.6 Dissertation layout.....	8
2 Literature review	11
2.1 Introduction	11
2.2 Climate and environmental change	11
2.2.1 Natural disasters	11
2.2.2 Extinction crisis.....	12
2.2.3 Heat wave.....	12
2.3 Mitigation measures on the effect of Greenhouse Gases (GHGs) emission	13
2.3.1 Non-renewable resources	13
2.3.2 Renewable energy	15
2.4 CO ₂ Capture and Storage (CCS).....	17
2.4.1 CO ₂ capture	18
2.4.2 Transport of captured CO ₂	19
2.4.3 Storage of captured CO ₂	19
2.5 Post-Combustion CO ₂ capture.....	20

2.6	Pre-Combustion CO ₂ capture	21
2.6.1	Reforming / gasification.....	22
2.6.2	Water gas-shift	24
2.6.3	CO ₂ capture	24
2.7	Oxy-fuel combustion	27
2.8	CO ₂ separation techniques.....	28
2.8.1	Absorption-based CO ₂ capture.....	28
2.8.2	Adsorption-based CO ₂ capture.....	29
2.8.3	Chemical looping separation.....	30
2.8.4	Cryogenic distillation	31
2.9	Membrane technology for CO ₂ capture.....	31
2.10	Organic membrane.....	33
2.10.1	Polymeric membrane	33
2.11	Inorganic membrane	33
2.11.1	Dense metallic membranes (Palladium).....	34
2.11.2	Mixed matrix membranes	34
2.11.3	Zeolite membrane.....	35
2.11.4	Gas separation mechanism in zeolite membranes.....	38
2.12	Membrane Selectivity in CCS	38
2.12.1	H ₂ selective membranes	39
2.12.2	CO ₂ selective membranes	39
2.13	In-situ crystallization	40
2.14	Chemical vapor phase transport technique	40
2.15	Secondary seeded growth method	41
2.16	Pore-plugging hydrothermal synthesis technique.....	41
2.17	Supported membrane for CO ₂ capture.....	42
2.17.1	Thin film membranes (TFM)	42
2.17.2	Nanocomposites architectural membrane	43
2.18	Zeolites membrane for H ₂ /CO ₂ separation	47
3	Experimental Procedures	54

3.1	Introduction	54
3.2	Materials and equipment used for the study.....	54
3.3	Experimental procedure	60
3.4	Support pre-treatment & preparation of precursor solution	60
3.5	Membrane synthesis	60
3.6	Membrane characterization	62
3.6.1	Static characterization	62
3.6.2	Dynamic characterization.....	63
3.7	Separation performance evaluation	66
4	Nanocomposite sodalite / ceramic membrane: synthesis, characterization and quality test	68
4.1	Introduction	68
4.2	Membrane synthesis & characterization	68
4.3	Membrane quality test	68
4.4	Result and discussion	68
4.4.1	Zeolite uptake in support of the membrane	68
4.4.2	SEM images	69
4.4.3	SEM image of membrane after 2-stage PPH synthesis.....	72
4.4.4	XRD analysis of crystals and membrane	74
4.4.5	Basic Desorption Quality Test (BDQT).....	76
4.5	Concluding remarks	78
5	Nanocomposite sodalite / ceramic membrane: separation performance and effects of operating variables.	80
5.1	Introduction	80
5.2	Results and discussion.....	80
5.2.1	Membrane separation performance.....	80
5.3	Effects of temperature on separation performance of sodalite membrane ...	88
5.4	Effects of pressure on separation performance of sodalite membrane.....	91
5.5	Effects of feed flow rate on separation performance of sodalite membrane	95
5.6	Separation performance.....	98

6	Conclusions.....	101
6.1	Recommendations	102
	Appendix A: Experimental equipment.....	118
	Appendix B: XRD data conversion.....	119
	Appendix C: Procedures for operating the membrane gas separation system	120
	Appendix D: Procedures for running JAD X-tract Extreme Version 1.4.5	122
	Appendix E: Data obtained from JAD X-tract Extreme	127
	Appendix F: MATLAB Code used for MS model.	138

LIST OF FIGURES

Figure 1.1: World energy consumption from 1990 to 2040 (adapted from <i>IEA</i> , (2016)).....	3
Figure 1.2: World energy consumption by energy sources (coal, renewables & nuclear), from 1990 to 2040 (Adapted from <i>IEA</i> , 2016).....	4
Figure 2.1: Schematic showing the three CO ₂ capture and storage chain.	19
Figure 2.2: Schematic depicting post-combustion CO ₂ capture (Adapted from Gibbins and Chalmers, (2008)).....	21
Figure 2.3: Schematic depicting the three main stages in pre-combustion CO ₂ capture process.....	22
Figure 2.4: Flue composition of air-blown reforming and IGCC pre-combustion.....	25
Figure 2.5: Schematic depicting Pre-combustion CO ₂ capture (Adapted from Gibbins and Chalmers, 2008)	26
Figure 2.6: Schematic depicting Oxyfuel combustion (Adapted from Gibbins and Chalmers, 2008)	28
Figure 2.7: Schematic of membrane gas separation in a tube and sheet configuration	32
Figure 2.8: Schematic depicting sodalite crystallite growth within / on porous support (adapted from Miachon et al., (2006)	45
Figure 2.9: Molecular structure of (a) SOD cage, (b) merged SOD cages in horizontal description, (c) merged SOD cages in cubic description, (Adapted from IZA (SOD))	51
Figure 3.1: Picture of a typical support (Picture not to scale).....	54
Figure 3.2: The cross-section of the asymmetrical α -Al ₂ O ₃ tube supplied by Fraunhofer IKTS, Germany.	55
Figure 3.3: Picture of the Teflon [®] -lined autoclave used for the pore-plugging hydrothermal synthesis for nanocomposite sodalite / ceramic membrane (Picture not to scale).	56
Figure 3.4: Schematic of membrane testing system used in this work.	57
Figure 3.5: Picture of the membrane gas separation system (Picture not to scale).....	58
Figure 3.6: Flow diagram showing a summary of the experimental procedure.....	60
Figure 3.7: Schematic of experimental procedure for membrane synthesis via pore-plugging hydrothermal route (Adapted from Daramola et al., (2015)).....	61
Figure 3.8: Temperature programme for sodalite membrane synthesis via pore-plugging hydrothermal route (Adapted from Daramola et al., (2015)).....	62
Figure 3.9 : Schematic of the membrane module employed for BDQT.	64
Figure 3.10: Picture of (a) graphite O-rings, (b) membrane module used for BDQT. 64	

Figure 3.11: Schematic of the experimental set-up used for the BDQT.	65
Figure 4.1: SEM image of hydroxy sodalite crystals obtained from the bottom of the Teflon®-lined autoclave during the pore-plugging hydrothermal synthesis.	70
Figure 4.2: SEM image showing the surface of the innermost layer of the nanocomposite sodalite / ceramic membrane obtained after the one-stage PPH synthesis.	71
Figure 4.3: SEM image showing the three asymmetric layers with the presence of sodalite crystals at 200 nm region after one-stage PPH synthesis.	72
Figure 4.4: SEM image showing the surface of the innermost layer of the nanocomposite sodalite / ceramic membrane obtained after the two-stage PPH synthesis.	73
Figure 4.5: SEM image showing the cross-sections of the three layers (200 nm, 800 nm & 1200 nm) with the presence of sodalite crystals at all layers.	74
Figure 4.6: XRD patterns of synthesized hydroxy sodalite crystals and simulated sodalite (IZA)(McCusker et al., 2007).	75
Figure 4.7: XRD patterns showing simulated sodalite pattern (IZA)(McCusker et al., 2007), synthesized sodalite crystals and sodalite membrane.	76
Figure 4.8: Basic Desorption Quality Test (BDQT) for the three as-synthesized nanocomposite membranes.	77
Figure 4.9: BDQT for membrane M1 after one and two-stage synthesis.	78
Figure 5.1: H ₂ and CO ₂ permeance through membrane prepared via one-stage synthesis.	86
Figure 5.2: H ₂ & CO ₂ permeance through membrane prepared via two-stage synthesis.	87
Figure 5.3: CO ₂ /H ₂ ideal selectivity in the one and two-stage nanocomposite membranes.	87
Figure 5.4: Membrane flux as a function of temperature (2-stage nanocomposite membrane).	89
Figure 5.5: Permeance as a function of temperature (2-stage nanocomposite membrane).	90
Figure 5.6: CO ₂ /H ₂ ideal selectivity as a function of temperature (2-stage nanocomposite membrane).	91
Figure 5.7: Flux as a function of pressure (2-stage nanocomposite membrane).	93
Figure 5.8: Permeance as a function of feed pressure (2-stage nanocomposite membrane).	94
Figure 5.9: Ideal selectivity as a function of pressure (2-stage nanocomposite membrane).	95
Figure 5.10: Flux as a function of feed flowrate on membrane obtained by the two-stage pore-plugging synthesis.	96

Figure 5.11: Permeance as a function of feed flowrate on the membrane obtained by two-stage pore-plugging synthesis..... 97

Figure 5.12: Ideal selectivity as a function of feed flowrate on the membrane obtained by two-stage pore-plugging synthesis. 98

Figure A.0.1: Picture of EcoTherm® oven used for membrane synthesis (Picture not to scale). 118

LIST OF TABLES

Table 2.1: Categories of water gas-shift catalyst and their properties.	24
Table 2.2: Classification of zeolite based on pore size	36
Table 2.3: Major differences between a thin-film membrane and nanocomposite architecture.....	46
Table 2.4: Zeolitic membranes reported for H ₂ separation / purification.	49
Table 3.1: Components in the membrane testing system.....	58
Table 4.1: Sodalite uptake within the α -Al ₂ O ₃ tubes after one-stage synthesis	68
Table 5.1: Comparison of permeation and selectivity result obtained and literature..	85

NOMENCLATURE

Basic Desorption Quality Test	BDQT
Carbon capture and storage	CCS
Chemical Vapor Deposition	CVD
Concentrating Solar Power	CSP
Deca-dodecasil 3R	DDR-3
Diethanolamine	DEA
Electrical Swing Adsorption	ESA
Enhanced Coal Bed Methane Recovery	ECBMR
Enhanced Oil Recovery	EOR
European Environment Agency	EEA
ExaJoules	EJ
Global Amphibian Assessment	GAA
Greenhouse Gas	GHG
Integrated Gasification of Combined Coal Cycle	IGCC
International Energy Agency	IEA
International Zeolite Association	IZA
Linde Type A	LTA
Metal Organic Framework	MOF
Methyldiethanolamine	MDEA
Methyldiethoxysilane	MDES
Mobil Composition of Matter	MCM

Monoethanolamine	MEA
Natural Gas Combined Cycle	NGCC
Organization for Economic Cooperation and Development	OECD
Permeance of component i	Π_i
Photovoltaics	PV
Polyethlenimine	PEI
Pore-Plugging Hydrothermal	PPH
Pressure Swing Adsorption	PSA
Research and Development	R & D
Scanning Electron Microscopy	SEM
Standard enthalpy of Reaction at 298 K	ΔH°_{298}
Standard Temperature and Pressure	STP
Sodalite	SOD
Temperature Swing Adsorption	TSA
Thin-film Membranes	TFM
Transmembrane Pressure	ΔP
United Nations Framework Convention on Climate Change	UNFCCC
X-ray diffraction	XRD
Zeolite Socony Mobile	ZSM

Chapter One

Introduction

1 Introduction

In this chapter, motivation, research objectives and justification are presented. Research contributions to the industrial and scientific community are outlined as well.

1.1 Motivation

The advent of the industrial revolution in 1760 marked the birth of world's energy crisis. Technological development, urbanization and improved standard of living have influenced greater demand in energy consumption worldwide (Houghton and IPCC, 2001; Ashton, 1948). Statistical analysis revealed that the world energy production and consumption are parallel (McHale, 1969). Also, Mchale (1969) and Ashton (1948) reported that there is an average annual increase of 3.25 % in world energy production between 1860 and 1958. In addition, an unprecedented rise of about 19 % in energy demands between 1961 and 1964 was recorded, this was attributed to growing population and industrialization in developing countries, mainly China and India (McHale, 1969). Recently, the International Energy Outlook estimated the energy demand over 28-year period from 2012 and projected to 2040 (IEA, 2016). However, the International Energy Outlook reported that 549 quadrillion British thermal unit (Btu) was consumed in 2012 and in the year 2040, it is estimated that 815 quadrillion will be consumed, indicating an increase of about 48 % in the energy consumption chain (IEA, 2016).

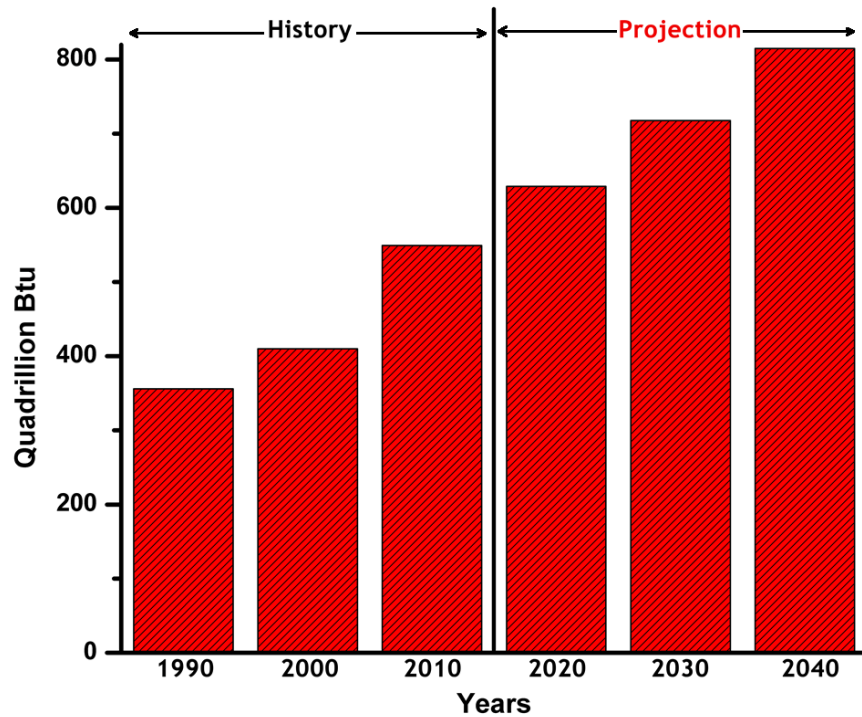


Figure 1.1: World energy consumption from 1990 to 2040 (adapted from *IEA*, (2016)).

Fossil fuels such as coal, natural gas and crude oil serves as a major source of world energy. Coincidentally, the discovery of coal occurs simultaneously with the emergence of industrial revolution between the 19th and 20th centuries (Ashton, 1948). Conventionally, coal is combusted for heating, powering of steam engine and electricity generation (Ashton, 1948). Up till now, the combustion of coal for energy is practiced by industrialized, developing and under-developed countries. Coal is identified as a non-renewable energy source and relatively in large abundance worldwide in comparison to all other sources of energy. Furthermore, noticeable annual average increase in coal, natural gas, nuclear power and hydrothermal power energy sources were observed between 1979 and 1983 (Colombo, 1984). This period is considered as the first and second major worldwide energy crisis in history. To date, energy crisis still persists and there has been an exponential increase in both energy supply and energy consumption.

Over the centuries, there has been tremendous reliance on non-renewable energy sources (fossil fuels) (Olajire, 2010; Houghton and IPCC, 2001). International Energy Agency (IEA) reported that 80 % of the total primary energy sources are from fossil fuels (oil, coal and natural gas) (IEA, 2013). In addition, the recent IEA Outlook, projection indicated that coal will persist as the main source of world energy in comparison with nuclear and renewable energy sources (IEA, 2016) (Figure 1.2)

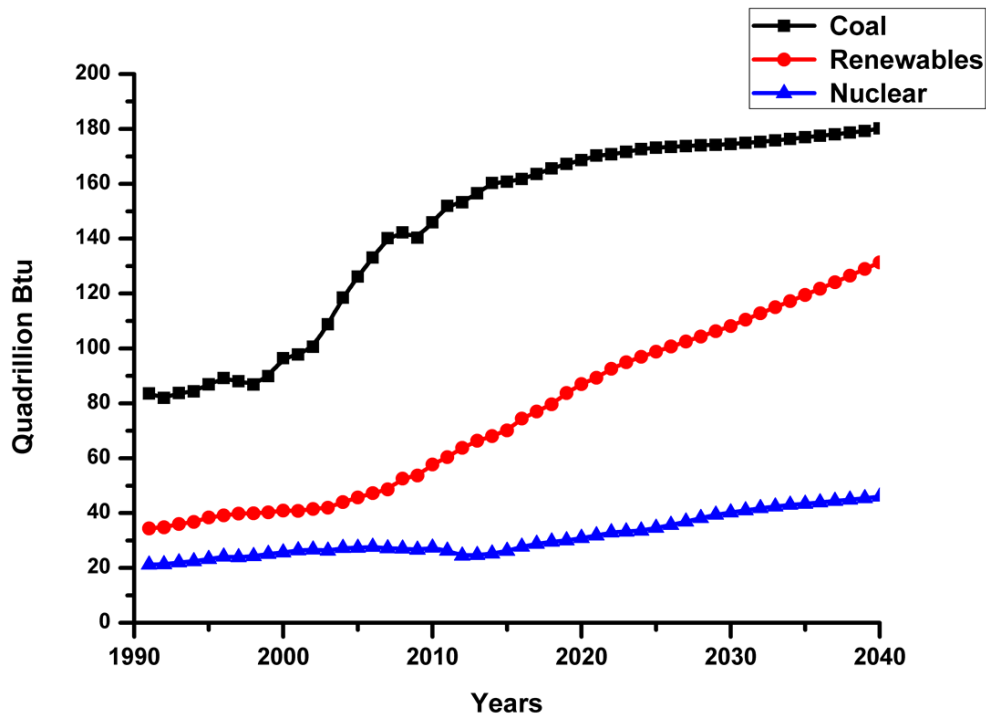


Figure 1.2: World energy consumption by energy sources (coal, renewables & nuclear), from 1990 to 2040 (Adapted from IEA, 2016).

Coal is the most abundant non-renewable fossil fuel readily available worldwide, having recoverable reserves in over 70 countries and possibly more. There is an approximate estimation of 150 to 200 years sufficient reserves of coal worldwide (IEA, 2015; Houghton and IPCC, 2001). It is to be noted that coal consumption exceeds all other combined sources of non-fossil fuels. Basically, the combustion of coal is likely to continue in next decades due to its abundance and continuous

use for energy generation that results in greenhouse gases emission (GHGs) leading to global climate change (Merkel et al., 2010).

The combustion of coal generates energy as main product and GHGs as its deleterious by-products. GHGs are released into the atmosphere as huge volumes of plumes either at a stationary or mobile point source. Stationary point sources generate higher volumes of plumes than the mobile point sources. An approximate one-third of carbon dioxide (CO₂) emissions is attributed to stationary point sources (e.g. coal fired power plants) (IEA, 2016; Metz and IPCC, 2005) A typical coal-fired power plants delivering between 500 and 1000 MW energy emits between 6 and 8 Mt CO₂ per year equivalent (IEA, 2015). This volume of CO₂ emitted is higher than CO₂ emission per year of combined oil-fired single cycle power plants and natural gas cycle power plants of same energy delivery capacity. In addition, atmospheric concentration of CO₂ in the energy demanding industrial age has been estimated to be about 379 ppm in 2004, whereas 280 ppm CO₂-equivalent was estimated in the years before industrial age. Currently, 400 ppm CO₂-equivalent has been recorded as the atmospheric concentration of CO₂ (Abas et al., 2015; IEA, 2013). The increment in the atmospheric concentration of CO₂ could be attributed to changes in energy demand. Energy demand is expected to keep rising due to industrialization in developing countries resulting from population growth, urbanization and technological development (Saidi and Hammami, 2015; IEA, 2013). Researchers in science and technology have attributed GHGs emission to a number of environmental issues (rising sea level, droughts, heatwave and etc.). Therefore urgent attention is required to reduce the level of CO₂ emission into the atmosphere.

1.2 Problem statement

Carbon Capture and Storage (CCS) has been identified as a promising technology to reduce CO₂ emission with the option of continuous combustion of coal. CCS is the process of capturing waste CO₂ form large point sources, such as fossil fuel power plants, transporting it to a storage site and safely deposit the captured CO₂, hindering it from reaching the atmosphere, such storage site could be geological formations.

The process of capturing CO₂ or carbon content of a fuel is the most essential stage of CCS and can be achieved by three main capture technologies; post-combustion, pre-combustion (fuel decarbonization) and oxyfuel combustion.

However, CCS in South Africa is still at the research phase, therefore, more efforts are needed to develop CCS technology in this country. Today, South Africa is ranked as highest emitter of GHGs in Africa and stands as 12th in the world with great dependency on coal as main source of energy. About 77 % of South Africa's energy needs are meant by coal-fired power stations. Advancement of CCS in South Africa could make this country the front runner in the mitigation of anthropogenic CO₂ emission in Africa. Recently, the government of South Africa appointed the South African Center for Carbon Capture and Storage (SACCCS) to research and implements CCS in the country within the next few decades.

CO₂ separation has been widely used in the natural gas processing since 1969, with the use of absorption technique. This conventional separation technique is cost inefficient and energy demanding. For example, monoethanolamine (MEA) is used in such processes and this requires enormous energy in the stripping process (Olajire, 2010). Alternatively, polymeric zeolitic membranes prove to overcome some of these shortcomings. Polymeric membranes are currently used commercially but battles with degradation in harsh conditions. Therefore, they are considered unsuitable for dehydration processes and labelled chemically unstable (Olajire, 2010; Chung et al., 2007; Kazemimoghdam and Mohammadi, 2005). Zeolite based membrane and zeolite membrane reactors provide CCS with vast amount of opportunities such as molecular size exclusion, uniform molecular sized pores, chemical inertness, high thermal and mechanical stability (for example, sodalite membranes are reported to be hydrothermally stable up to 723 K), making them material of choice in separation and catalytic applications (Daramola et al., 2016, 2015, 2012, 2009b; Kalantari et al., 2015; Olajire, 2010; Khajavi et al., 2010b, 2007a). However, zeolite membranes are faced with problems such as reproducibility.

Frequently used supports include; stainless steel, alumina, porous glass, titania and anodic alumina. In addition, asymmetric porous supports are found to provide low flow resistance, good strength and optimal permeance, example of such material is α - Al_2O_3 . Alumina is mostly used to synthesis high silica zeolite membrane and they provide best support because it only dissociate at high alkalinity (Chiang and Chao, 2001). However, the synthesis procedure dictates the membrane architecture either as a thin-film membrane (TFM) or nanocomposite membrane.

Nanocomposite membrane has been synthesized via pore-plugging hydrothermal route with high degree of membrane reproducibility(Daramola et al., 2009b; Miachon et al., 2006). In addition, Daramola et al.(2012) reported that nanocomposite membranes possess higher selectivity as compared with thin-film membranes. Sodalite is “a porous crystalline zeolite made of cubic array of β -cages as primary building block with 4 & 6-rings and a cage aperture in the range of 0.26 and 0.29 nm making it a good candidate for separation / purification of light gases such as helium (0.26 nm), water (0.27 nm) and hydrogen (0.27 nm) under certain process conditions” (Daramola et al., 2016; Khajavi et al., 2009, 2007b)

In this work, nanocomposite sodalite / ceramic membrane was synthesized via the pore-plugging hydrothermal route by adapting the experimental procedures of Daramola et al. (2016). The as-synthesized membranes was characterized and evaluated for gas separation.

1.3 Research questions

The following research questions were addressed in the course of this project;

- Can nanocomposite ceramic-sodalite membrane be successfully reproduced via pore plugging hydrothermal synthesis technique?
- What will be the separation performance of the nanocomposite ceramic-sodalite membrane during the separation of H_2 from CO_2/H_2 gas mixture for a CO_2 pre-combustion capture?

- What optimal operating conditions will favor the separation of H₂ from CO₂/H₂ in a pre-combustion carbon capture at industrially relevant feed compositions using nanocomposite ceramic-sodalite membrane?

1.4 Research aim and objectives

The aim of this research was to synthesize, characterize and evaluate the separation performance of as-synthesized nanocomposite sodalite / ceramic membrane. The following statements were the objectives of this study;

1. To successfully synthesize a reproducible nanocomposite ceramic-sodalite membrane via hydrothermal technique. Also, to evaluate the quality of the membranes using static and dynamic characterization techniques.
2. To methodically evaluate the separation performance of the as-synthesized nanocomposite ceramic-sodalite membrane during H₂/CO₂ mixture at pre-combustion CO₂ capture conditions and compare results with literature.
3. To investigate the effects of operating variables (temperature and pressure) on the as-synthesized membrane; and evaluate operational stability of the membrane during pre-combustion CO₂ capture.

1.5 Expected outcomes

- i. Successful synthesis of a reproducible nanocomposite sodalite ceramic membrane via hydrothermal route.
- ii. Information on the effects of operating variables on the separation performance of the as-synthesized nanocomposite membranes.
- iii. A well-documented report in the form of a dissertation.

1.6 Dissertation layout

The structure of the dissertation is presented as follows:

Chapter 1 provides detailed background information on the project; highlighting the current technological challenges with traditional capture techniques and membrane

based technology. In addition, the shortcomings associated with nanocomposite architecture were highlighted.

Chapter 2 presents in-depth literature review of previous studies on zeolitic membrane with a focus on zeolite membrane in gas separations especially for pre-combustion CO₂ capture. A brief review on conventional synthesis techniques and improvement to synthesis techniques used for development of zeolite membrane are provided. More emphasis is on zeolite membranes used in gas separation applications.

Chapter 3 describes experimental procedure used in the synthesis and characterization techniques of nanocomposite hydroxy sodalite crystal and membrane.

Chapter 4 discusses the results of the synthesis, characterization techniques employed in this work. Scanning electron micrographs and X-ray powder diffraction results were compared with literature results.

Chapter 5 outlines the results of the separation performance of the nanocomposite sodalite / ceramic membrane. In addition, separation performance on the synthesized nanocomposite sodalite / ceramic membrane using gases (CO₂ & H₂) and modelling of experimental results using a deduced expression from the Maxwell Stefan model.

Chapter 6 summarizes the research work and conclusions which have been deduced from the experimental work. In addition, recommendation for current work and future works are provided.

Chapter Two

Literature Review

2 Literature review

2.1 Introduction

Studies indicated that there is a global average temperature rise from 0.70 – 0.75 °C per 100 years between 1910 and 2009 (IPCC and Edenhofer, 2014; Jian-Bin et al., 2012). The global average temperature rise has been attributed to greenhouse gases (GHGs) emission (IPCC and Edenhofer, 2014). In an attempt to mitigate GHGs emission, a non-legal binding document by United Nations Framework Convention on Climate Change (UNFCCC), the European Council and Parliament was signed in 2005 (Kyoto Protocol) (IPCC and Edenhofer, 2014). This was commissioned with the goal to limit the global average temperature rise to 2 °C above the pre-industrial level (European Commission, 2007; Krewitt et al., 2007). Notwithstanding, a notable rise in sea levels, effects of the bad weather, damages to economic sectors, threats to human health and agriculture, drought and cyclones still persist. These problems require more drastic actions to be channeled towards the mitigation of the effects of GHGs emission. The last 10 years recorded an annual increase in atmospheric CO₂ at a rate of 2.11 ppm. In 2004, statistics showed an increase in atmospheric CO₂ at the rate of 1.87 ppm per year in comparison to 1.42 ppm per year in last decades. Whereas in the 60s, 0.73 ppm average annual increase of atmospheric CO₂ was witnessed (IPCC and Edenhofer, 2014; Edenhofer et al., 2012). On this note, numerous events as discussed below have been reported and attributed to the effects of GHGs emission where CO₂ is categorized as a major pollutant.

2.2 Climate and environmental change

Emission of the greenhouse gases has impacted on climate and environment. Below are few of the noticeable incidents; which are caused by anthropogenic carbon dioxide emission.

2.2.1 Natural disasters

Natural disasters such as earthquakes, volcanic eruptions, flooding, landslides, wave/surges and wildfire claimed unprecedented 220,000 lives in the first quarter of

2005 (IPCC and Edenhofer, 2014; Edenhofer et al., 2012). A total of 238 flood events were recorded between 1975 and 2001, causing adverse physical and psychological human health consequences (IPCC and Edenhofer, 2014; Edenhofer et al., 2012). Scientific observation and reports concluded that the events occurred due to continuous anthropogenic carbon dioxide emission. These disasters are rapid, however, some other effects are long term (IPCC and Edenhofer, 2014; Edenhofer et al., 2012).

2.2.2 Extinction crisis

Ocean sequestration of CO₂ which occurs both naturally and artificially absorbs about 30 % of anthropogenic CO₂ emission. Noticeable effects of ocean sequestration take more time (years). In addition, some reports indicated the dissociation of organic minerals into water bodies which consequently resulted in the change of pH levels (Czaun et al., 2013; Yang et al., 2008; EEA, 2004) The acidification of the water bodies eventually leads to dissolution of marine carbonates and noticeable impacts on the biological systems (Czaun et al., 2013). For instance, massive pollution along the Yangtze River in China led to extinction of Baiji White Dolphin (Le Page, 2007). Moreover, there is a great reduction in amphibians, largely as a result of their permeable skin making them vulnerable to effects of pollution and climate change. Global Amphibian Assessment (GAA) believes that over one third of amphibians will go into extinction if GHGs emission continues (UNEP, 2005).

Furthermore, glaciers are gradually retreating from the Alps. About one third of the glaciers and one half of glaciers' mass was lost in the European Alps between 1850 and 1950. Also, 10 % of glacier was lost alone in the hot summer of 2003 (heatwave period) and 10 % of the snow cover has been lost in the northern hemisphere since 1966 (UNEP, 2005; EEA, 2004).

2.2.3 Heat wave

Europe witnessed heatwave in the summer of 2002 and 2003. Records provided in 2004 could ascertain that the heatwave experienced, was as a result of continuous

emission of GHGs. EEA predicted that in 2040s', more than half of Europe's summer will be warmer than what was experienced in 2003 (Saidi and Hammami, 2015; Le Page, 2007; EEA, 2004). Heatwave-related health issues such as tick-borne disease and lyme borreliosis have been projected to escalate even further in the future (EEA, 2004). In addition, records indicated that number of summer days and heatwaves have increased tremendously in the last 100 years. For instance, northwest Russia and Iberian Peninsula experience higher temperatures in winter than in summer (EEA, 2004).

These incidents have influenced research and development in science and technology to seek for alternative energy sources that are environmentally friendly, renewable and cost effective. Some of these alternative sources includes CCS, hydrogen fuel cells, wind, solar, geothermal and nuclear energy. Notwithstanding, technologies are being developed for the mitigation of the effects of GHGs emission but the commercial applications of some of these technologies is hampered due to technology maturity, cost, environmental friendliness etc. (Metz and IPCC, 2005).

2.3 Mitigation measures on the effect of Greenhouse Gases (GHGs) emission

Numerous strategies are being applied today to mitigate the effect of continuous emission of GHGs by ensuring a tremendous decline in the emission, these application include; increasing the energy efficiency of electrical appliances, fuel substitution, emissions trading, changes in combustion practices and the use of renewable energy (biomass, geothermal, solar, tidal, water and wind energy), hydrogen fuels, less carbon intensive sources, natural gas and nuclear energy, afforestation and carbon sequestration. These proposed strategies could enable the continuous use of fossil fuels with reduced GHGs emissions (Houghton and IPCC, 2001). Brief and careful examinations of some of the mitigation measures that dominate research topics are presented below.

2.3.1 Non-renewable resources

Non-renewable resources, also known as finite resources, are resources that their economic value cannot be readily replaced and/or does not renew itself at a

sustainable rate in comparison to its rate of consumption in meaningful human time-frames (IPCC and Edenhofer, 2014). They are categorized into two groups; fossil fuels (coal, natural gas and oil) and nuclear fuels.

Nuclear energy is a contending energy sources accounting for about 12.3 % of world electricity supply according to a report by Rogner, (2013). Globally, about 375.5 gigawatt energy are being generated from 437 reactors as at November 2012. However, nuclear stations are primarily stationed close to water bodies (sea, large rivers, lake or massive cooling towers) for cooling of the reactor rods submerged in them. The case of the Fukushima Daiichi accident of 11th March, 2011 caused by earthquake and subsequent tsunami has created a gap in nuclear technology. The accident has stimulated countries like Germany, Belgium, Spain and Switzerland to phase out their nuclear power stations within the next two decades (Rogner, 2013; Scott, 2013). In addition, Italy has shut down all its functioning nuclear power stations while countries like Cuba, Kuwait and Libya have outrightly cancelled plans to introduce nuclear sources due to financial, political and technical reasons (Rogner, 2013). By way of conclusion, nuclear energy sources are faced with poor public acceptance, nuclear economics, strict public policy, security and environmental concerns in waste disposal (Broecks et al., 2016). Although, they are known to deliver unlimited energy and zero emissions (Kidd, 2013; Rogner, 2013). However, coal, natural gas and oil are increasingly being the major energy sources in power generation.

Natural gas and oil were simultaneously discovered in 1821 and 1859, respectively, during the industrial revolution. Both fuels are considered to be reaching the peaking era and it is predicted that natural gas peaks will occur within a decade of oil peaking (Abas et al., 2015). Coal was also discovered during the industrial revolution and it played a major role especially in coal-fired steam engines and development of earlier rail system. However, coal production and consumption has surpassed natural gas and oil due to the fast depletion in oil and gas reservoirs (Abas et al., 2015). Moreover,

cleaner energy sources such as renewable energy are being investigated with aim of mitigating GHGs emissions and meeting world energy demands.

2.3.2 Renewable energy

Renewable energy also known as alternative energy source provides the world with potentials of conserving fossil fuels for other applications and future use. Renewable energy is defined as “any form of energy from solar, geophysical or biological source that is replenished by natural process at a rate that equals or exceeds its rate of use” (Edenhofer et al., 2012). Observable increase in global contribution of this source of energy was recorded in the last decades. In 1990s, it was observed that renewable energy sources increased by only 2 % and impressive increment of 5 % in recent years. Renewable energy represents a total of 12.9 % of global primary energy of about 492 EJ (exaJoules) (IPCC and Edenhofer, 2014; Edenhofer et al., 2012). Biomass, geothermal, ocean, solar, tidal, wind energy and hydropower are all sources of renewable energy.

A prominent source of renewable energy, solar energy technology refers to “the harnessing of solar irradiance to generate electricity via photovoltaics (PV) and concentrating solar power (CSP) to produce thermal energy” (Salame et al., 2015). In spite of being the most abundant renewable resources, solar energy only accounts for about 0.04 % of basic power used by human (Salame et al., 2015). This energy source could be used in heating and cooling, as well as, to produce fuels, useful for transportation and other purposes (Salame et al., 2015). However, solar energy application is still within the research and development (R&D) and mature phase. In addition, commercial application of solar energy technology is being hampered by a number of factors; high cost of solar panels and storage system. Advancement in technology and production of cheap solar panels and storage system could create a platform for wide commercial applications and harnessing of solar energy (Salame et al., 2015; Amponsah et al., 2014; IPCC and Edenhofer, 2014). However, there is more focus on biofuel as a source of energy. In fact, countries like Brazil and Norway

have already introduced biofuel into their energy mix and made it available in commercial quantities.

Biofuels, a renewable energy source, are majorly produced from biomass feedstock such as agricultural and livestock waste. Biofuel such as ethanol produced from sugar and starch are commercially available (Salame et al., 2015; Amponsah et al., 2014; IPCC and Edenhofer, 2014). Biomass has been co-fired and co-gasified with fossil fuel with or without CCS. In retrospect, this has reduced the high demand on fossil fuels especially at geographical locations where biofuels are produced. Also, biofuels has acted as alternative fuels, cutting off the huge demands resulting from fluctuations in supply of fossil fuels (Gibbins and Chalmers, 2008). However, biofuel energy is insufficient source of energy compare to fossil fuels. In addition, environmental impact of biofuels production from land use could lead to land erosion as result of the removal of green vegetation. Alternatively, hydropower energy is a clean and renewable energy source possessing economic, technical and environmental benefits over biofuels.

Hydropower energy exploits kinetic and potential energies stored in water as a result of its movement from a much higher to lower elevations, this in turn, generates electricity with aid of a turbine engine. The technology is in its mature phase and it is known to exploit mechanical energy of flowing water by forcing it through a piping known as penstock, which turns a generator. Hydropower technology are known to provide multiple uses such as irrigation, flood / drought control and energy supply (Salame et al., 2015; Amponsah et al., 2014; IPCC and Edenhofer, 2014). Hydropower is a proven technology with high efficiency and very low operating and maintenance costs. However, hydropower energy is limited to availability of water bodies such as river, seawater in a geographical location. In addition, high initial cost of hydropower facilities, inundation of land and wildlife habit as well as displacement of people living in the reservoir area serve as short comings (Salame et al., 2015). However, geothermal energy could serve as an alternative to hydropower energy and

it is considered an efficient supply of clean energy with minimal impact to its surroundings (Salame et al., 2015).

Geothermal energy utilizes thermal energy from the earth's interior using up geothermal reservoirs with the aid of wells. Three known use of geothermal energy are system heating, electricity generation and use in geothermal heat pumps. Geothermal energy is a sustainable and safe source of energy for the environment with minimal emission. However, this technology is at the research and development (R & D) phase (Amponsah et al., 2014; IPCC and Edenhofer, 2014). A major drawback with geothermal energy is suitable locations. Suitable geothermal power plants must be located where there are hot rocks that can be easily drilled. For example, China possess richest geothermal resources, other countries include Japan, USA, Iceland and Turkey. In addition, geothermal energy could only provide relatively small amount of energy compared with other renewable energy sources. Moreover, they are faced with safety concerns (Salame et al., 2015; Amponsah et al., 2014; IPCC and Edenhofer, 2014).

Fossil fuel combustion is a proven technology which could sufficiently meet the energy demand in next few decades. However, with advent of new technology such as carbon capture and storage (CCS), there is provision for continuous combustion of fossil fuel but with an option of capturing GHGs emission after or prior to combustion. Despite the advent of CCS, the mitigation of GHGs with CCS remains scientific challenge. Moreover, the commercial application of CCS has been hampered due to its energy penalties, high operating and capital cost and technology maturity.

2.4 CO₂ Capture and Storage (CCS)

CCS is a technology in which CO₂ is separated from other gases after final combustion at a point source or carbon content of a fuel is separated prior to final combustion of the fuel, compressed, transported and stored in various geological formations (Hammond and Spargo, 2014; Pires et al., 2011). CO₂ capture could be achieved by incarcerating the carbon in flue gases or fuel (feedstock) prior to final

combustion. The technology employed in the capture process pivot on the type of combustion / combustion equipment, fuel source and fuel composition (Metz and IPCC, 2005). CO₂ capture constitute about 70 - 80 % cost of the total CCS chain (Metz and IPCC, 2005). Diverse CO₂ capture technologies are commercially available, but cost and energy penalty have limited their applications (Olajire, 2010).

CO₂ capture and storage provides us with continuous combustion of fossil fuels and control of the emission of GHGs. The reduction of CO₂ emission could be applied to both stationary point and mobile sources, but this attracts some penalties. Report indicated that CCS could assist in about 19 % of total global emission reduction in next few decades (L'Orange Seigo et al., 2014). However, the application of CCS still battles with environmental challenges, regulatory issues varying from country to country, public perception especially with issues that are related to possible risks of leakage in storage site and clear legal framework (L'Orange Seigo et al., 2014; Jan et al., 2012). In addition, public perception of CCS is relatively low with little acceptance based on statistics, when compared with other climate change mitigation options such as geothermal energy and wind energy (Broecks et al., 2016; Jan et al., 2012). CCS public perception could be motivated with advancement in R&D, technology advancement and public awareness through social media. However, CCS involves three main stages, which are the CO₂ capture, transport and storage.

2.4.1 CO₂ capture

CO₂ capture is witnessing more attention from researchers today as a result of limitation with the present technologies, such as absorption, adsorption, cryogenic distillation and membrane, employed in capturing CO₂ (Pires et al., 2011; Yang et al., 2008). These techniques have their own limitations and constraints in capturing CO₂ from point sources. However, after the CO₂ is captured at the point sources, it is compressed and transported to various geographical storage site. Figure 2.1 shows the three stages of CO₂ capture and storage chain.

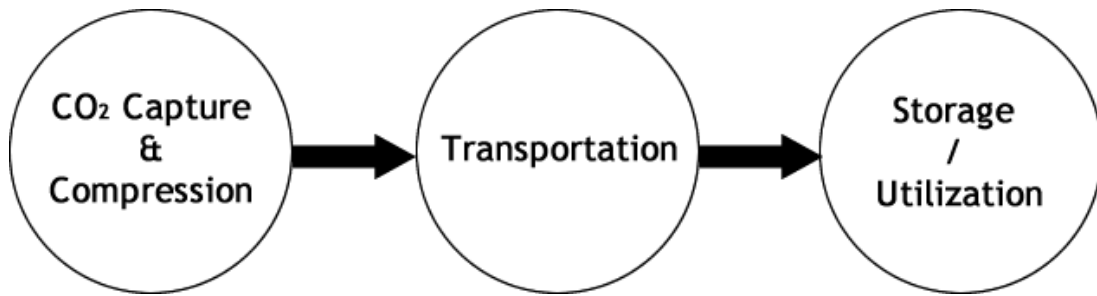


Figure 2.1: Schematic showing the three CO₂ capture and storage chain.

2.4.2 Transport of captured CO₂

Transport of the captured CO₂ involves the movement of the compressed CO₂ from a capture point to its storage site and it is the most technically matured stage of CCS today (Bouzalakos and Maroto-Valer, 2010). Captured CO₂ could be transported to its final destination (a storage site or utilization site) via tankers, ships or pipeline. The mode of transportation chosen is a factor of the volume of captured CO₂ and the proximity to the storage or utilization site. Transport of captured CO₂ via pipelines is the most viable and mature technology. In addition, the transport of CO₂ to storage site via ship has also improved significantly. However, local conditions and regional economic circumstances can play a major role in evaluation of the cost of transporting the captured CO₂ to its storage site (IEA, 2013). Factors limiting the transport of CO₂ via pipelines include corrosion due to presence of water in the captured CO₂, crack formation in pipelines and adverse effects of impurities (Olajire, 2010). However, majority of pipelines, transport CO₂ for utilization purposes. For example, 225 kilometers pipeline built in 1972 at Texas Canyon Reef Carriers is devoted for Enhanced Oil Recovery (EOR). Over 6000 kilometers of CO₂ pipeline exist in the United State and there are offshore pipelines transporting CO₂ in Snohvit Project, Norway for EOR (Olajire, 2010).

2.4.3 Storage of captured CO₂

Storage of captured CO₂ in geological formation involves injecting the captured CO₂ into geological formations located in the depth more than 1 - 3 kilometers below

ground level (Gibbins and Chalmers, 2008; Metz and IPCC, 2005). These geological formations or geological reservoirs can be basalts, deep unused saline water-saturated reservoir rocks, depleted oil and gas reservoirs, unmineable coal seams, oil shales and cavities. However, deep saline aquifers have the highest CO₂ storage potential which could reach between 400 – 10,000 GT of CO₂ storage, followed by depleted oil and gas fields (920 GT), with the least storage potential to be unmineable coal seams (15 GT) (Leung et al., 2014). Concentration of compressed CO₂ for sequestration either in deep underground geological formations or ocean is recommended to be more than 90 % (Irfan et al., 2011). However, the use of depleted oil reserves and other technology has made CO₂ storage a bit lucrative such as Enhanced Coal Bed Methane Recovery (ECBMR) as well as Enhanced Oil Recovery (EOR) (Leung et al., 2014). For example, Weyburn project in Saskatchewan, Canada is a typical case of EOR project with storage capacity of 30 million tons of CO₂ transported via 320 kilometers pipeline from a gasification plant situated at North Dakota, USA (Leung et al., 2014). However, storing CO₂ in depleted hydrocarbon fields, deep saline formations generate no income but rather increases the cost of storage because of monitoring of such sites (IEA, 2016, 2013). These technologies are still active topics of investigation. In addition, advancement of CCS technology differs from country to country. Industrialized countries are front runners in CCS. Recently, more focus is on developing countries as they tend to meet their energy demand, consequently emit more CO₂.

However, the separation of carbon content in end-of-pipe or chemical process can be achieved using some available technologies; Post Combustion, Pre Combustion, Oxy Fuel Combustion (Olajire, 2010).

2.5 Post-Combustion CO₂ capture

Post-combustion CO₂ capture (PCC) is one of the CO₂ capture technologies. It provides a viable potential of retrofitting with existing power plants. Post-combustion is a downstream process and categorized as an end-of-pipe technology. Report indicated that the technology could lead to an increase in energy cost by 32 % and 65

% in gas and coal-fired power plants, respectively (Leung et al., 2014; Olajire, 2010). This huge increase in energy cost has been attributed to low concentration and relatively low partial pressure of CO₂ in the flue gases of power plants (Luis et al., 2012). Therefore, PCC requires a source of driving force in concentrating the flue gas for separation. However, coal-fired power plants are known to emit about 7 – 14 % CO₂ and gas-fired power plants emit about 4 % (Leung et al., 2014; Olajire, 2010). Furthermore, enormous energy is required for regeneration of chemical solvents (for example monoethanolamine, MEA) used in the capture process (Leung et al., 2014; Olajire, 2010). About 4 to 6 GJ / tonne energy is consumed during the regeneration process of CO₂ recovered (Bounaceur et al., 2006). The technology is termed energy inefficient and least efficient among competing capture technologies. However, advances in research and development (R&D) could alleviate some of these shortcomings in post-combustion carbon capture. Figure 2.2 shows the main features of a post combustion capture process.

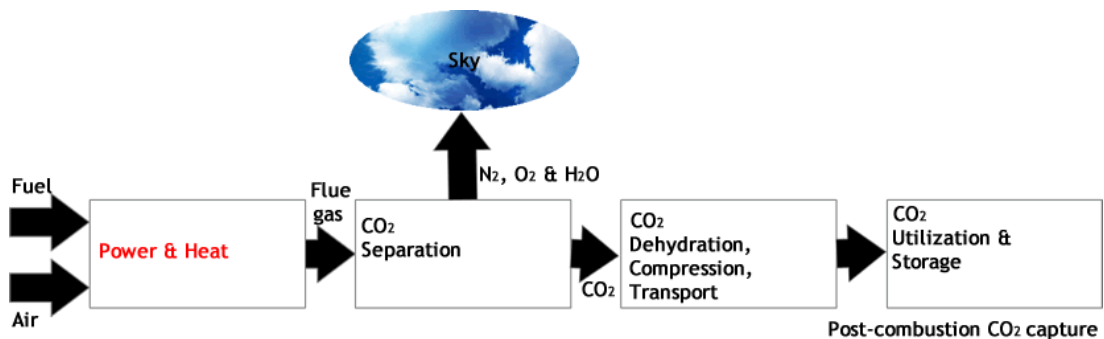


Figure 2.2: Schematic depicting post-combustion CO₂ capture (Adapted from Gibbins and Chalmers, (2008))

2.6 Pre-Combustion CO₂ capture

Pre-Combustion CO₂ capture aims to provide a carbon-free fuel (fuel decarbonization). This could be hydrogen fuel and other hydrogen fuel based technology (Olajire, 2010). Pre-Combustion technology is primarily applied before final combustion of the carbon-free fuel such that the heating value of the fossil fuel is transferred to H₂ (Olajire, 2010). In pre-combustion CO₂ capture process, the fuel could be conventionally coal or natural gas which liberates mainly carbon monoxide

and hydrogen (Figure 2.3 and Figure 2.5). Recent advancements in pre-combustion CO₂ capture technology have biomass a potential feedstock. Other components of pre-combustion are air, steam or controlled amount of oxygen which serves as the oxidizing agent necessary for the gasification process (Leung et al., 2014; Olajire, 2010). Pre-combustion CO₂ capture is a three stage process, first stage being the gasification / reforming process followed by water-gas shift reaction stage and the CO₂ capture as seen in Figure 2.3.

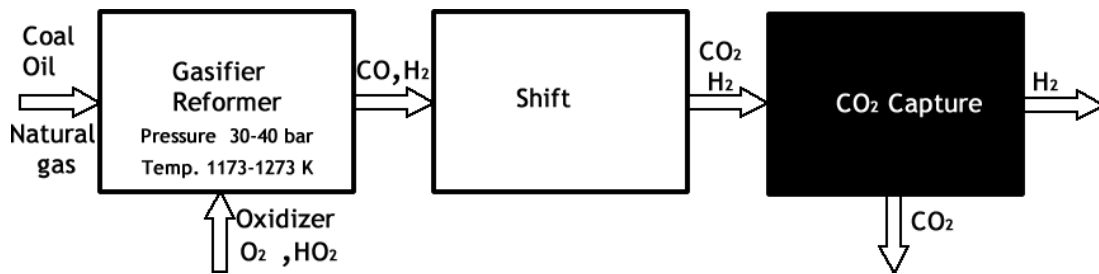


Figure 2.3: Schematic depicting the three main stages in pre-combustion CO₂ capture process.

2.6.1 Reforming / gasification

Pre-reforming occurs prior to the reforming process by reducing the steam-to-carbon ratio in the main reformer, translating into a reduction in the energy required in the main reformer. However, the pre-reformer can also acts as “sulfur guard” by removing all sulfur to protect the main reformer catalyst and improve efficiency. The pre-reformer catalyst could be nickel based on either a magnesium oxide or magnesium alumina. Reforming of fossil fuel (natural gas) is normally by the steam reforming or partial oxidation. Steam methane reforming is commercializing technology which was first developed in 1868 by Tessie du Motay and Marechal. This is a catalytic process occurring at temperature of 700 – 1000 °C and pressure between 3 – 25 bar (Equation 1) (Michalkiewicz and Koren, 2015).

In case of partial oxidation, the heat required for reforming is generated within the reformer and there are three classes of partial oxidation, namely;

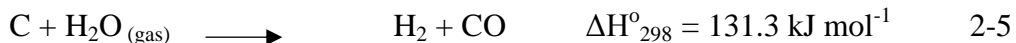
- (i) Partial oxidation with no catalyst
- (ii) Autothermal reforming and
- (iii) Catalytic partial oxidation.

For natural gas steam reforming and autothermal reforming, Equation 2.1 and Equation 2.2 depict the chemical reactions, respectively.

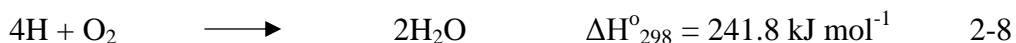


Gasification which is applied mainly to coal, occurs at a higher temperature, thus requires cooling and scrubbing before water gas shift reaction. This pretreatment often increases H₂O to CO ratio as well as temperature depletion to suite the water gas shift reaction. Gasification process could involve either carbon or oxygen.

The following chemical equations depict the reactions involving carbon in gasification:

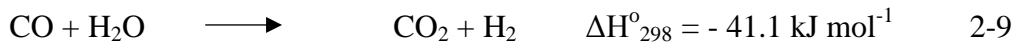


Also, the gasification involving oxygen is represented by the following chemical equations:



2.6.2 Water gas-shift

Water gas shift reaction is an exothermic reaction which liberates additional H₂, the water gas-shift reaction is depicted by Equation 2-9. The CO liberated in the gasification / reforming process reacts further to give additional H₂ and CO₂. However, lower temperatures favor optimum conversion of CO to H₂ and steam in the presence of catalyst (see Table 2.1). In addition, by integrating water gas-shift and CO₂ capture processes, CO₂ or H₂ can be continuously removed from the reactor, therefore, the equilibrium is shifted to the product side.



Furthermore, the water gas-shift catalyst is categorized into three;

- (i) High-temperature shift,
- (ii) Low-temperature shift and
- (iii) Sour shift catalyst (see Table 2.1).

Table 2.1: Categories of water gas-shift catalyst and their properties.

	Active components	Operating conditions (°C)	Sulfur content in feed gas (ppmv)
High-temperature shift	Fe ₃ O ₄ with Cr ₂ O ₃ as stabilizer	350-500	<100
Low-temperature shift	Cu supported by ZnO and Al ₂ O ₃	185 -274	<0.1
Sour shift	Sulfided Co and Mo (CoMoS)	250 – 500	>300

2.6.3 CO₂ capture

This stage, the CO₂ could be separated from H₂, where H₂ could serve as fuel for gas turbine combined-cycle plants, fuel cells, and chemical feedstocks for production of

ammonia (Leung et al., 2014; Olajire, 2010). Also, captured CO₂ could be stored or used as refrigerants, fire extinguisher gases, food beverages and production of urea (Leung et al., 2014; Olajire, 2010). Conventionally, absorption process using monoethanolamine (MEA), Selexol, Rectisol or Purisol are employed for separating CO₂ / H₂. However, pre-combustion carbon capture using membrane technology has been postulated to provide the least energy penalty and best for coal-fired power plants (Bounaceur et al., 2006). Pre-combustion carbon capture has numerous advantages including the production of carbon-free fuel and capture of CO₂ at relatively high pressure. Pre-combustion CO₂ capture occurs at a pressure of about 20 to 70 bar and CO₂ partial pressure between 3.5 and 27 bar, this translate to a reduction in the energy requirement for the separation. Moreover, the composition of the flue gas is a function of the feed and the system configuration used in pre-combustion process, see Figure 2.4. In addition, this technology could be applied in an integrated gasification combined cycle (IGCC) (Scholes et al., 2010).

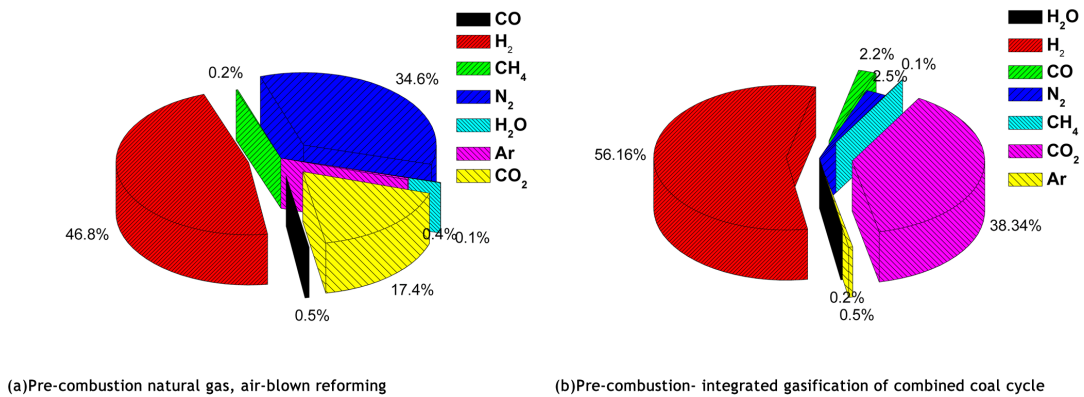


Figure 2.4: Flue composition of air-blown reforming and IGCC pre-combustion

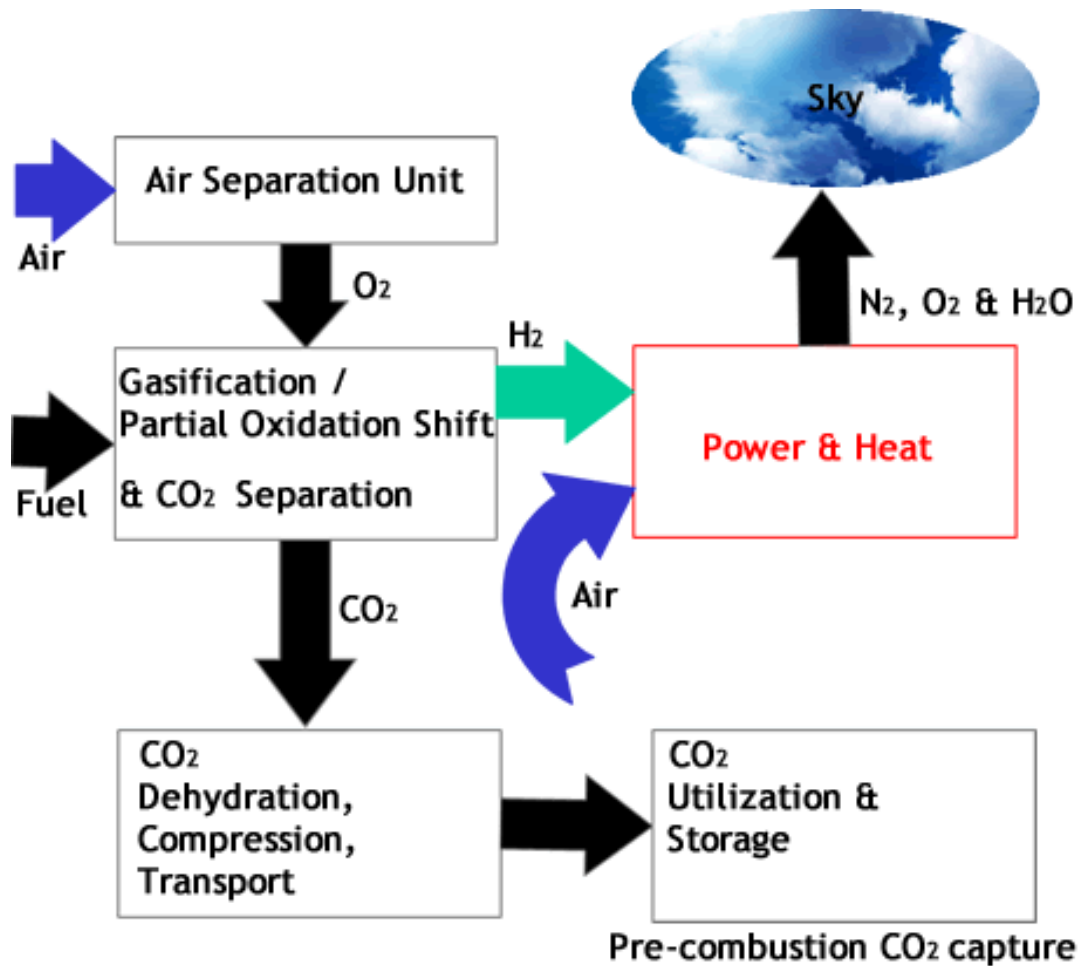


Figure 2.5: Schematic depicting Pre-combustion CO₂ capture (Adapted from Gibbins and Chalmers, 2008)

Integrated gasification of combined coal cycle is rooted known technology of natural gas combined cycle (NGCC). Pre-combustion carbon capture technology employs IGCC technique. This is a technique of producing synthesis gas mainly H₂, CO and very often CO₂ from the heating of carbon-based fuels such as coal, biomass and natural gas in the presence of air, O₂ or steam as oxidant (Scholes et al., 2010). It is known to have high CO₂ concentration between 35 and 40 % with a total pressure of about 20 bar or more. The CO₂ in the exit stream is known to have high pressure but low temperature, which forms a good basis for CO₂ pre-combustion capture. Yang et al., (2008) reported that pre-combustion capture systems are less expensive in comparison with post-combustion capture system. Also, pre-combustion capture

plants incorporated with IGCC are more efficient than the conventional pulverized coal-fired power plants (Yang et al., 2008).

2.7 Oxy-fuel combustion

Oxy-fuel combustion, which is also known as oxy firing and oxy combustion, is a modified post-combustion technology. In this scenario, the two main combustion components are O₂ and fuel. However, oxyfuel combustion entails the separation of oxygen from air using cryogenic separation process or membrane based technology (Figure 2.1) (Olajire, 2010). The combustion of oxygen and fuel in oxyfuel combustion emits SO₂, water, particulate matters and highly concentrated CO₂. The SO₂ could be separated by desulphurization technology and particulate matter removed by the use of electrostatic precipitators. CO₂ concentration in oxyfuel combustion is in the range of 80 – 98 % and could be removed by physical method such as distillation, then compressed, transported and stored (Leung et al., 2014; Olajire, 2010). Oxy-fuel combustion flue gas has a concentrated amount of CO₂ approximately 80 – 90 %, 5 % N₂ and 5 % O₂ by volume compared to flue obtained from direct combustion with air which contains approximately 79 % N₂, 13 – 15 % CO₂ and 5 % O₂. The major limitation with this technology is the associated capital and energy cost required for production of pure O₂ or separation of O₂ from air. In addition, high concentration of SO₂ could create severe corrosion damage to the system (Leung et al., 2014; Olajire, 2010). Although, the applications of these carbon capture technologies requires some separation techniques for successful operation at the industrial level.

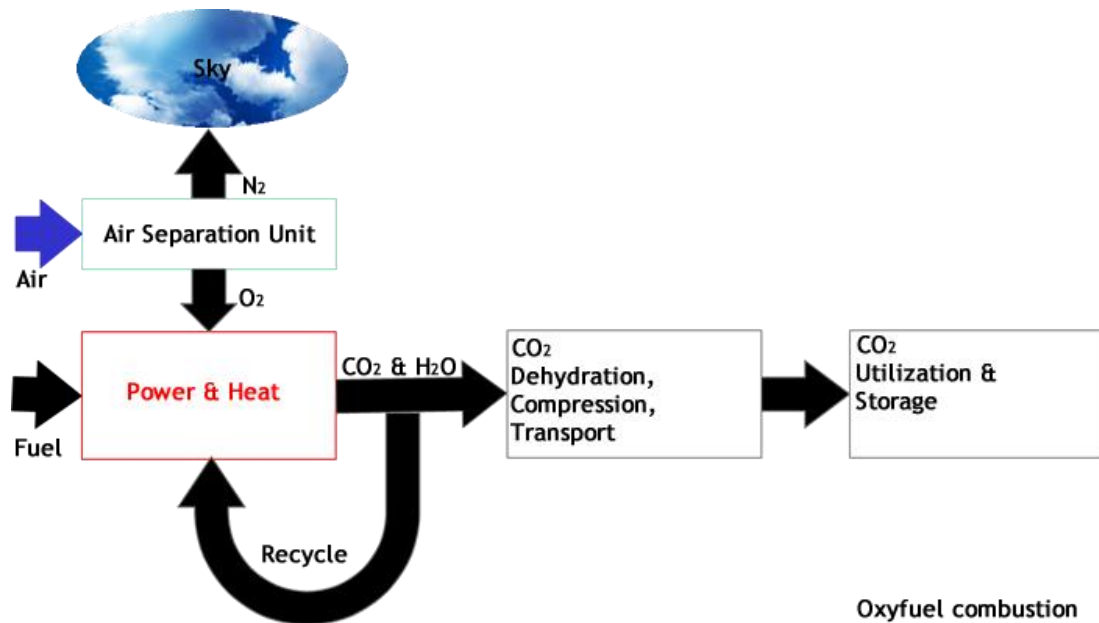


Figure 2.6: Schematic depicting Oxyfuel combustion (Adapted from Gibbins and Chalmers, 2008)

2.8 CO₂ separation techniques

In order to successfully separate CO₂, some separation techniques are employed. Some of these techniques use solvents (physical and chemical) and membranes to capture/separate CO₂ content. A brief examination of the separation techniques are presented below;

2.8.1 Absorption-based CO₂ capture

Absorption technology is a mature technology for CO₂ capture (Olajire, 2010). Absorption technologies are applied in capture processes either as chemical and physical sorbents. Chemical sorbents such as monoethanolamine (MEA), diethanolamine (DEA), methyl diethanolamine (MDEA), piperazine, anion-functionalized ionic liquid and potassium carbonates have been used in CO₂ separation. MEA has been commercially available for over 60 years, the use of MEA in CO₂ separation is a mature technology that has been commercialized. It has been used extensively in natural gas industry for the capture of CO₂. In this process, the MEA solution is contacted with the flue gas in a packed absorber column, where the CO₂ is preferentially absorb from other flue gases (Leung et al., 2014; Olajire, 2010).

This solvent is later sent to a regeneration unit where CO₂ is stripped off in a counter flowing stream at a temperature range of 100 – 200 °C. The CO₂ content stripped from the solvent is highly concentrated (about 99 %), this could be compressed for storage or serve as chemical feedstock in food industries, intermediates and value-added products (Leung et al., 2014; Olajire, 2010). Nevertheless, the absorption process is considered energy inefficient and also suffers from excessive equipment corrosion, solvent loss, amine degradation and susceptible to emission of volatile degradation compounds (Leung et al., 2014; Olajire, 2010).

However, in physical absorption of CO₂, the process relies on the solubility of the CO₂ which is a factor of the partial pressure and temperature. Elevated partial pressures or lower temperatures are known to favor the solubility of CO₂ in physical absorbents (Olajire, 2010). However, solvent regeneration occurs at elevated temperature or lowering the pressure of such system. In addition, the technology has been commercialized for acid gas removal in natural gas processing and CO₂ removal from syngas in the production of methanol, hydrogen and ammonia (Olajire, 2010). For example, Great Plains Synfuels plant located at North Dakota, USA uses this technology for the production of synthetic natural gas for over 20 years. Notwithstanding, the solvents (Selexol) used in physical absorption has a very high affinity for hydrocarbons which usually results in loss of hydrocarbons. Also, the process is adequately efficient at high operating pressure but at low pressure, causing loss of system efficiency (Olajire, 2010).

2.8.2 Adsorption-based CO₂ capture

Adsorption is a thermodynamic process that involves a shift of the effluent component from the gas phase (feed) by attaching itself onto the surface or within the pores of the solid material, that is, the adsorbent (Olajire, 2010). The adsorbent could be an activated carbon, zeolite or metal oxides. Adsorption could be a physical (physisorption) or chemical (chemisorption) process followed by adsorbent regeneration (desorption). Desorption of the adsorbent could be achieved in a number of ways; Electrical Swing Adsorption (ESA), Pressure Swing Adsorption (PSA),

Temperature Swing Adsorption (TSA) or washing (Olajire, 2010). A brief discussion on some of adsorbents use in CO₂ capture is given below;

Molecular sieve are crystalline substances (especially zeolite) with pores of molecular dimensions which allow the passage of molecules below its molecular size or mass. Molecular sieve has been studied and improved to modify their chemistries, in other to adapt for various chemical separation especially carbon capture and sequestration (Olajire, 2010). Some of the reported materials include silica, MCM-41 and MCM-48. These materials are reported to be cost and energy efficient and with great potentials in carbon sequestration (Olajire, 2010).

Activated carbon performance depends largely on the surface chemistry. The surface chemistry is dominated by heteroatoms which could exist in the form of acidic, basic or neutral organic functional groups. Activated carbons have been applied to a variety of industrial processes (Olajire, 2010). Chemical modification of activated carbon has been reported to enhance its adsorption behavior in capturing CO₂. For example, activated carbon has been chemically modified with NH₃ and polyethlenimine (PEI) impregnation which increased the CO₂ capture capacity at elevated temperature (Olajire, 2010).

2.8.3 Chemical looping separation

A metal oxide is a metallic compound which is formed from metal and O₂ in the form of oxide ion and are referred to as oxygen carriers which are often used for combustion, instead of using pure oxygen as in the case of oxyfuel combustion. In the process of combustion, metal oxides are burned to form CO₂ and water only, thus, reduced back to metal (Leung et al., 2014). A further oxidation reaction, leads to release and recycle of the metal and removal of water by condensation. In general, this process is termed chemical looping separation and they have great potentials, for example, low cost of metal oxides (Leung et al., 2014).

2.8.4 Cryogenic distillation

Cryogenic distillation of gas mixtures relies on fractional condensation and distillation at low temperature and high pressure into gas components. This process is analogous to traditional distillation processes with the exception that it only applies to gaseous mixtures (Leung et al., 2014; Olajire, 2010). It is a commercial process used to liquefy and purify CO₂ from high purity and it involves cooling at very low temperature. CO₂ recovery in this process could be in the range of 90 - 95 % of the entire flue gas (Leung et al., 2014; Olajire, 2010).. However, the process is hampered by intensive energy demand of CO₂ recovery in liquid form (Leung et al., 2014; Olajire, 2010).

2.9 Membrane technology for CO₂ capture

Modern membrane technology is novel capture concept which could be applied across all carbon capture technology, that is, post, pre and oxyfuel combustion technique) (Olajire, 2010). Membrane is defined as a selective semi-permeable barriers that separate mixtures, restricting the transport of various chemical species (Daramola et al., 2012; Olajire, 2010; Yang et al., 2008). This technology provides an important technique whereby process intensification can be implemented; such strategy is known to couple both the reaction and separation process together. Membrane technology, reduces production cost, maximize energy utilization and enhance waste reduction (Daramola et al., 2012; Bernardo et al., 2009). Membrane gas separation is pressure driven process and operates on a variety of mechanism; adsorption/diffusion, solution/diffusion, molecular sieve and ionic transport. However, membrane performance is a function of its permeability and selectivity. Permeability is described as the flux of a specific gas over the membrane (in units of mol s⁻¹ m⁻² Pa⁻¹) and selectivity is the preferential selection of a gas species or molecule over the other (s). Membrane selectivity is described as the “ability to separate a desired component from the feed mixture” (Daramola et al., 2012; Olajire, 2010). These functions are inverse of each other, for a highly permeable membrane, it does possess a low selectivity and vice versa (Daramola et al., 2012; Olajire, 2010).

Among the common configuration for membrane technology are the tube and sheet type membrane (Figure 2.7).

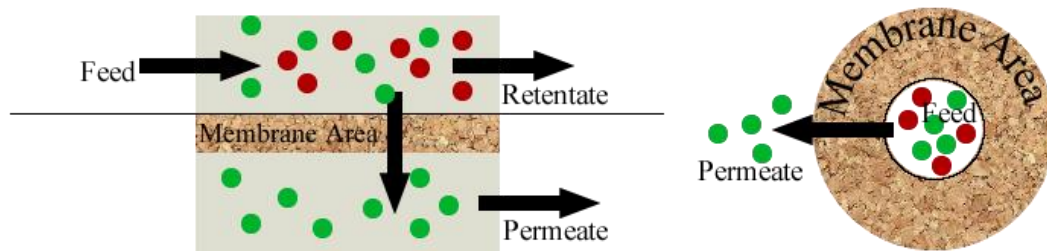


Figure 2.7: Schematic of membrane gas separation in a tube and sheet configuration

Membrane technology possesses great potential in the separation of CO_2 and H_2 with superior efficiency over conventional thermal separation processes (such as absorption). Membrane efficiency is about 10 times more than conventional separation processes (Bernardo et al., 2009). Furthermore, membranes possess noticeable advantages over absorption and adsorption processes, they have simple modular system, no waste streams and no regeneration energy required. Membrane technology eliminates limitations of conventional gas absorption towers and adsorption processes, thus, offers high selectivity and high driving force with a simple modular design (Daramola et al., 2012; Luis et al., 2012; Olajire, 2010)). Membrane separation is a proven technology which has been applied in natural gas sweetening and commonly used in H_2S recovery in refineries (Scholes et al., 2010). However, chemical and physical properties of a membrane play a dominant role in gas separation. Some of the properties include membrane structure and thickness, configuration, module, system design and choice of material (permeability and separation factor) (Bernardo et al., 2009). Remarkable success recorded with membrane technologies have led to its implementation in power generation, for instance, FutureGen power plant located at Coles County, Illinois, USA was planned

to operate on IGCC technology, for electricity and hydrogen production with the use of membrane (Yang et al., 2008).

However, membranes can be categorized into two major class based on nature of membrane materials, organic and inorganic membranes.

2.10 Organic membrane

Organic membrane such as polymers have been extensively studied for gas separation and as supports for catalytic membranes, however, they receive limited commercial applications due to their decomposition and failure at high temperature (Daramola et al., 2012; Armor, 1998). As a result of this limitation, numerous inorganic (ceramic) membranes, possessing greater thermal and mechanical stability and chemical inertness, have been made commercially available (Daramola et al., 2012; Armor, 1998).

2.10.1 Polymeric membrane

Polymeric membranes possess reasonable process-ability, economic competitiveness and scalability (Kosinov et al., 2016). However, major limitations with polymer membrane include plasticization when exposed to hydrocarbons or CO₂ and permeability/selectivity trade-off. In addition, they are chemically unstable and deteriorate at high temperatures. Despite these major limitations, they are forefront and dominate commercial separation applications. Moreover, their separation performance is reduced drastically in ;such process conditions (Bernardo et al., 2009). Most polymeric membranes are more selective to CO₂ and some has shown great potentials in CO₂/H₂ separation, for example, polyphosphazenes and PDMS (Bernardo et al., 2009). However, due to low thermal and mechanical stability and poor chemical fastness, polymeric membranes are unfit for hydrogen separation (Michalkiewicz and Koren, 2015).

2.11 Inorganic membrane

Inorganic membranes are interesting materials and have shown enormous potential in gas separation applications. Owing to their superior thermal resistance, they possess great potential application in high temperature membrane reactors for integration in

carbon capture power generation plants (Bernardo et al., 2009). For instance, silica, carbon molecular sieves and zeolite inorganic membranes are known to be chemically, thermally stable and can also withstand high pressure operations (Kosinov et al., 2016). Major advantage of inorganic membranes over other membranes is that they are highly selective. However, high cost and reproducibility of such membrane has posed serious challenges. Brief discussion of some inorganic membranes is presented below:

2.11.1 Dense metallic membranes (Palladium)

Dense phase metallic membranes such as palladium and perovskites offer very high permeability and produce nearly pure H₂. Dense metallic membranes faces serious limitations which has limited their application (Michalkiewicz and Koren, 2015). Palladium membranes can be poisoned by chemicals such as H₂S, CO and H₂S. Palladium membrane are exceptionally sensitive to H₂S, a 1ppm concentration of H₂S affects the membrane separation performance. In addition, Pd is an expensive material and Pd membrane could undergo phase changes resulting in crack formation at higher temperature and pressure (Michalkiewicz and Koren, 2015; Daramola et al., 2012).

2.11.2 Mixed matrix membranes

Mixed matrix membranes (MMMs) are conventionally developed to enhance the physical and chemical properties of polymeric membranes. They comprise of an inorganic material as fillers incorporated into a polymer matrix. In this configuration, there is a synergistic combination of polymeric membranes process-ability and the superior separation performance of inorganic membranes (Bernardo et al., 2009).

MMMs possess superior physical and mechanical properties for aggressive separation processes over inorganic membranes. However, presence of interfacial defects between the inorganic filler and polymeric membrane hampers its industrial application. Careful selection of materials and preparation route could enhance the synergetic combination by improving MMMs gas separation performance (Mahajan and Koros, 2000).

More research effort needs to be geared towards MMMs fabrication for the development of thin or nanocomposite defect-free mixed membrane structures.

2.11.3 Zeolite membrane

First report on zeolite dates back to the late 1930s and they have been extensively studied for membrane applications. Some of those studied include zeolite MFI (ZSM-5 & silicalite-1), zeolite X & Y, zeolite NaA and sodalite (Daramola et al., 2009). Zeolites are best described as porous crystalline, aluminosilicates of alkaline or alkali earth metals; either on micro, meso or nano scale (Aoki et al., 2000). Zeolites are porous crystalline aluminosilicates with a uniform pore structure and a controlled channel diameter which could range between 0.3 and 1.0 nm, this property makes them ideal membrane materials (Michalkiewicz and Koren, 2015). By aluminosilicates definition; it has a framework composition of SiO_4^{4-} and AlO_4^{5-} with corner sharing, forming open structures (Petrov and Michalev, 2012). Zeolites are also known as molecular sieves, named as a result of their molecular pore size structures, with ability to sieve larger pore size molecules shape and also adsorption properties (Bernardo et al., 2009; Chiang and Chao, 2001). The general formula for the framework material is given as $\text{M}_m[\text{TO}_x]_t\text{X}_t$ where T represents the framework atom, X the non-framework and M represents the alkali or alkaline earth atom (Khajavi et al., 2007a). The T atoms are tetrahedrally coordinated with O_2 and are connected to other T atoms forming alternating connection of corner sharing TO_4 tetrahedra (Khajavi et al., 2007a). Zeolites membrane possesses superior thermal and chemical resistance over polymeric membranes. However, they have been extensively studied in last two decades as a result of ease of preparation and separation performance.

Major drawback of zeolite membrane is associated with the ease of formation of non-zeolitic pores which are larger than the zeolite pores. Non-zeolitic pores are formed during zeolite membrane synthesis due to draw backs associated with traditional membrane synthesis route. This in-turn reduces the selectivity and separation performance. However, with the advent of the temperature controlled crystallization

route whereby the active separation layer is grown within the pores of the macro-porous support, the aforementioned challenge has been eliminated, hence a robust and defect free nanocomposite membrane is developed (Daramola et al., 2016; Li et al., 2008a; Miachon et al., 2006; Chau et al., 2003).

In addition, transport of gas in a zeolite membrane is described using the Stefan Maxwell approach at low temperatures which considers the effect of adsorption, and at higher temperature Knudsen diffusion is dominant (Bernardo et al., 2009). For instance, pore plugged MFI membrane prepared by Miachon et al., (2006) could best be fitted with the Maxwell-Stefan model alone. However, permeance after the lower temperature maximum remains constant (Bernardo et al., 2009)

Nonetheless, natural occurring zeolites possess some limitations of non-uniformity in pore size, purity of the crystalline layers and thermal stability. However, synthetic zeolites can be size-modified for a wide variety of chemical properties (Petrov and Michalev, 2012; Gorgojo et al., 2008). A tabular classification of zeolite based on pore size distribution is given Table 2.2.

Table 2.2: Classification of zeolite based on pore size

Description (Pore)	Rings	Range (nm)	Types	Reference
Extra Small	6	0.26 – 0.29	SOD	(Khajavi et al., 2009)
Small	8	0.30 – 0.45	Zeolite A	(Petrov and Michalev, 2012)
Medium	10	0.45 – 0.60	ZSM-11	(Tuan et al., 2001)
Large	12	0.60 – 0.80	FAU	(Lassinantti et al., 2000)
Extra Large	14	0.80 – 1.00	UTD-1	(McCusker et al., 2001)

Numerous zeolites minerals have been used in commercial applications; Mordenite, Chabazite, Erionite and the synthetic zeolites types A, X, Y, L, ZSM-5, ZSM-11 and many more. These zeolites have flexibility with size, shape of framework and pore corresponding to change in temperature and support (Petrov and Michalev, 2012). In past 20 years, efforts have been made to make zeolite a perfect molecular sieve with intensive research on growing a thin and continuous membrane on a porous/non-porous support. Various materials has been used as support for zeolite, these supports provide the zeolite membrane with mechanical strength, high area density packing, thermal and chemical stability (Daramola et al., 2012; Chiang and Chao, 2001). Materials frequently used as supports include stainless steel, alumina, porous glass, titania and anodic alumina, there are numerous factors to be considered in choosing a support for zeolite membrane; low flow resistance and good strength from asymmetric support provides optimal permeance and flow resistance and bonding with the zeolite (Chiang and Chao, 2001).

Moreover, hollow fiber membrane are preferred to disk or tubular support, they provide greater surface to volume ratio which could facilitate easy scale-up in industrial applications (Daramola et al., 2012). These support types have been investigated by various authors. For instance, Alshebani et al., (2008b) gave a detailed report on synthesis of MFI nanocomposite on alumina ceramic hollow fiber using the pore-plugging hydrothermal route. However, a major breakthrough with zeolite membrane has been reported for LTA zeolite membranes. LTA zeolite membranes witnessed one of the first commercial applications of zeolite membrane. LTA zeolite membranes was synthesized hydrothermally on the surface of porous tubular support and applied for solvent dehydration by pervaporation. Numerous plants have been installed since 2001 using LTA zeolite membranes for pervaporation (Morigami et al., 2001). Various techniques have been employed in synthesizing zeolite membrane on support, synthesis procedure dictate the nature of the as-synthesized membrane. Some of the reported zeolitic membranes are known to be

hydrogen or carbon dioxide selective. A brief discussion on gas separation mechanisms in zeolite membrane and membrane selectivity is provided below.

2.11.4 Gas separation mechanism in zeolite membranes

Gas permeation through zeolitic membranes could undergo a combination of adsorption selectivity, diffusion selectivity and size exclusion. In the case of adsorption selectivity, adsorption of molecules precludes all separation which occurs at the surface of the zeolitic membrane pores (Kosinov et al., 2016). In addition, adsorption selectivity is dominant at low temperature and is influenced by adsorbate and adsorbent interaction. This mechanism is suitable for dewatering applications and CCS (Kosinov et al., 2016).

Diffusion selectivity occurs at moderate temperature which could be best described as “hopping of molecules from one adsorption site to another” (Kosinov et al., 2016). This occurs when the diffusivity of the smaller molecule is much faster than the larger components in the zeolite micropores (Kosinov et al., 2016). However, molecular sieving, also referred to as size exclusion, is an extreme scenario of diffusion selectivity. Molecular sieving occurs when a component of a gas mixture can be totally screened out (not allowed to permeate) within the zeolite micropores (Kosinov et al., 2016).

2.12 Membrane Selectivity in CCS

Generally, metallic membranes are selective towards hydrogen with high degree of purity. Conversely, rubbery polymeric membranes are known to be selective towards carbon dioxide. Membrane selectivity is majorly influenced by

- (i) Difference in the motilities of the components and
- (ii) Difference in the adsorption behaviors of the each species.

However, a membrane selectivity could either be towards hydrogen or carbon dioxide, a brief review is presented below;

2.12.1 H₂ selective membranes

Hydrogen is an energy carrier which could be used in fuel cells. Conventionally, hydrogen production is by steam-methane reforming and subsequent water-gas shift reaction which produced additional H₂ by conversion of carbon monoxide to carbon dioxide (Bux et al., 2009; Nanyi Wang et al., 2015). Hydrogen could be recovered from numerous mixtures, hydrocarbon separation and CO₂ capture from the following; syngas, biogas, flue gas and natural gas (Kosinov et al., 2016). Numerous hydrogen selective membranes have been developed from inorganic membranes (zeolites, Pt-alloys, microporous amorphous silica, doped silica membranes and carbon molecular sieve (CMS) membranes) and organic membranes (polymer) (Nanyi Wang et al., 2015). Metallic membranes are known to produce hydrogen of high purity up to 99.99 % and are generally based on palladium and its alloys. The separation of hydrogen is achieved by dissociative chemisorption of hydrogen at the surface of the metallic membrane to produce atomic hydrogen (Scholes et al., 2010). The atomic hydrogen diffuses through the metal lattice as a result of partial pressure across the membrane. However, the atomic hydrogen recombine into molecular hydrogen and diffuses away at the other end of the metallic surface (Scholes et al., 2010). Conclusively, the process makes metallic membrane highly selective towards hydrogen, however, no other gas molecule undergo such dissociation process.

2.12.2 CO₂ selective membranes

CO₂ selective membranes are membranes that restrict the passage of smaller molecules such as H₂ but larger molecules such as CO₂ permeate. The development of such membranes remains a technological challenge till date. Porous inorganic membranes, polymeric membranes and facilitated transport membranes have been used as CO₂ selective membranes. However, porous inorganic membranes require a form of surface modification to enhance its capillary condensation which results in rapid diffusion within the pores (Scholes et al., 2010). In case of polymeric membranes, solubility selectivity must support CO₂ and diffusivity selectivity of H₂

must be minimal. Example of such polymers are the rubbery polymeric membranes which possess similar characteristics (Scholes et al., 2010).

In the development of membrane, the synthesis material, synthesis procedure and support materials play a major role. Studies indicated that synthesis route employed determines the type of membrane being developed such as the thin-film and nanocomposite membrane. In addition, numerous synthesis procedures have been investigated thoroughly in order to find economically viable synthesis solution. Conventional synthesis routes include in-situ crystallization, secondary seeded growth synthesis and most recently the pore-plugging hydrothermal synthesis.

2.13 In-situ crystallization

In-situ crystallization involves a single step process, such that the nucleation and zeolite growth takes place in the presence of the support (Daramola et al., 2012; Caro and Noack, 2008; Miachon et al., 2006; Caro et al., 2000; Davis et al., 1990). This entails the deposition of a layer containing the Si and Al precursor as a dry amorphous aluminosilicates gel onto a support using sol-gel technique followed by zeolitization under vapor (Daramola et al., 2012; Caro et al., 2000). The single step method in in-situ crystallization is preferred in order to simplify the synthesis procedure. However, the experimental number of synthesis runs depends on the zeolite of interest and the preparation conditions. A report by Gorgojo et al., (2008) who studied the growth mechanism in in-situ crystallization revealed that the concentrations of the reactants in the synthesis gel is reduced during synthesis process, the heterogeneous nucleation gets halted and only crystal growth proceeds, this only occurs even when dissolved nuclei is used as a feed. In addition, they concluded that the nuclei coexist with the crystal for a long time during the synthesis of the zeolite material (Gorgojo et al., 2008).

2.14 Chemical vapor phase transport technique

The chemical vapour transport method, also referred to as sol-gel conversion and vapor phase transport technique, favors nucleation process by a dry-gel conversion. Chemical vapor transport is a two-step synthesis technique that involves the coating

of a support with amorphous gel containing silica and aluminum. Then, it is followed by crystallization under autogenous pressure (Daramola et al., 2012; Miachon et al., 2006; Caro et al., 2000; Matsufuji et al., 2000; Xu et al., 1990). However, crack formation in the amorphous layer is experienced with chemical vapor phase transport technique due to competition of the growth process and the nucleation process. In addition, the formation of cracks within the amorphous layer results into a major setback of obtaining reproducible membranes.

2.15 Secondary seeded growth method

Various seeding techniques have been reported and proposed in literature. Secondary seeded growth technique has been reported to provide an enhanced reproducibility and quality as a result of decoupling of the crystal growth and the nucleation process. Secondary seeded growth is a two stage process, firstly, an ex-situ seeding of the support, during which a previously synthesized zeolite crystals are deposited on the surface of a support and then followed by hydrothermal synthesis (Daramola et al., 2012; Bonilla et al., 2001; Caro et al., 2000; Gouzinis and Tsapatsis, 1998). Such techniques was reported by Boudreau et al., (1999), in the report, they varied the pH of the synthesis solution in order to match the zeta potential of alumina supports and thus enhance the seeding process. Another notable contribution to secondary seeded growth method was reported by Hedlund et al., (2002) for ZSM-5 membranes on non-porous planes like gold plates, the seeding process was enhanced by using cationic polymer, thus, promoting the seeds to stick to the surface of the support via electrostatic forces.

2.16 Pore-plugging hydrothermal synthesis technique

Pore-plugging hydrothermal synthesis technique is “a one-stage technique involving growing zeolite crystals within the pores of a support until the pores are completely blocked by the zeolite materials” (Daramola et al., 2016, 2015; Deng et al., 2010; Li et al., 2008a; Miachon et al., 2006; Chau et al., 2003). Membranes obtained via pore-plugging hydrothermal synthesis techniques are reported to possess minimal cracks, which usually results from thermal expansion mismatch between the zeolite crystals

and the support tube, easy scale up and easiness of membrane handling and module assembling (Li et al., 2008). Despite the fact that membranes fabricated via pore-plugging hydrothermal synthesis technique are reported to have very high selectivity, they do have low membrane fluxes (Daramola et al., 2012, 2009b). The low membrane fluxes could be attributed to totally plugged support materials.

However, the strength of zeolite membranes is enhanced by the type of support materials. The support materials provide both mechanical and thermal strength to the zeolite. Supported zeolite membrane could be in the form of thin-film or nanocomposite membrane.

2.17 Supported membrane for CO₂ capture

Suzuki, (1987) patented the first supported zeolite membrane, since then, numerous supported membranes have been produced especially for gas separation application and pervaporation. Traditionally, supported membranes are developed via sol-gel or chemical vapor deposition (CVD) techniques, micro-wave heating, secondary seeded growth, direct hydrothermal synthesis and most recent pore-plugging hydrothermal technique with stainless steel, alumina, porous glass, titania and anodic alumina as support (substrate). Basically, thin-film membranes and nanocomposite architecture have been reported as supported membranes and have been evaluated for CO₂ capture. In addition, the synthesis technique employed determines the type of supported membrane to be fabricated.

2.17.1 Thin film membranes (TFM)

Thin-films or better described as thin-film selective layers of approximate 1000 nm thickness on highly porous substrate. They have been extensively studied since 1970s and applied commercially for large scale separation (Yave et al., 2010). They have been developed, employing numerous methods depending on the specific target requirements. Some of the techniques employed in developing thin-film membranes are spin coating, dip coating and interfacial polymerization. Thin-films are largely used in science and technology in separation units, sensors display, optical instrument, coatings and membranes (Daramola et al., 2012; Yave

et al., 2010); consequently they are of interest in various field of science and technology.

Thin-film configurations have thickness between some microns which subsequently affects the flux of material through the membrane. However, this limit the separation performance, thus, reducing the technical and economic advantage of thin-film membranes (Daramola et al., 2012; Li et al., 2008b; Chau et al., 2003). Thin-film membranes in CO₂ capture is still within the development phase because of their low permeance. This makes thin-film membrane faces limiting applications for large scale gas applications (Daramola et al., 2012; Yave et al., 2010). State-of-the-art CO₂ selective thin-film membranes only possess permeance of about 0.3 m³ (STP) m⁻².h⁻¹.bar⁻¹, which is not high enough for large scale carbon sequestration in coal-fired power plants (Yave et al., 2010).

For example defect-free thin-film membranes were synthesized and reported by Khajavi et al., (2007). The group prepared hydroxy sodalite membrane on an alumina support which was evaluated through gas permeation test using N₂ and He and applied for pervaporation.

2.17.2 Nanocomposites architectural membrane

Nanocomposite is “a multiphase solid material where one of the phases has one, two or more dimensions of less than 100 nm” (Daramola et al., 2016, 2015; Miachon et al., 2006; Chau et al., 2003). Nanocomposite architecture can also be described as structures having nanoscale repeating distances between the different phases that makes up the material; porous media, colloids, gels and copolymers.

In nanocomposite architecture membrane, the active phase is embedded within the pores of the porous support which could be achieved via pore-plugging hydrothermal synthesis (Daramola et al., 2016, 2015; Miachon et al., 2006; Chau et al., 2003). The pore-plugging hydrothermal synthesis described by some authors as temperature controlled crystallization (Daramola et al., 2016, 2015; Li et al., 2008a; Khajavi et al.,

2007; Chau et al., 2003). Basically, the following outlines the process involve in this synthesis;

- Formation of solution which constituent is a mixture of zeolite active materials (chemical precursor) and bringing it in contact with the porous support (host).
- Embedding zeolite crystals within the pores of the support by employing a non-isothermal thermal program using a multi-stage succession processes.
- Eliminating the residual chemical precursor.

Interruption time is always introduced to promote the growth of the nuclei or nutrient diffusion in the porous structure (Daramola et al., 2009b; Alshebani et al., 2008; Chau et al., 2003). In nanocomposite architecture, the zeolite crystal size is subjected to the pore diameter of host, thereby, limit differences in thermal expansion. Also, active phase in a nanocomposite architecture is within the pores of the porous support, transport of materials occur within this phase (Daramola et al., 2016, 2015; Alshebani et al., 2008; Li et al., 2008a). Obviously, it enhances higher separation performance (selectivity) and protects the membrane layer from abrasion and shock. These properties make nanocomposite architecture membrane better than the thin film-like. Moreover, transport of material occurs within zeolite pores instead of intercrystalline openings. A schematic comparison of thin-film membranes and nanocomposite architecture is illustrated in Figure 2.8.

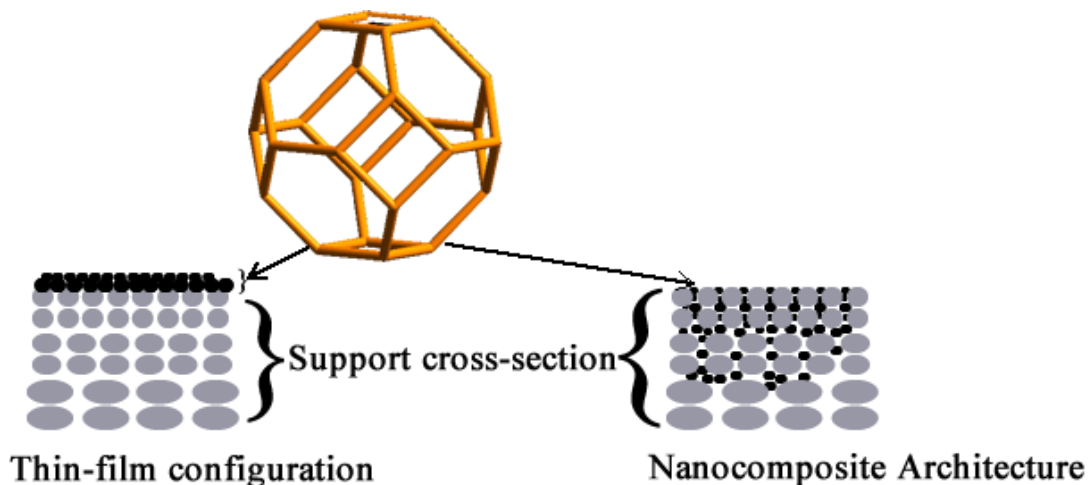


Figure 2.8: Schematic depicting sodalite crystallite growth within / on porous support (adapted from Miachon et al., (2006))

Table 2.3: Major differences between a thin-film membrane and nanocomposite architecture.

Thin-film membrane (TFM)	Nanocomposite architecture membrane
Low membrane selectivity with high flux	High membrane selectivity coupled with low flux
Active phase forms a layer of thickness > 1000 nm	Active phase is embedded within porous support with dimension < 100 nm
Poor mechanical and thermal stability	Superior mechanical and thermal stability
Crack formation due to thermal shocks	Limited crack formation control from thermal shocks
No report has indicated interruption time during TFM synthesis	Interruption time is always introduced to promote growth of the nuclei
In use industrially for large scale separation	Still in the research phase

(Daramola et al., 2009b; Miachon et al., 2006; Chau et al., 2003)

2.18 Zeolites membrane for H₂/CO₂ separation

Numerous zeolite membranes have been reported for hydrogen separation / purification. A comprehensive review on silica membranes for H₂ separation was reported by Khatib et al., (2011), Wirawan et al., (2011) reported and prepared silicalite-1 composite membrane by secondary seeded growth method and evaluated it for H₂/CO₂ permeation. Also, Rezakazemi et al., (2012) reported on H₂ separation and purification using crosslinkable PDMS/zeolite-A nanoparticles mixed matrix membranes, other reports provide detailed information on hydrothermal stability, gas permeation properties, synthesis technique as well as performance of zeolite membranes for H₂ separation (Daramola et al., 2016, 2015; Y. Gu et al., 2008; Gu and Ted Oyama, 2007; Giessler et al., 2003; Lee and Oyama, 2002). Among the most researched zeolites for H₂ separation / purification includes LTA (Huang and Caro, 2011; Varela-Gandía et al., 2011, 2010; Huang et al., 2010; Guan et al., 2001), DDR (Bose et al., 2014; Kanezashi et al., 2008; Tomita et al., 2004), silicalite (Wang and Lin, 2012; Wirawan et al., 2011; Moon et al., 2008; Gu and Ted Oyama, 2007; Giessler et al., 2003), SAPO (Das et al., 2012) and sodalite (Daramola et al., 2016, 2015). These zeolite materials possess small pore diameter, making them material of interest in light gas / molecule separation (H₂) (see Table 2.4). Zeolite pore diameter, a major factor affecting their molecular sieving ability, influences the gas separation performance and separation mechanism. In addition, the nature of zeolite, pore volume, surface area, chemical inertness and thermal stability play major roles in the separation performance of zeolite membranes (Kosinov et al., 2016; Tomita et al., 2004; Morigami et al., 2001).

Furthermore, Gascon and Kapteijn, (2010) reported that high temperature causes a reduction in pore volume due to condensation of S-OH groups in silica membranes. Silica membranes have been reported to possess high permeability, high selectivity but thermally unstable at high temperatures. The presence of steam (H₂O) makes silica membrane to lose permeability (Michalkiewicz and Koren, 2015).

Investigation on MFI membranes concluded that MFI membranes are not effective for H₂ separation (Michalkiewicz and Koren, 2015; Hong et al., 2005; Lovallo and Tsapatsis, 1996). However, most reports on MFI for H₂ separation recorded a low permeance (Hong et al., 2005; Lovallo and Tsapatsis, 1996). In addition, it has been reported that diffusion of small gas molecules such as H₂, CO and CO₂ at high temperature in MFI zeolites membrane can be best described by the Knudsen diffusion (Michalkiewicz and Koren, 2015; Daramola et al., 2009b). In contrast, sodalite and silicalite-1 membrane with high silica content are hydrothermally stable and possess high resistance to sulfur compounds. In addition, silicate-1 and sodalite membranes are relatively cheap and highly selective to H₂ over water and CO₂, due to their hydrophobic surface and molecular sieving ability, respectively (Daramola et al., 2016, 2012; Michalkiewicz and Koren, 2015).

However, these zeolitic membranes are yet to be commercialized for industrial gas applications as a result of major set-backs due to crack formations in thin-film membranes leading to permeation of light gases through non-zeolitic pores, complex synthesis techniques, challenges with zeolite membrane reproducibility, poor chemical stability and separation performance (Daramola et al., 2016, 2015, 2012; Giessler et al., 2003).

Table 2.4: Zeolitic membranes reported for H₂ separation / purification.

Zeolite / Support	Membrane type	Preparation technique	Zeolite (nm)	pore	Reference
LTA					
LTA / AlPO ₄ / α -alumina	Thin film, Composite	Secondary seeded growth	0.4		(Huang et al., 2010; Huang and Caro, 2011)
NaA (Ion exchanged Ca ²⁺ & K ⁺) / α -alumina	Thin film, Composite	In-situ hydrothermal	0.3, 0.5		(Guan et al., 2001)
Cs-LTA / Carbon	Thin film, Composite	In-situ hydrothermal	0.4		(Varela-Gandía et al., 2011)
PDMS Zeolite A	Thin film, Mixed matrix membrane	Solution-casting	-		(Rezakazemi et al., 2012)
DDR					
DDR	Thin film, Composite	Secondary seeded growth	0.36 X 0.44		(Bose et al., 2014)
SAPO-34					
SAPO-34 / α -alumina	Thin film composite	In-situ hydrothermal	0.38		(Poshusta et al., 1999)
SAPO-34 / Stainless steel tubes	Thin film composite	In-situ hydrothermal	0.38		(Hong et al., 2008)
MFI					
Silica / γ -alumina	Thin film, Composite	Chemical vapor deposition	0.45, 0.60		(Gu and Ted Oyama, 2007)
Silica / vycor glass	Thin film, Composite	Chemical vapor deposition	0.45, 0.60		(Lee and Oyama, 2002)
ZSM-5 Silicalite / α -alumina	Bilayer thin-	Direct hydrothermal	0.45, 0.60		(Wang and Lin, 2012)

alumina	film					
Silicalite-1 / α -alumina	Thin film, Composite	Secondary growth	seeded	0.45, 0.60		(Wirawan et al., 2011)
Silicalite-1 / α -alumina	Thin film, Composite	In situ nucleation & secondary growth	& seeded	0.45, 0.60		(Algieri et al., 2003)
Silicalite-1 /stainless steel	Thin-film, Composite	Direct hydrothermal		0.45, 0.60		(Kapteijn et al., 1995)
Silicalite-1 /silicalite-1 graphite paper SOD	Thin film, Composite	Direct hydrothermal		0.45, 0.60		(Akhtar et al., 2015)
Sodalite / α -alumina	Nanocomposite	Pore-plugging hydrothermal		0.26 – 0.29		(Daramola et al., 2016)

Recently, Daramola et al., (2016, 2015) reported the synthesis of nanocomposite hydroxy sodalite ceramic membrane in view of H_2/CO_2 separation. However, numerous reports have appeared in the past for synthesis of sodalite membrane but a few of these reports have characterized such membrane for H_2 separation (Kalantari et al., 2015; Naskar et al., 2011; Moteki et al., 2008; Zheng et al., 2008; Lee et al., 2006; Kazemimoghadam and Mohammadi, 2005).

Sodalite is “a porous crystalline zeolite made of cubic array of β -cages as primary building block. It has a cage aperture in the range of 0.26 and 0.29 nm making it a potential candidate for the separation/purification of light gas (for example hydrogen (0.27 nm)) under specific process conditions” (Daramola et al., 2015; Khajavi et al., 2010b). Sodalite possesses a framework structure with cubic symmetry from vertex-linking of SiO_4 and AlO_4 into four and six membered oxygen-rings (Figure 2.9). Thus, the flexible framework, allows the structure to accommodate anions with different geometries (Khajavi et al., 2010b).

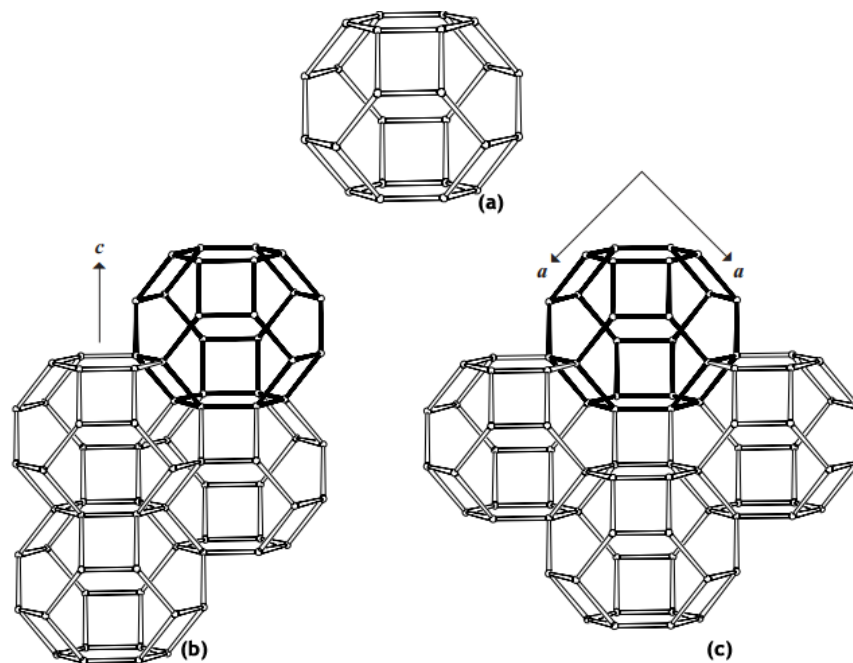


Figure 2.9: Molecular structure of (a) SOD cage, (b) merged SOD cages in horizontal description, (c) merged SOD cages in cubic description, (Adapted from *IZA (SOD)*)

Hydroxy sodalite, which is an interesting member of the sodalite family, has attracted application in selective water removal (e.g. water desalination) (Khajavi et al., 2010, 2007), dehydration (Rohde et al., 2008) and gas separation (Daramola et al., 2016; Zheng et al., 2008). Thin-film hydroxy sodalite membranes have been reported and synthesized via direct hydrothermal synthesis (Wang et al., 2015; Rohde et al., 2008; Khajavi et al., 2007), secondary seeded growth method (Zheng et al., 2008; Lee et al., 2006; Kazemimoghadam and Mohammadi, 2005) and microwave synthesis (Xu et al., 2004; Julbe et al., 2003). Recently, nanocomposite sodalite membrane was synthesized via the so-called pore-plugging hydrothermal synthesis (Daramola et al., 2016, 2015). Traditional synthesis techniques (such as secondary seeded growth method and microwave synthesis) develop thin-film membranes (TFM), however, TFM presents some serious impediments to its commercial application in gas separation and dehydration applications due to defect and crack formation as a result of thermal shock, low membrane selectivity, poor thermal and mechanical stabilities (Daramola et al., 2012). However, nanocomposite hydroxy sodalite membrane has been reported to possess superior quality, coupled with higher degree of reproducibility, as compared to its counterpart (thin-film membranes) (Daramola et al., 2015).

Chapter Three

Experimental Procedures

3 Experimental Procedures

3.1 Introduction

This chapter discusses the experimental procedures and materials employed in this study.

3.2 Materials and equipment used for the study

Anhydrous sodium metasilicate (Na_2SiO_3 , 99%), anhydrous sodium aluminate (NaAlO_2 , 99%) and sodium hydroxide (NaOH , 99%) were all purchased from Sigma Aldrich (Pty) South Africa. The gaseous H_2 and CO_2 were of analytical grade obtained from Afrox, South Africa. The deionized water was prepared within the School of Chemical and Metallurgical Engineering, University of the Witwatersrand. In addition, all chemicals used in the project were used as-supplied. The supports used for sodalite membrane synthesis were asymmetrical $\alpha\text{-Al}_2\text{O}_3$ tubes (inner diameter / outer diameter = 7 mm / 10 mm, length 150 mm), sealed with 10 mm enamel at both ends. The cross-sectional layers of the substrate were of dimensions: outer layer, 1200 nm; intermediate layer, 800 nm; inner layer, 200 nm (Figure 3.1 & Figure 3.2) supplied by Fraunhofer IKTS, Germany.



Figure 3.1: Picture of a typical support (Picture not to scale).

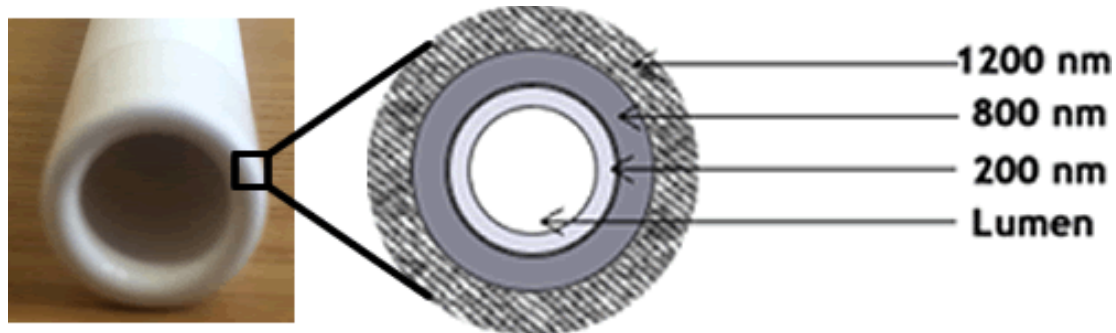


Figure 3.2: The cross-section of the asymmetrical α -Al₂O₃ tube supplied by Fraunhofer IKTS, Germany.

The equipment used in this research was; magnetic stirrer, Teflon® lined stainless steel autoclave, LABOTEC EcoTherm® oven, filtration setup, membrane module and membrane testing system. The heating plate served two purposes during the course of the research. Firstly, the heating plate was used during the pretreatment of the support, for boiling the supports in de-ionized water, in order to remove dirt and loose particles. Secondly, the heating plate was used to mix the precursor solution to obtain homogeneous solution. The Teflon® lined stainless steel autoclave of 125 mL volume, model 4748A was purchased from Parr Instrument Company, U.S.A (Figure 3.3). The autoclave was employed for the synthesis of the nanocomposite sodalite membranes. LABOTEC EcoTherm® oven was used for hydrothermal synthesis and post-drying supports and membranes. The membrane testing system was designed by CHEMVAK cc South Africa, Pty and it was used for evaluation of separation performance of the synthesized membranes (Figure 3.4 & Figure 3.5).



Figure 3.3: Picture of the Teflon[®]-lined autoclave used for the pore-plugging hydrothermal synthesis for nanocomposite sodalite / ceramic membrane (Picture not to scale).

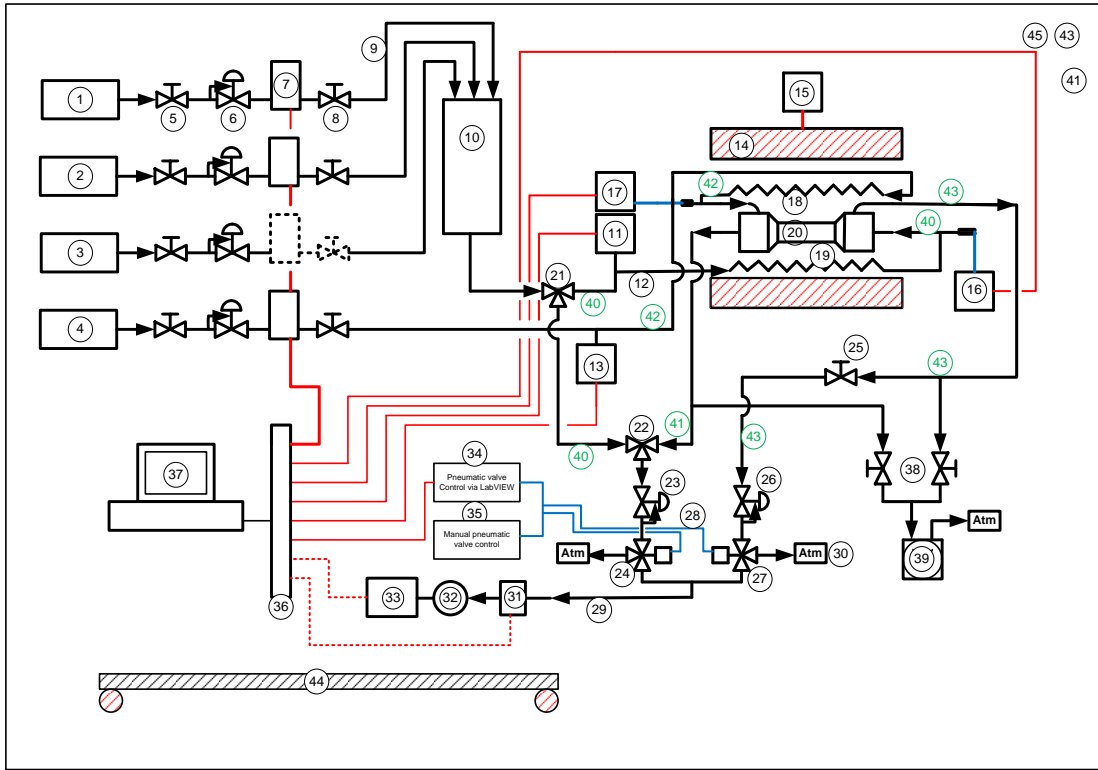


Figure 3.4: Schematic of membrane testing system used in this work.



Figure 3.5: Picture of the membrane gas separation system (Picture not to scale).

Table 3.1: Components in the membrane testing system.

No	Description
1	Main feed gas: CO ₂
2	Make-up gas: N ₂
3	Secondary feed gas: CH ₄ , etc.
4	Sweep gas: N ₂
5	Shut-off valves; 4x
6	Single-stage in-line regulators + 1/8" BSP fittings; 4x

- 7 Mass Flow Controllers + 1/8" BSP fittings; 3x
- 8 1/8" shut-off valves
- 9 1/8" SS tubing and Swagelok fittings
- 10 Gas mixer unit + 1/8" fittings
- 11 **Feed gas** electronic pressure transducer + 1/8" fittings + display + connector to NI LabVIEW DAC system.
- 12 **Feed gas** mixture gas line; 1/8" SS tubing + fittings.
- 13 **Sweep gas** electronic pressure transducer + 1/8" fittings + display + connector to NI LabVIEW DAC system.
- 14 Split level, ceramic band, clamp-on heater; ambient - 500°C.
- 15 Temperature control unit for heater.
- 16 Digital thermometer + type-K thermocouple (TC1) + DAC unit
- 17 Digital thermometer + type-K thermocouple (TC2) + DAC unit
- 18 Sweep gas heat exchanger.
- 19 Feed gas heat exchanger.
- 20 Membrane reactor + insert/membrane + seals.
- 20 Residue gas line + 1/8" fittings for easy access and membrane change.
- 21 1/8" Swagelok SS 3-way valve.
- 22 1/8" Swagelok SS 3-way valve.
- 23 GO Back-pressure regulator for feed/retentate gas line + fittings.
- 24 ASCO 3-way electro-pneumatic valve.
- 25 1/8" Swagelok SS ball valve.
- 26 GO Back-pressure regulator for permeate gas line + fittings.
- 27 ASCO 3-way electro-pneumatic valve.
- 28 Electric lines to the manual operation switch and the NI LabVIEW control system
- 29 1/8" SS gas line to the MFM, GC and column.
- 30 Exhaust to atmosphere.
- 31 Mass flow meter (MFM).
- 32 GC gas sampling valve + 1/8" fittings
- 33 GC
- 34 NI 240 VAC relay module to control the 3-way electro-pneumatic valves.
- 35 Manual valve control system.
- 36 NI LabVIEW DAC interface modules for recording temperature, pressure, and pneumatic valves.
- 37 PC/Laptop with LabVIEW customized software.
- 38 1/8" Swagelok SS metering valves.
- 39 Vacuum pump + fittings.
- 40 **Feed** gas mixture gas lines.
- 41 **Retentate** gas mixture gas lines.

- 42 **Sweep** mixture gas lines
 - 43 **Permeate** gas mixture gas lines
 - 44 Custom built trolley, instrument panels, support framework, power supplies etc.
-

3.3 Experimental procedure

The experimental procedures were conducted in four main stages as depicted in Figure 3.6.

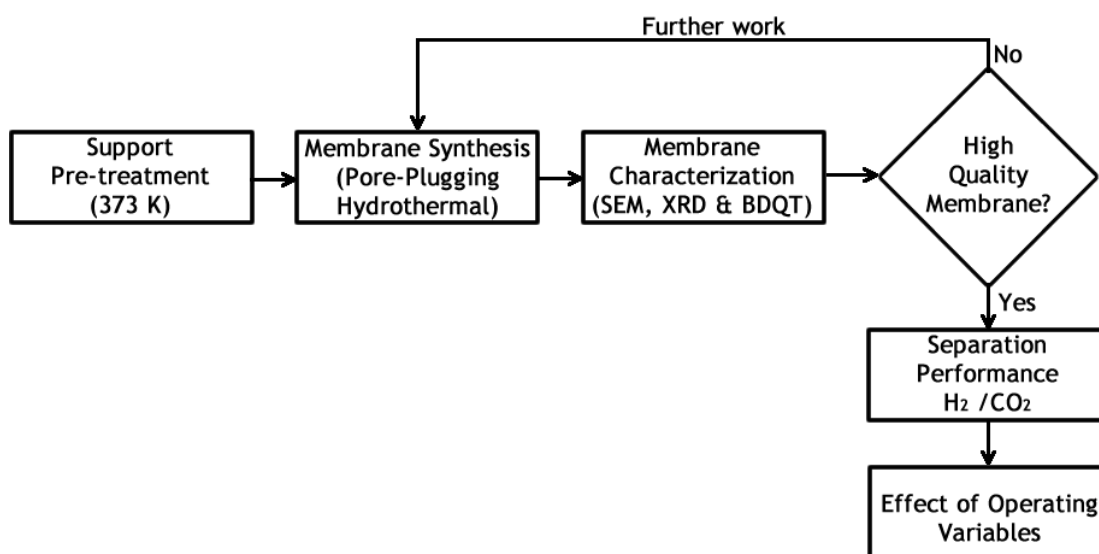


Figure 3.6: Flow diagram showing a summary of the experimental procedure.

3.4 Support pre-treatment & preparation of precursor solution

In preparation for the synthesis, three supports (M1, M2 & M3) were totally immersed in de-ionized water in a 2 L volumetric flask and heated for about an hour to remove loose particles and dirt from the porous structure of the supports. Then, the supports were dried in a LABOTEC EcoTherm[®] oven at 100 °C for an hour and allowed to cool down to ambient temperature. Figures 3.1 and 3.2 presents picture and schematic cross-section of the asymmetrical α -Al₂O₃ tube used in this work, respectively (Daramola et al., 2016, 2015).

3.5 Membrane synthesis

The chemicals used were anhydrous sodium metasilicate (Na₂SiO₃), anhydrous sodium aluminate (NaAlO₂), sodium hydroxide (NaOH) and deionized water. The

chemicals were then mixed together as-supplied in a polytetrafluoroethylene (PTFE) bottle and continuously stirred for an hour using a magnetic stirrer, in order to obtain an homogeneous precursor of molar composition ratio: $5\text{SiO}_2:\text{Al}_2\text{O}_3:50\text{Na}_2\text{O}:1005\text{H}_2\text{O}$ (Daramola et al., 2015). Figure 3.7 depicts schematic of the experimental procedure for membrane synthesis via pore-plugging hydrothermal route.

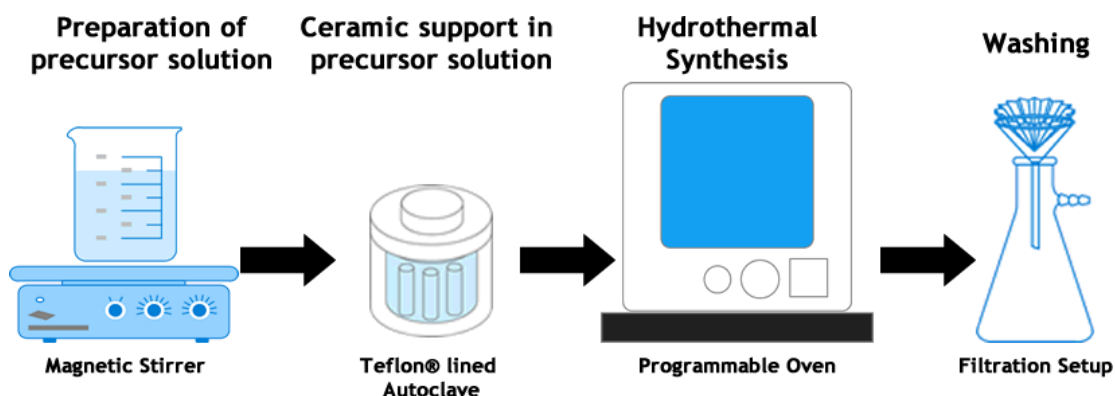


Figure 3.7: Schematic of experimental procedure for membrane synthesis via pore-plugging hydrothermal route (Adapted from Daramola et al., (2015)).

For the membrane synthesis, about 250 mL of the precursor solution was poured into a Teflon®-lined stainless steel autoclave (Figure 3.3) and the pretreated supports were totally immersed. The content was left for about 15 minutes to allow the penetration of the precursor into the pores of the substrates and displacement of air from the pores of the supports. Then, the sealed Teflon® stainless steel autoclave was placed in a LABOTEC EcoTherm® oven and subjected to pore-plugging hydrothermal (PPH) synthesis according to the temperature programme depicted in Figure 3.8. However, no structure directing agent was used for the membrane synthesis. The membrane was successfully synthesized via pore-plugging hydrothermal route, however, the synthesis procedure employed produce occluded sodalite cages. After the completion of the PPH synthesis, the synthesized membranes and crystals formed at the bottom of the autoclave were thoroughly washed with de-ionized water until the pH of the wash-water was 7. The washed membranes and the sodalite crystals were dried in an oven overnight (12 hours) at

100 °C. The weight of sodalite grown within the pores of the support was obtained by subtracting the weight of the support before the synthesis from the weight of the membrane after synthesis.

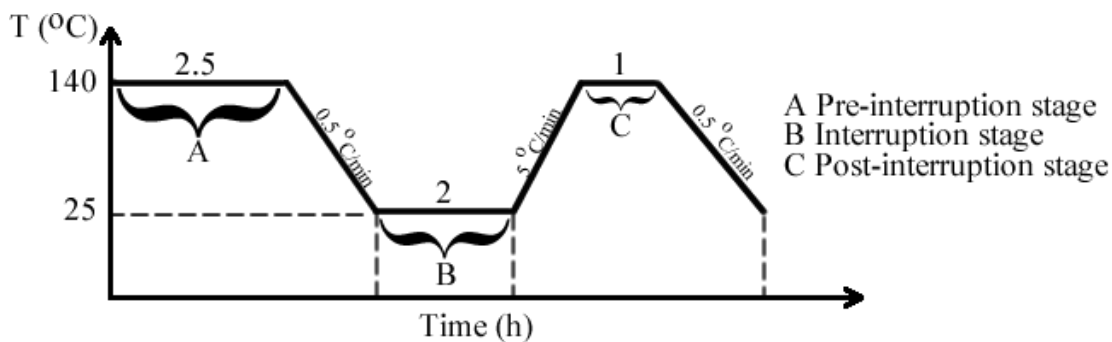


Figure 3.8: Temperature programme for sodalite membrane synthesis via pore-plugging hydrothermal route (Adapted from Daramola et al., (2015)).

3.6 Membrane characterization

Scanning electron microscopy (SEM), X-ray Diffraction (XRD) and Basic Desorption Quality Test (BDQT) were performed to characterize the as-synthesized nanocomposite sodalite ceramic membranes and the techniques are discussed below.

3.6.1 Static characterization

Static characterization of the as-synthesized membrane was conducted with scanning electron microscopy (SEM) and X-ray diffraction (XRD).

Scanning electron microscopy is a powerful magnification tools that utilizes focuses beams of energetic electrons to obtain visual images of materials (McMullan, 1995). Sodalite crystals were examined with SEM to confirm that sodalite crystals were indeed embedded within the α -alumina support. A portion of the membrane was cut and subjected to SEM analysis as well. A Sigma Zeiss SEM housed in the School of Chemical and Metallurgical Engineering at the University of the Witwatersrand, Johannesburg was used for SEM analysis.

X-ray Powder Diffraction (XRD) is “a rapid analytical technique primarily used for phase identification of a crystalline material” (Bragg, 1914). It is used to study crystal

structure based on constructive interference of monochromatic x-rays and a crystalline sample. Sodalite crystals obtained from the bottom of the autoclave and finely crushed nanocomposite sodalite / ceramic membrane were used for the XRD analysis to ensure the purity of the membranes. A Bruker D8 advance X-ray diffractometer using Co K α radiation ($\lambda = 0.179$ nm) at a scan rate of 0.25 sec / step and a step size of 0.02 $^\circ$ situated at the School of Chemistry, University of the Witwatersrand, Johannesburg was employed.

3.6.2 Dynamic characterization

Basic Desorption Quality Test (BDQT) was employed to evaluate the quality of the as-synthesized nanocomposite sodalite ceramic membrane. Prior to the BDQT, the membranes were subjected to thermal treatment at temperature of 100 $^\circ$ C for time duration of 1.5 hours to remove moisture that might have been absorbed within the membrane pores. Then, the membranes were allowed to cool to ambient temperature before n-butane saturation. Afterwards, H $_2$ single gas permeation (Π_{H_2}) was carried out at 25kPa transmembrane pressure and ambient temperature. This was conducted to obtain the maximum H $_2$ gas permeance through the membrane. The synthesized nanocomposite sodalite / ceramic membranes were saturated with n-butane for a duration of 1.5 hours at ambient temperature and a partial pressure of 14 kPa. Hydrogen was used as the non-condensable gas to open the blocked pores of n-butane at room temperature. Figure 3.9a shows a schematic of the membrane module employed for thermal treatment and BDQT. Graphite O-rings were used as seals between membrane and at both ends of the module to ensure that the module was gas-tight (Figure 3.9b)

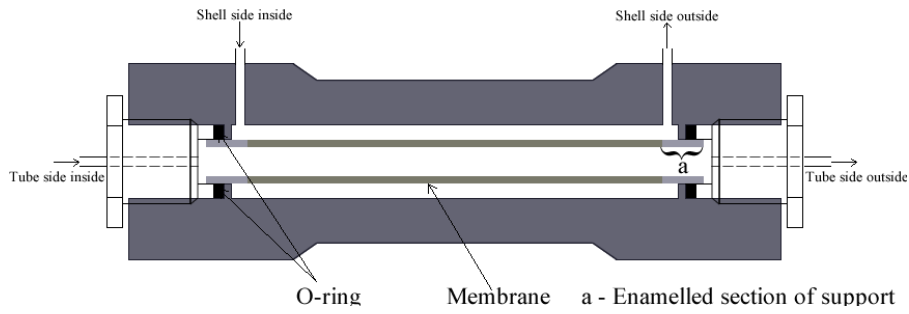


Figure 3.9 : Schematic of the membrane module employed for BDQT.

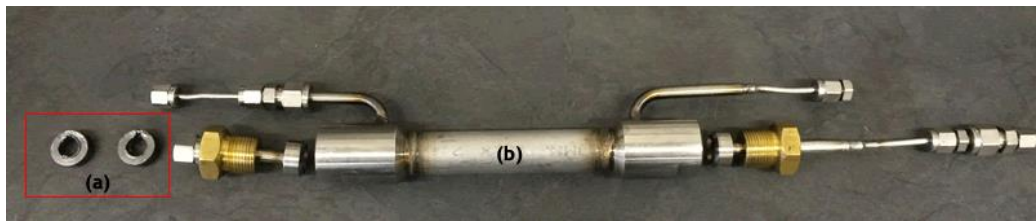


Figure 3.10: Picture of (a) graphite O-rings, (b) membrane module used for BDQT.

For the BDQT, the experimental setup depicted in Figure 3.10 was used. It is to be noted that results obtained from the BDQT was reproducible. The experiment was repeated at least twice for each of the membranes.

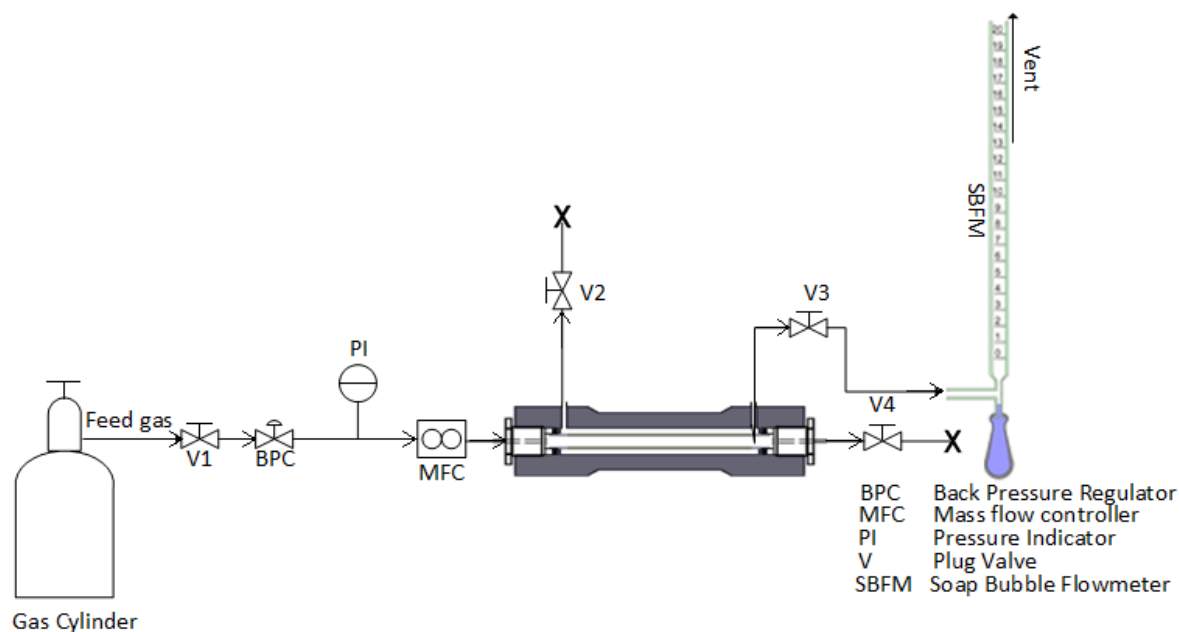


Figure 3.11: Schematic of the experimental set-up used for the BDQT.

Amongst the techniques commonly used for zeolite membrane defect characterization are mercury porosimetry (Manickam et al., 2014; Jareman et al., 2004) and permoporometry (Karimi et al., 2016, 2015, Tsuru et al., 2003, 2001), bubble point technique (Maghsoudi, 2016; Jakobs and Koros, 1997) and adsorption-desorption technique (Pachtova, 2003). These techniques have either been applied directly or modified due to their complexity and unsatisfactory results obtained (Karimi et al., 2016, 2015; Maghsoudi, 2016; Manickam et al., 2014; Peinador et al., 2010).

However, Pachtova, (2003) reported a simplified adsorption-desorption technique for zeolite membranes characterization. The simplified techniques involves the dynamic desorption of adsorbed gas on the zeolite membrane, desorption process is conducted under a pressure difference of a non-adsorbed gas.

Adsorption process involves subjecting the zeolite membrane to partial pressure of an adsorbing molecule (water or n-butane). The basic assumption is that zeolite pores are filled up and plugged for all sizes, up to a certain diameter known as “critical diameter”, with the exception of non-zeolitic pores. However, non-zeolitic pores

(inter crystalline zeolite pores) would allow the permeation of non-adsorbing gas (N₂ or H₂). According to Daramola et al., (2009), permeation commences via pores larger than the critical diameter and the permeation will increase significantly with time. Therefore, a relative and absolute low permeance is expected for a high quality zeolite membrane while a poor quality membrane should show a higher relative and absolute permeance with time.

In this work, normal butane (n-butane) was used to saturate the membrane and it is known to condense into the zeolite pores and block permeation of non-condensable gases (e.g. N₂, H₂) through the pores of the membranes. However, in the presence of defect or non-zeolitic pores, non-condensable gases will permeate during the BDQT. The permeance of hydrogen through the n-butane saturated membrane was obtained with the use of Equation 3.1.

$$\Pi_i = \frac{V_i}{A\Delta P} \quad 3-1$$

Π_i is H₂ permeance, V_i volumetric flowrate, A is the membrane effective area and ΔP is the transmembrane pressure.

3.7 Separation performance evaluation

Separation performance of the nanocomposite sodalite ceramic membranes were conducted via single gas permeation using H₂ and CO₂. The separation set-up depicted in Figure 3.4 was used. The membrane separation testing comprised of NI LabVIEW DAC interface modules, NI 240VAC relay module, back-pressure regulator, mass flow meter, gas mixer unit, digital thermometer etc. The permeation experiments were carried out at room temperature and at transmembrane pressure of 25 kPa. The flow rate of the permeate gas was measured using a soap bubble flowmeter. During the gas permeation, plug valve 2 and 4 were closed.

Chapter Four

Nanocomposite Sodalite / Ceramic Membrane:
Synthesis, Characterization & Quality Test

4 Nanocomposite sodalite / ceramic membrane: synthesis, characterization and quality test

4.1 Introduction

This chapter discusses the results obtained from the synthesis, characterization and quality test. Part of the results discussed in this chapter have been published in a peer-reviewed journal (See Appendix G)

4.2 Membrane synthesis & characterization

Nanocomposite hydroxy sodalite / ceramic membrane prepared via pore-plugging hydrothermal synthesis was synthesized according to Section 3.5. The membranes were synthesized using one-stage PPH and two-stage PPH using the temperature programme depicted in Figure 3.8. The morphology of the crystals obtained from the bottom of the autoclave and the as-prepared membranes was checked as previously described in Chapter 3. In addition the phase identification of the membrane and the crystals was done with XRD as previously described in Chapter 3.

4.3 Membrane quality test

Quality of the as-synthesized membranes was evaluated using the Basic Desorption Quality Test (BDQT) (Pachtova, 2003) described in Section 3.6.2.

4.4 Result and discussion

4.4.1 Zeolite uptake in support of the membrane

Mass of sodalite grown within the supports was estimated before and after the synthesis. Table 4.1 shows the initial weight, the final weight and percentage uptake of sodalite crystals within the supports after one-stage PPH synthesis.

Table 4.1: Sodalite uptake within the α -Al₂O₃ tubes after one-stage synthesis

Support	Initial weight	Final weight	Weight uptake (g)	Percent weight uptake (%)
M1	16.25	16.82	0.57	3.39
M2	16.28	16.97	0.69	4.07
M3	17.27	17.73	0.46	2.59

4.4.2 SEM images

After the one-stage synthesis, the sodalite crystals obtained from the bottom of the autoclave were examined. The SEM micrograph of the sodalite crystals obtained at the bottom of the autoclave is presented in Figures 4.1. Figure 4.1 shows crystals with cubic and nanorod-like shape. The observed shapes are consistent with literature. Urchin, thread-ball, flower-like, coral-like and cubic-octahedral have been reported for hydroxy sodalite crystals (Kalantari et al., 2015; Naskar et al., 2011; Kundu et al., 2010; Bayati et al., 2008). The cubic and nanorod-like shapes obtained in this study could be attributed to the interplay between growth and nucleation processes that both proceeded in parallel at high temperature (Chen et al., 2007).

A small portion of the nanocomposite sodalite / ceramic membrane (Membrane M2) was crushed and prepared for SEM micrograph. The inner surface of nanocomposite sodalite ceramic membrane (Figure 4.2) seems to be totally plugged with sodalite crystals. Figure 4.3 depicts the cross section of nanocomposite sodalite / ceramic membrane with three asymmetric layers (top, middle and bottom). However, the 800 nm and 1200 nm layers (as seen in Figure 3.2) are partially pore-plugged with sodalite crystals and it is envisaged that a multi-layer pore-plugging hydrothermal synthesis could totally plug these two regions.

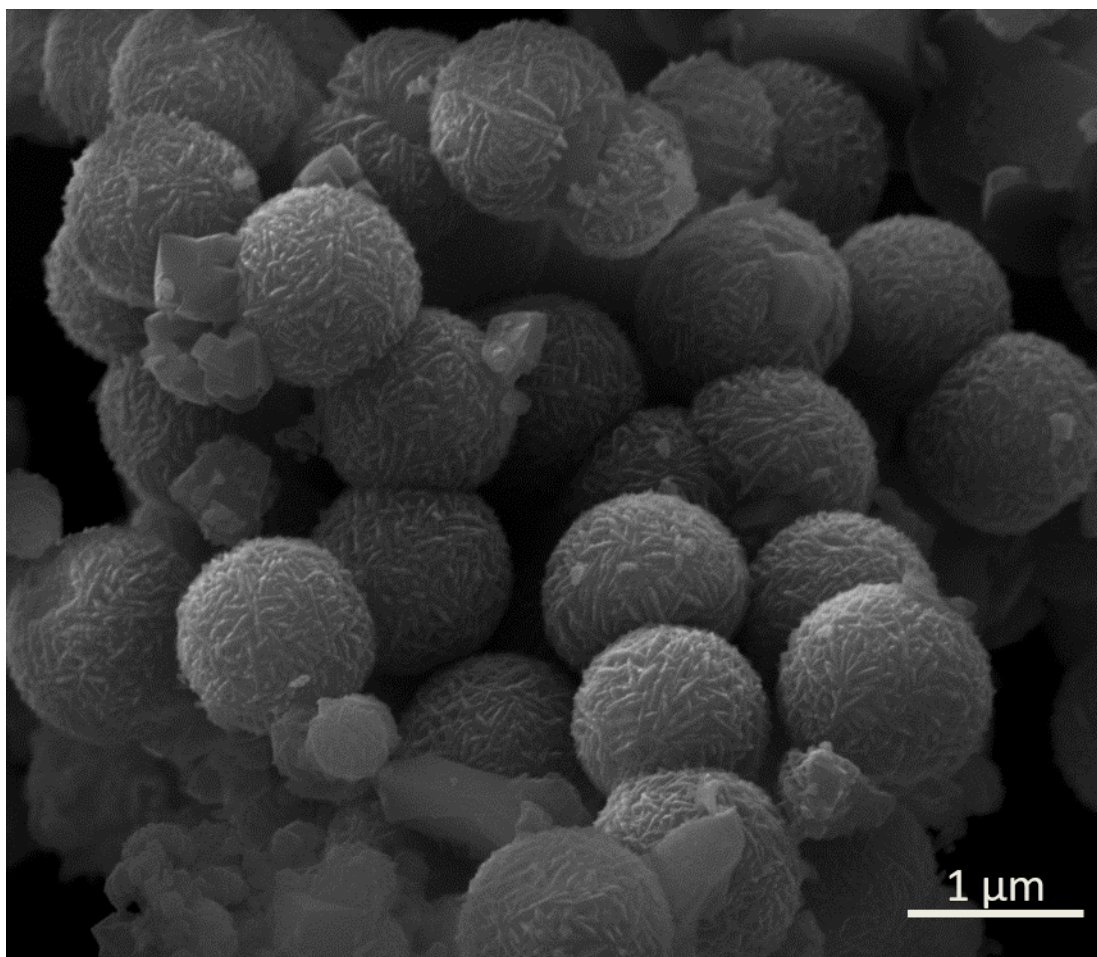


Figure 4.1: SEM image of hydroxy sodalite crystals obtained from the bottom of the Teflon®-lined autoclave during the pore-plugging hydrothermal synthesis.

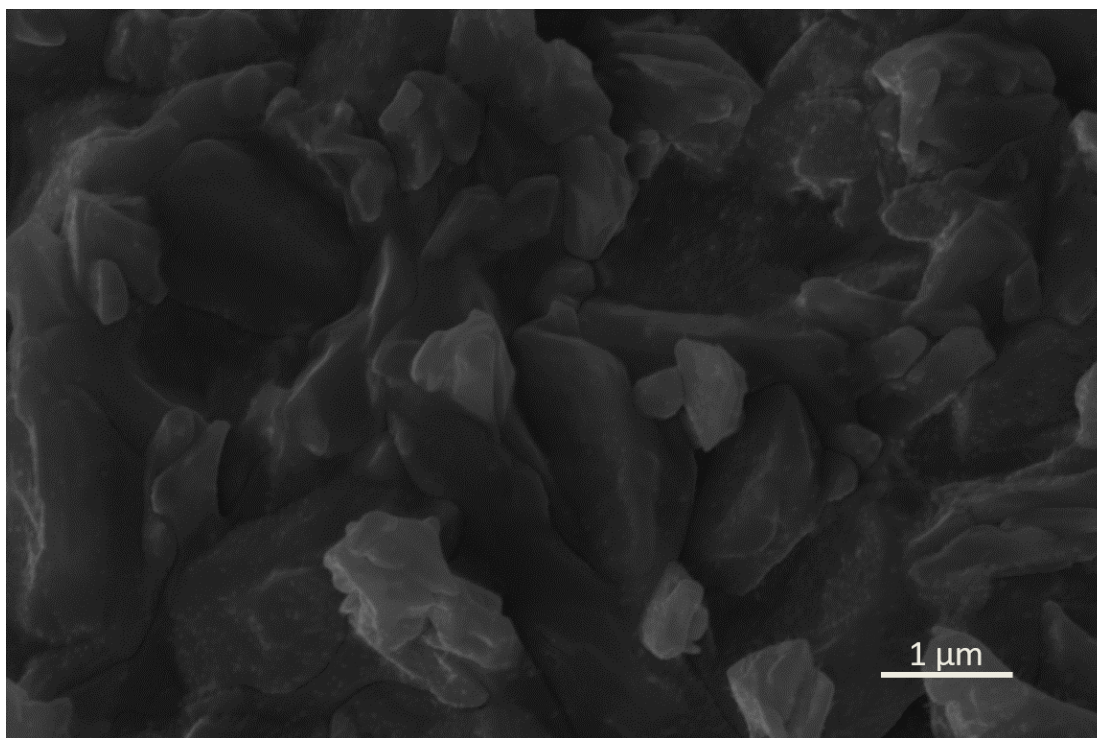


Figure 4.2: SEM image showing the surface of the innermost layer of the nanocomposite sodalite / ceramic membrane obtained after the one-stage PPH synthesis.

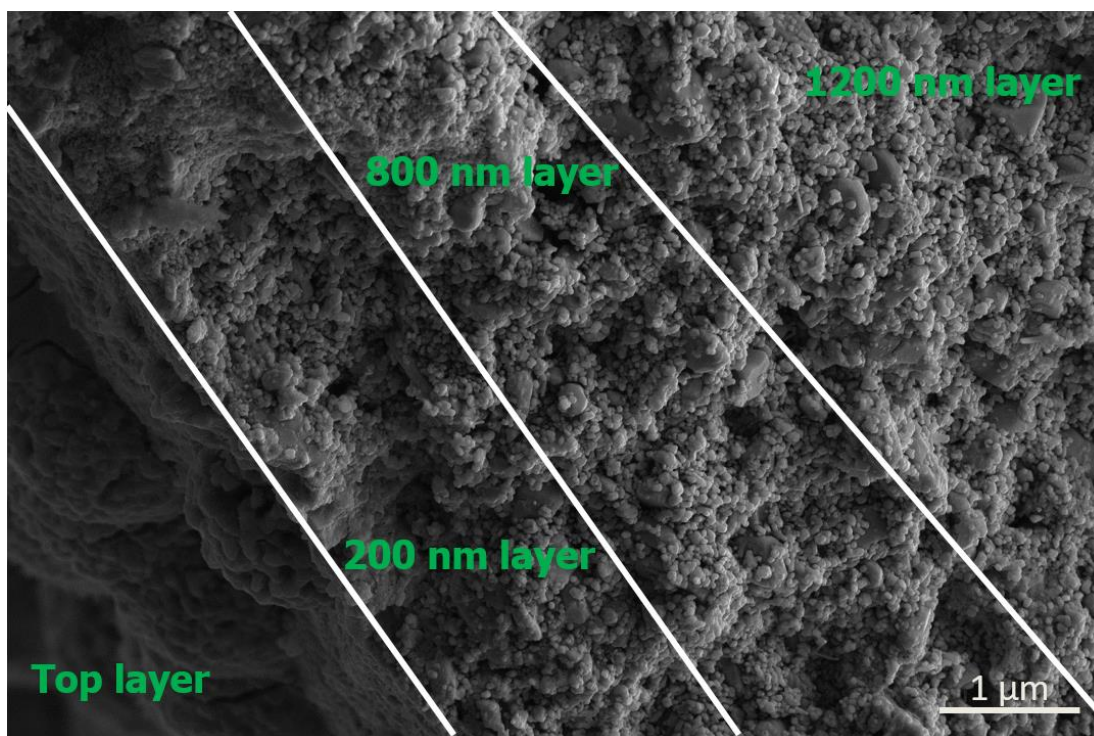


Figure 4.3: SEM image showing the three asymmetric layers with the presence of sodalite crystals at 200 nm region after one-stage PPH synthesis.

4.4.3 SEM image of membrane after 2-stage PPH synthesis

SEM micrograph of the inner surface (Figure 4.4) and cross-section (Figure 4.5) of the nanocomposite membrane obtained after the two-stage PPH synthesis shows that the sodalite crystals are fully grown in the 200 nm layer of the support. The SEM micrograph of the cross-section of the membrane (Figure 4.5) shows that the membrane has been fully pore-plugged in comparison to SEM micrograph of Figure 4.3 of membrane obtained from one-stage synthesis, which was partly pore-plugged. Multi-stage synthesis have been reported to enhance zeolite membrane quality, formation of a uniform and inter-grown zeolite phase. Huang et al., (2012) reported on synthesis of multi-layer zeolite LTA membranes with enhanced gas separation performance.

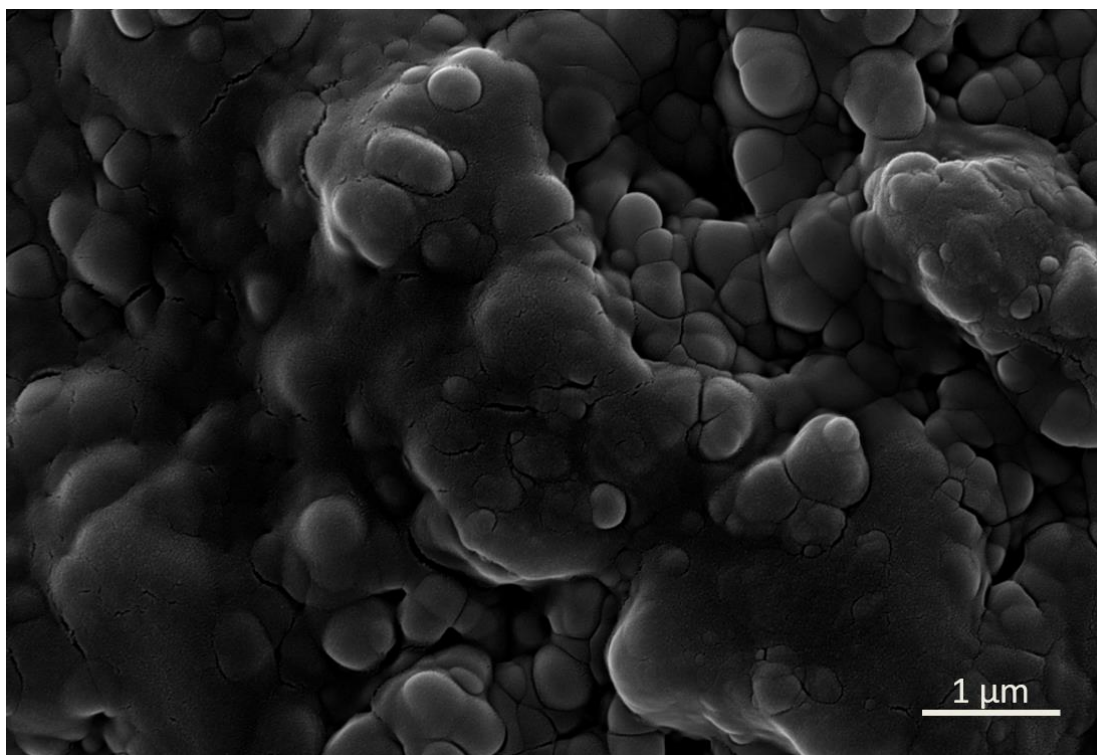


Figure 4.4: SEM image showing the surface of the innermost layer of the nanocomposite sodalite / ceramic membrane obtained after the two-stage PPH synthesis.

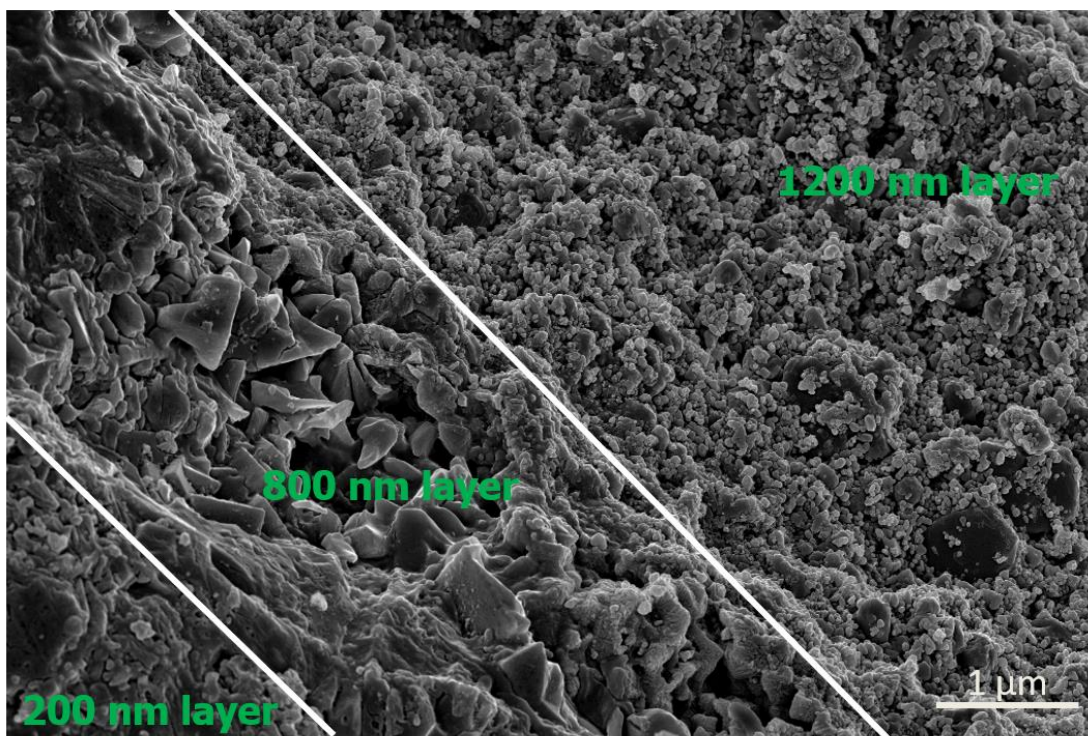


Figure 4.5: SEM image showing the cross-sections of the three layers (200 nm, 800 nm & 1200 nm) with the presence of sodalite crystals at all layers.

4.4.4 XRD analysis of crystals and membrane

The XRD pattern of the hydroxy sodalite crystals obtained from the bottom of the autoclave confirms that sodalite crystals were indeed obtained from the one-stage pore-plugging hydrothermal synthesis. (Figure 4.6)

The powder XRD pattern of the finely grinded membrane obtained after the two-stage PPH synthesis is depicted in Figure 4.6. The patterns (Figure 4.6 and 4.7) obtained are in agreement with reported XRD patterns for sodalite and it also correlate with simulated XRD pattern from the International Zeolite Association (IZA) (McCusker et al., 2007). In addition, the pattern reported also agrees with reported pattern for hydroxy sodalite (Daramola et al., 2016; Ding et al., 2010; Khajavi et al., 2007b; Xu et al., 2004).

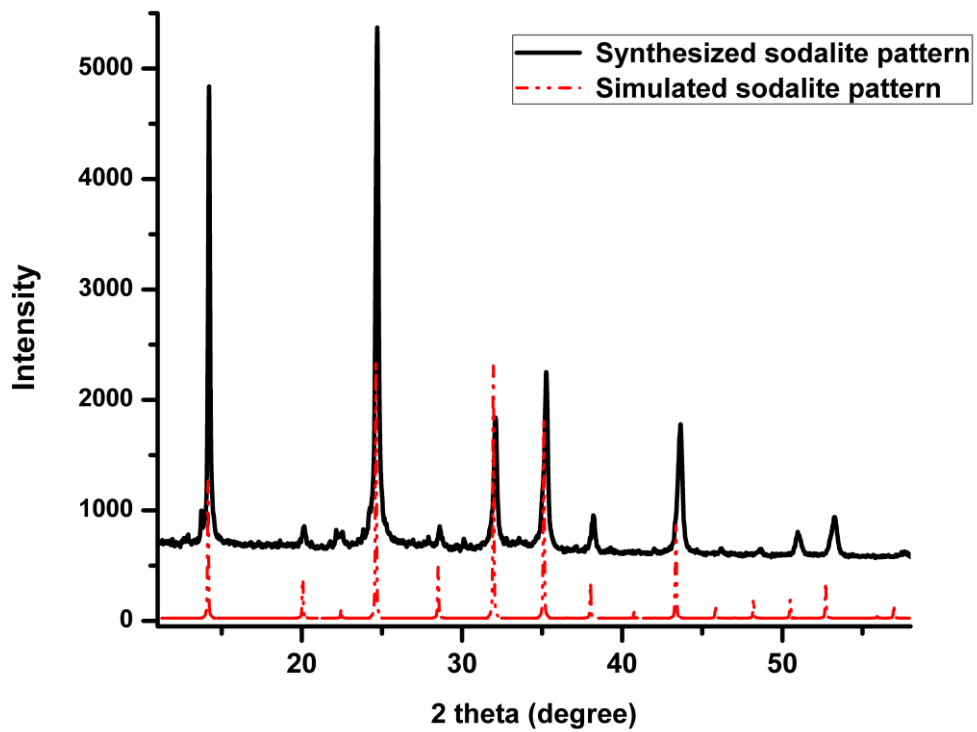


Figure 4.6: XRD patterns of synthesized hydroxy sodalite crystals and simulated sodalite (IZA)(McCusker et al., 2007)

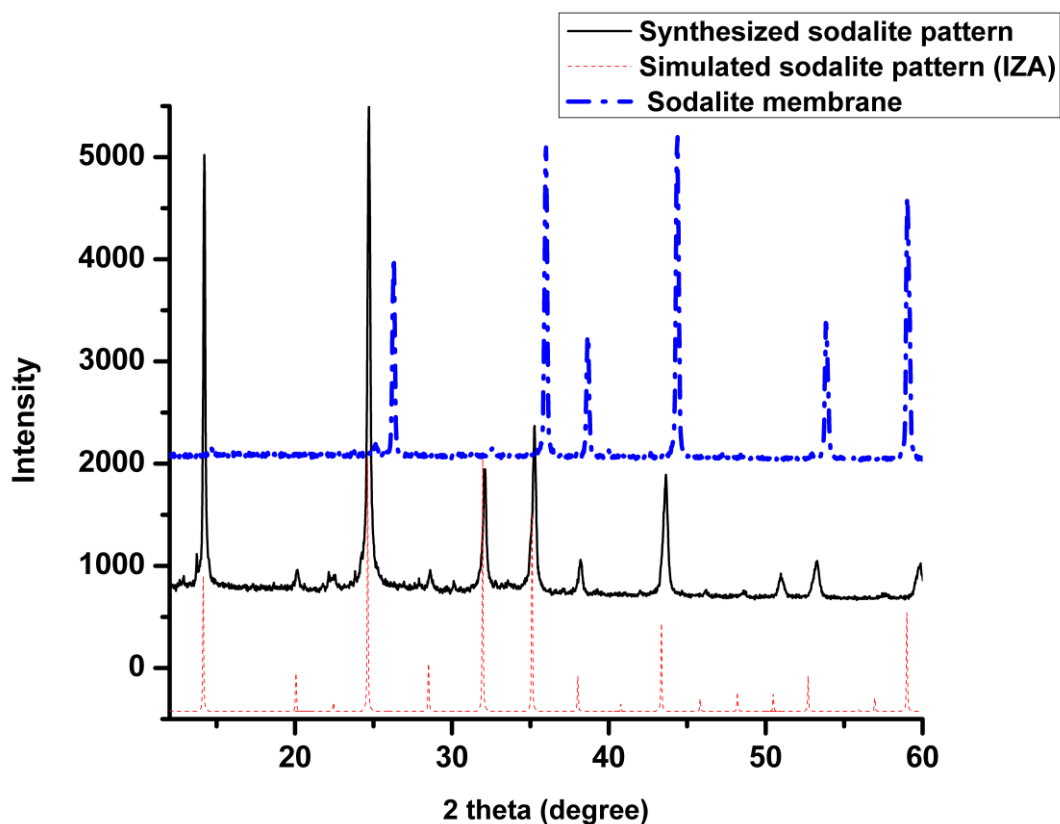


Figure 4.7: XRD patterns showing simulated sodalite pattern (IZA)(McCusker et al., 2007), synthesized sodalite crystals and sodalite membrane.

4.4.5 Basic Desorption Quality Test (BDQT)

Figure 4.8 shows the hydrogen permeance through sodalite membranes during the BDQT. The strong adsorption of n-butane in the nanocomposite sodalite / ceramic pores blocks the permeation of H₂ through the pores. Hydrogen permeation through the sodalite/ceramic membranes (M2 & M3) evolved relatively faster in comparison with membrane M1 and reached about 90% of the original H₂ permeance (Π_{H_2}). Enhanced permeance through the nanocomposite sodalite/ceramic membrane M2 & M3 could be attributed to fast desorption of n-butane from the membrane pores (inter-crystalline and intra-crystalline pores). Membrane (M1) displayed the least H₂ permeance of the three (3) membranes as observed in Figure 4.8. M1 possess the best quality and was subsequently used for separation performance evaluation during the separation of H₂ & CO₂.

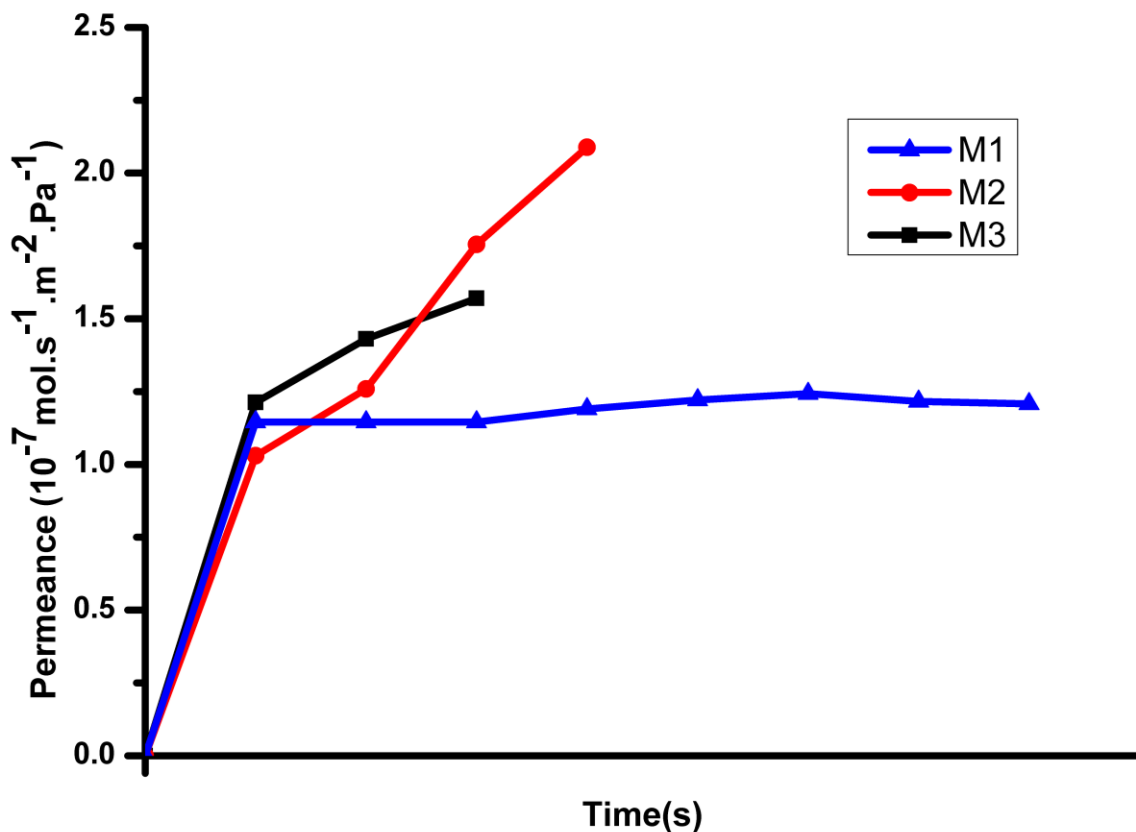


Figure 4.8: Basic Desorption Quality Test (BDQT) for the three as-synthesized nanocomposite membranes.

The membrane M1, which was subjected to two-stage PPH synthesis, showed a greater improvement (Figure 4.9). Desorption of condensable gas within the sodalite membrane showed a relatively low permeance with time. This is an indication that the porous support are sufficiently plugged with sodalite crystals.

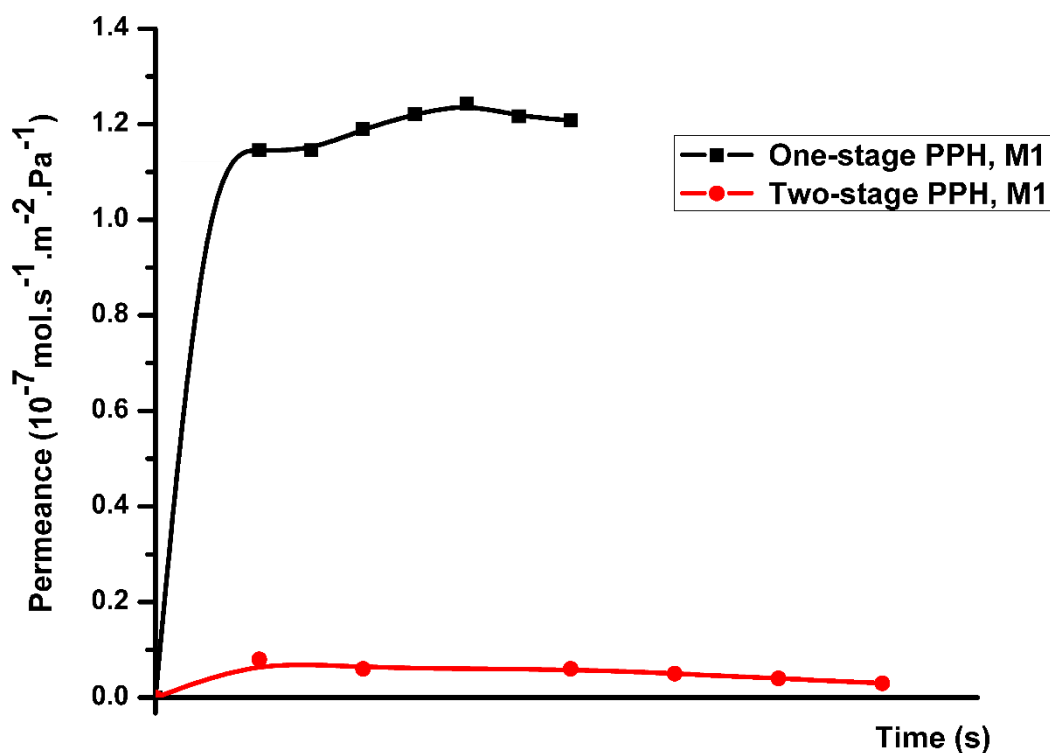


Figure 4.9: BDQT for membrane M1 after one and two-stage synthesis.

4.5 Concluding remarks

In this chapter, nanocomposite sodalite / ceramic membrane was successfully synthesized via one-stage PPH and two-stage PPH synthesis. The membranes were characterized using SEM and XRD. The quality of the membrane was checked using BDQT. The SEM images confirmed that sodalite crystals were grown within the pores of the three (3) layers of the support with the 200 nm layer totally pore-plugged. In addition, the XRD pattern re-affirms that pure sodalite was synthesized via the synthesis route. To evaluate the quality of the as-synthesized membranes, basic desorption and quality test was performed. The BDQT confirmed that the membrane improved tremendously after the two-stage PPH synthesis.

Chapter Five

Nanocomposite Sodalite / Ceramic Membrane:
Separation Performance and Effect of Operating
Variables.

5 Nanocomposite sodalite / ceramic membrane: separation performance and effects of operating variables.

5.1 Introduction

In this chapter, results of separation performance of the membranes are presented. Separation of H₂ from H₂/CO₂ mixtures was measured using single gas components of H₂ and CO₂. Membrane M1 obtained from the two-stage PPH synthesis was used in the investigation. The gas separation experiments were carried out at room temperature and at transmembrane pressure of 25 kPa. During the gas separation experiment, plug valve 2 and 4 were closed in Figure 3.10. The measurement was obtained using the set-up depicted in Figure 3.4 & Figure 3.5. Flow rate of the permeate gas was measured using a soap bubble flowmeter. The permeance of the H₂ and CO₂ from the membrane and the H₂/CO₂ ideal selectivity (S_{H_2/CO_2}), were calculated using Equation (3.1) and Equation (5.2), respectively:

$$S_{H_2/CO_2} = \frac{\Pi_{H_2}}{\Pi_{CO_2}} \quad 5-1$$

Π_{H_2} & Π_{CO_2} are the H₂ and CO₂ permeance in mol.s⁻¹.m⁻².Pa⁻¹, respectively.

5.2 Results and discussion

5.2.1 Membrane separation performance

Further investigation was conducted on the membrane (M1) to evaluate its separation performance during H₂/CO₂ mixture separation. H₂ and CO₂ permeation measurements were carried out at ambient temperature and transmembrane pressure of 25 kPa over a permeation period of 170 s. Results obtained reveal that H₂ has the highest permeance through membrane (see Figure 5.1). The observation could be attributed to the small kinetic diameter of H₂ (0.27 nm) in comparison with CO₂ (0.33 nm).

In principle, gas permeation through porous media is described by mechanism such as Knudsen diffusion, surface diffusion, Poiseuille flow and molecular sieving (Abas et al., 2015). Gas separation in sodalite membrane could be described by molecular sieving and adsorption-diffusion mechanism. In such mechanism, the ratio of pore

diameter (sodalite crystal pore diameter) to molecular diameter (for example, hydrogen) tends to unity. This is an indication that separation is being effected by the molecular structure, as a result of interactions between permeating molecules and pore walls.

In this work, the permeance of H₂ and CO₂ through the sodalite membrane synthesized using the one-stage PPH synthesis reached a value of about 3.9×10^{-7} mol.s⁻¹.m⁻².Pa⁻¹ and 8.38×10^{-8} mol.s⁻¹.m⁻².Pa⁻¹, respectively (Figure 5.1 and Figure 5.2). In addition, the permeance of H₂ and CO₂ decreased in the membrane obtained from the two-stage PPH synthesis with an increase in ideal selectivity (Figure 5.2 and Figure 5.3). The gas permeation measurement shows that the nanocomposite membrane displayed H₂ permeance and CO₂ permeance of 7.37×10^{-8} mol.s⁻¹.m⁻².Pa⁻¹ and 1.14×10^{-8} mol.s⁻¹.m⁻².Pa⁻¹, respectively. In addition, the ideal selectivity of the membrane improved from 4.6 to 6.5 for the membrane obtained via one-stage to two-stage PPH synthesis, respectively.

Table 5.1 presents a comparison of this work and other reported zeolite membranes that were evaluated for gas permeation in similar experimental conditions. Experimental result obtained in this work is in close agreement with values reported for multi-layer LTA membranes evaluated for single gas permeation of H₂ and CO₂ by Huang et al., (2012), although LTA has a wider cage dimension in the range of 0.30 & 0.45 nm in comparison with sodalite cage dimension (0.26 and 0.29 nm). Huang et al., (2012) prepared multilayer (three layer) NaA zeolite using α -Al₂O₃ support and evaluated it for gas permeation. However, Huang et al., (2012) reported a higher ideal selectivity (12.50) in their work, also, the work was conducted at a much higher temperature and transmembrane pressure. The average pore dimension of LTA, 0.41 nm, and the experimental conditions used in the evaluation of the LTA membrane could be responsible for the higher ideal selectivity obtained by Huang et al., (2012).

Also, gas permeation reported by Wang et al., (2015); Huang et al., (2012); Hosseini et al., (2008); Guan et al., (2003, 2001) were evaluated at higher transmembrane

pressure when compared to this present work. In the work, Gu et al., (2008) prepared modified-MFI which was supported on alumina and prepared via direct hydrothermal synthesis. The gas permeation was conducted between 296 and 723 K. However, Gu et al., (2008) reported a higher ideal selectivity from their modified MDES MFI membrane in comparison with this work. The higher temperature and wider average pore dimension of MFI, in range of 0.45 & 0.60 nm, could be a factor responsible for the higher ideal selectivity (17.50) reported by Gu et al., (2008). However, the higher selectivity reported by Gu et al., (2008) was traded for a lower H₂ and CO₂ flux. In this work, sodalite / ceramic membrane possessed a higher flux but low selectivity. Nanocomposite membranes have been reported to possess higher flux but low selectivity (Daramola et al., 2009)

In addition, DDR-3 membrane prepared via modified secondary seeded growth by Kanazashi et al., (2008) was evaluated at temperatures between 298 K and 773 K for single gases (H₂ & CO₂). The DDR-3 membrane is selective to H₂ with a permeance of $2.18 \times 10^{-8} \text{ mol.s}^{-1}.\text{m}^{-2}.\text{Pa}^{-1}$ and ideal selectivity of 5.59. DDR-3 is highly siliceous zeolite with average pore size 0.36 nm, making it a good candidate for comparison with the synthesized nanocomposite ceramic/sodalite membrane. Kanazashi et al., (2008) conducted single gas permeation experiments using H₂, CO and CO₂ using a stainless steel cell and an experimental setup similar to the one used in this work. Kanazashi et al., (2008) reported an ideal selectivity of 5.59 at a temperature range of 298 & 773 K. The ideal selectivity obtained in this work shows superior membrane quality in comparison with DDR-3 membrane prepared by Kanazashi et al., (2008). It should be noted that sodalite has a smaller cage dimension of 0.26 nm in comparison with DDR-3 of 0.36 nm and experimental conditions used by Kanazashi and co-worker is much wider in terms of temperature (298 -773 K). Therefore, the nanocomposite sodalite / ceramic membrane reported in this work, outperformed the DDR-3 thin-film membrane by Kanazashi et al., (2008).

Aluminophosphate (AlPO₄) mainly composed of AlO₂⁻ and PO₂⁺ tetrahedra was prepared on a porous alumina tube by Guan and his co-workers in the presence of HF

and using tetraethylammonium hydroxide (TEAOH) as template. AlPO_4 is a microporous crystal that is thermally stable up to 873 K with limited ion-exchange potentials. The thermal stability of AlPO_4 is higher in comparison with sodalite thermal stability which is about 450 K. In addition, Guan and his co-worker experimental conditions are higher than experimental conditions in this work. Guan conducted the gas permeation at 310 K and 101 kPa, whereas, sodalite / ceramic membrane was only evaluated at 298 K and 25 kPa in this work. Ideal selectivity obtained by Guan and his co-worker indicated that the AlPO_4 membrane is highly selective towards H_2 . Moreover, a relatively higher H_2 permeance and lower CO_2 permeance was reported by Guan. However, sodalite / ceramic membrane evaluated in this work, is selective towards H_2 with high H_2 permeance but the CO_2 permeance is slightly high. This CO_2 permeance through sodalite / ceramic membrane effect the low ideal selectivity.

Zeolitic Imidazolate Framework, such as ZIF-7, is formed by bridging benzimidazolate anions and zinc cations usually resulting in a sodalite topology with a pore size of about 0.3 nm. Li et al., (2010) reported on gas permeation properties of ZIF-7 supported on alumina and prepared by microwave-assisted secondary growth. The gas permeation experiment was conducted at 493 K and transmembrane pressure of 101 kPa, the experimental conditions reported by Li et al., (2010) is higher than experimental condition used in evaluating sodalite / ceramic membrane in this work. H_2 and CO_2 permeance through the ZIF-7 membrane is relatively low in comparison to sodalite / ceramic membrane reported in this work. However, Li et al., (2010) reported a higher ideal selectivity of 13.6, which is higher than selectivity reported for sodalite / ceramic membrane reported in this work. The higher selectivity reported by Li et al., (2010) could be due to relatively low H_2 permeance and a much lower CO_2 permeance within the ZIF-7 membrane.

Conclusively, experimental conditions such as temperature, transmembrane pressure and etc. affect the separation performance of zeolitic membranes. In addition, the type of zeolitic materials used in the development of the membrane is a key factor to

consider towards enhancing the separation performance. Zeolite materials having an average pore dimension similar to the molecular size of H_2 but smaller than the kinetic diameter of CO_2 will result in better separation performance in terms of selectivity. It is noteworthy to mention that the presence of defects in the membrane will dramatically reduce the membrane selectivity.

Table 5.1: Comparison of permeation and selectivity result obtained and literature.

Membrane Support	/ Synthesis method	Permeation conditions		Ideal selectivity (H ₂ /CO ₂)	Permeance (10 ⁻⁷ mols ⁻¹ m ⁻² Pa ⁻¹)		Reference
		Temperature (K)	Transmembrane pressure (kPa)		H ₂	CO ₂	
Hydroxy sodalite / α -Al ₂ O ₃	Pore-plugging hydrothermal (1-stage synthesis)	298	25	4.63	3.89	0.84	This work
Hydroxy sodalite / α -Al ₂ O ₃	Pore-plugging hydrothermal (2-stage synthesis)	298	25	6.46	7.37	1.14	This work
Multi-Layer LTA (3- layers) / α -Al ₂ O ₃	<i>in-situ</i> hydrothermal (3 step synthesis)	373	101	12.50	2.10	0.17	Huang et al., (2012)
MDES modified MFI / α -Al ₂ O ₃	<i>in-situ</i> crystallization	296-723	-	17.50	1.86	0.11	Gu et al., (2008)
AlPO ₄ / α -Al ₂ O ₃	Two-step hydrothermal	310	101	23.90	3.36	0.14	Guan et al., (2003)
ZIF-7 / Al ₂ O ₃	Microwave-assisted secondary growth	493	101	13.6	0.45	0.03	Li et al., (2010)
Ni-MOF-74 / α -Al ₂ O ₃	Two-stage (layer by layer seeding and secondary solvothermal crystallization)	298	-	9.1	127	0.07	Lee et al., (2012)
CVD modified DDR-3 / α -Al ₂ O ₃	Secondary seeded growth	298-773	-	5.59	2.18	0.39	Kanezashi et al., (2008)

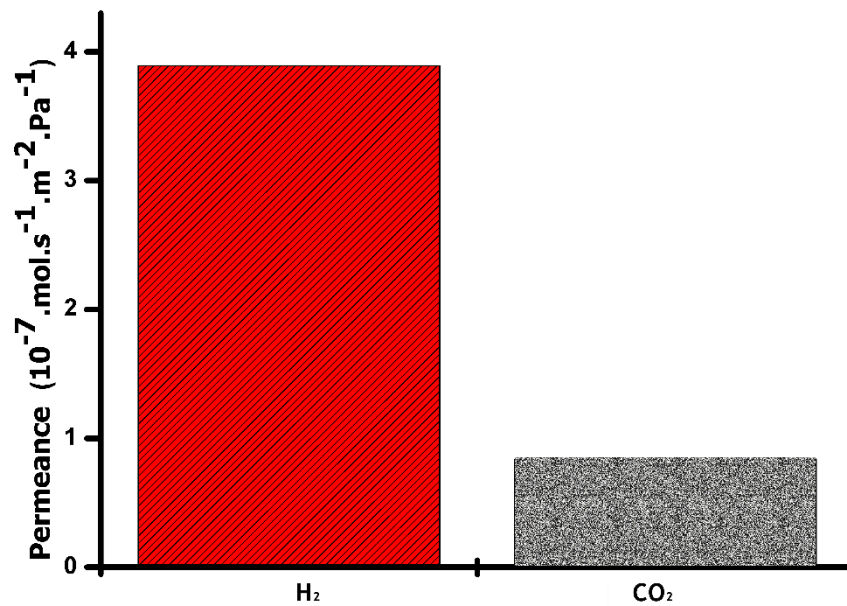


Figure 5.1: H₂ and CO₂ permeance through membrane prepared via one-stage synthesis.

In addition, because of the kinetic diameter of H₂ (0.27 nm) which is smaller than that of CO₂ (0.33 nm), higher permeance of H₂ through the defect-free nanocomposite sodalite/ceramic membrane is expected. Ideal selectivity of 4.6 was obtained for the permeance of H₂ and CO₂ through the one-stage membrane. This value is slightly lower than the Knudsen separation coefficient 4.7 for H₂/CO₂. For the two-stage membrane, ideal selectivity of 6.5 was obtained. The lower selectivity obtained in this work could be attributed to the occluded water present in sodalite cage (see Table 5.1).

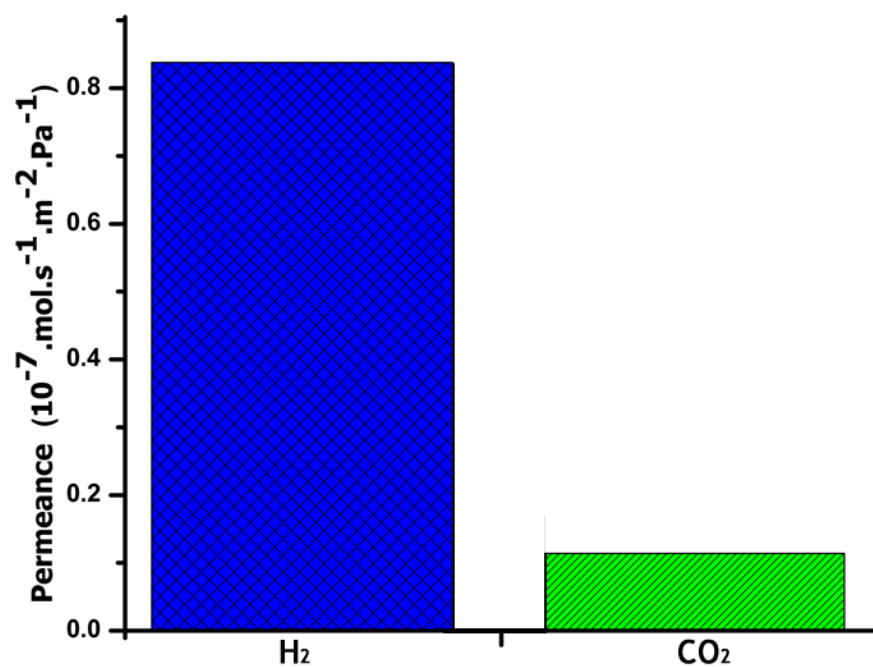


Figure 5.2: H₂ & CO₂ permeance through membrane prepared via two-stage synthesis.

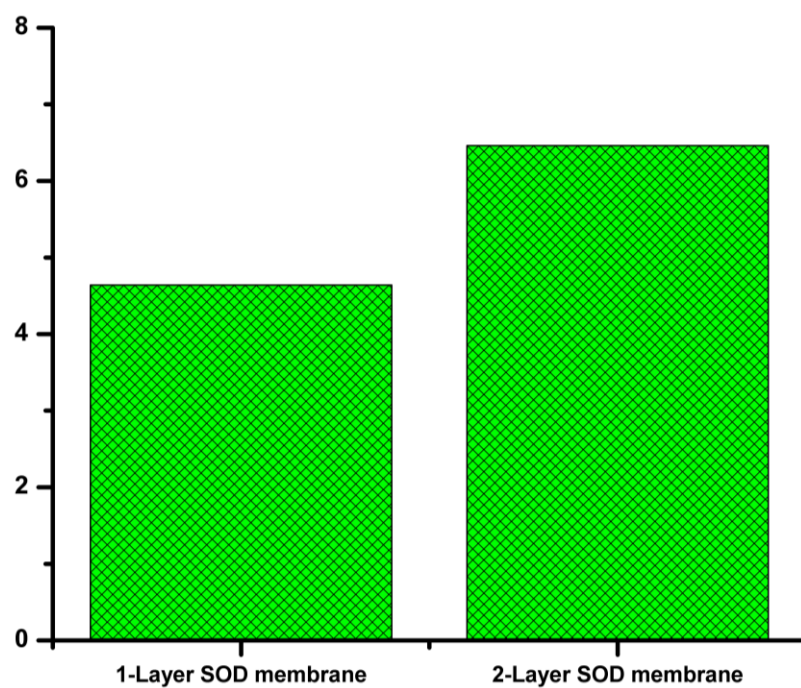


Figure 5.3: CO₂/H₂ ideal selectivity in the one and two-stage nanocomposite membranes.

5.3 Effects of temperature on separation performance of sodalite membrane

The effect of temperature was investigated on the two-stage synthesized membrane using H₂ and CO₂. Figure 5.4 shows membrane flux as a function of temperature on the nanocomposite membrane. The plot shows a continuous decrease in molar flux of H₂ and CO₂ with increasing temperature (373 K through 423K, till 473K). Maximum molar flux for H₂ and CO₂ was observed at $1.5 \times 10^{-3} \text{ mol.s}^{-1}.\text{m}^{-2}$ and $0.4 \times 10^{-3} \text{ mol.s}^{-1}.\text{m}^{-2}$ at 373K, respectively. Figure 5.5 depicts permeance as a function of temperature on the two-stage synthesized nanocomposite sodalite ceramic membrane of $5.8 \times 10^{-8} \text{ mol.s}^{-1}.\text{m}^{-2}.\text{Pa}^{-1}$ and $1.4 \times 10^{-8} \text{ mol.s}^{-1}.\text{m}^{-2}.\text{Pa}^{-1}$, respectively. For nanocomposite materials, gas permeance is generally described by adsorption driven mechanism after the maximum gas permeance has been reached (Miachon et al., 2007). At elevated temperature, the flux of gas components (H₂ and CO₂) are decreases monotonically, this could imply that the maximum H₂ and CO₂ permanence has been reached in the sodalite membrane, which is in agreement with literature (Daramola et al., 2009a; Miachon et al., 2007). In addition, Miachon and co-workers (2007) reported a continuous decrease in flux for gas permeation using H₂ in the nanocomposite MFI-alumina membranes prepared via pore-plugging hydrothermal route. The continuous flux decrease in nanocomposite membranes at higher temperature has been attributed to the distinctive nanocomposite structure. In addition, the membrane material such as low silicon/aluminum ratio materials which give rise to acidic sites, such sites are very strong adsorption sites which maybe characterized by adsorption-driven mechanism. It should be noted that H₂ permeance through the sodalite / ceramic membrane is much higher than CO₂ permeance, though H₂ permeance and CO₂ permeance decreased with increasing temperature. Also, the presence of intercrystalline pathways such as non-zeolitic pores could be responsible for the decrease in membrane selectivity towards a single gas component (H₂), as seen in this work. Figure 5.6 depicts the ideal selectivity as a function of temperature in the nanocomposite membrane at the maximum permeance obtained using H₂ and

CO₂. As can be seen, the ideal selectivity increased with increasing temperature, the ideal selectivity increased from 373 K through 423 K until 473 K.

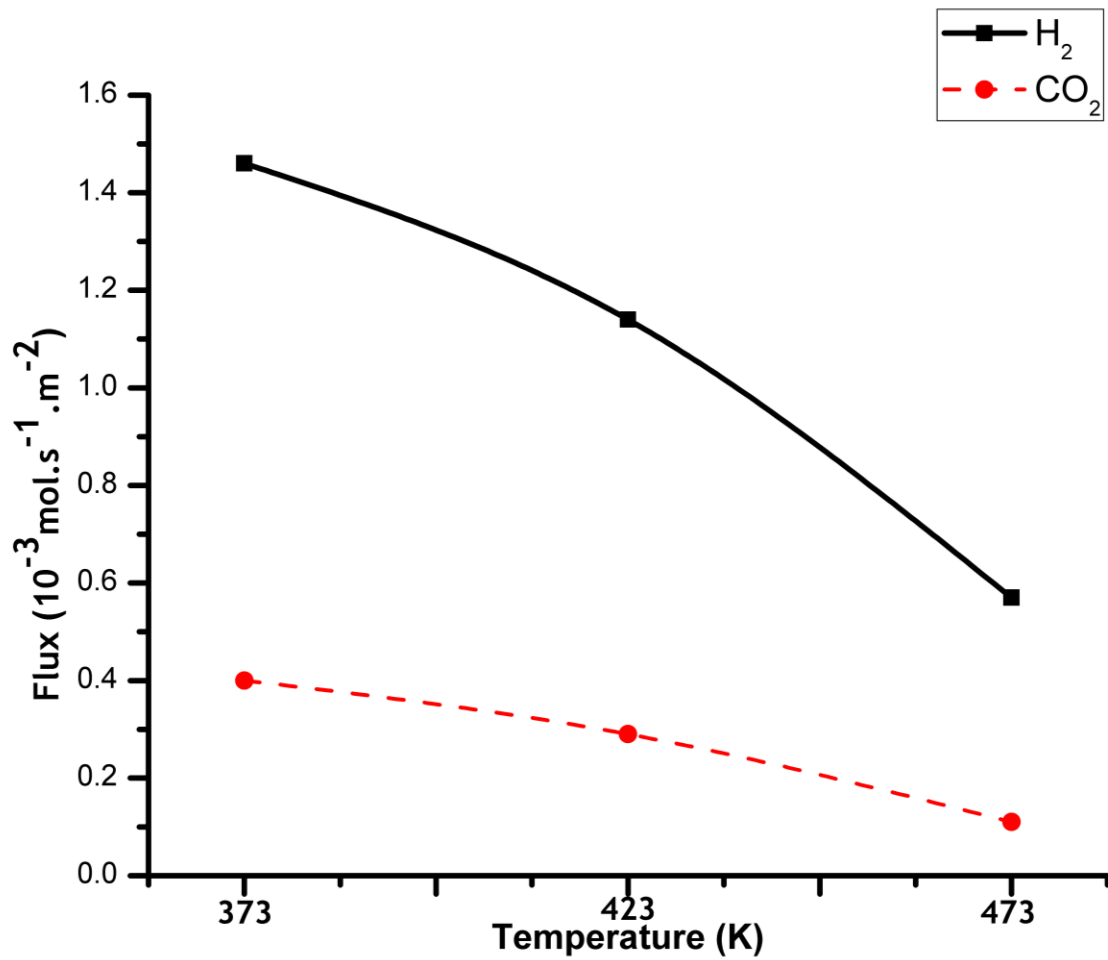


Figure 5.4: Membrane flux as a function of temperature (2-stage nanocomposite membrane).

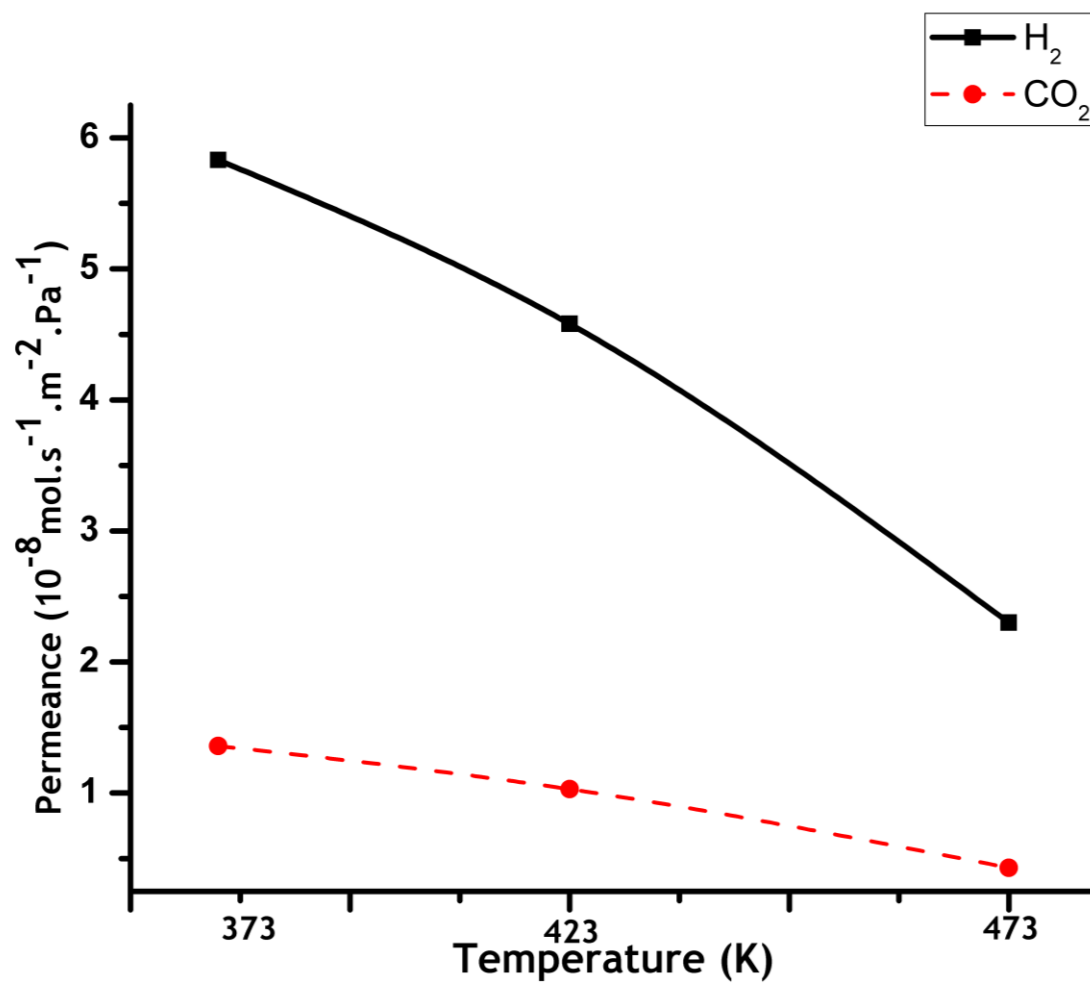


Figure 5.5: Permeance as a function of temperature (2-stage nanocomposite membrane).

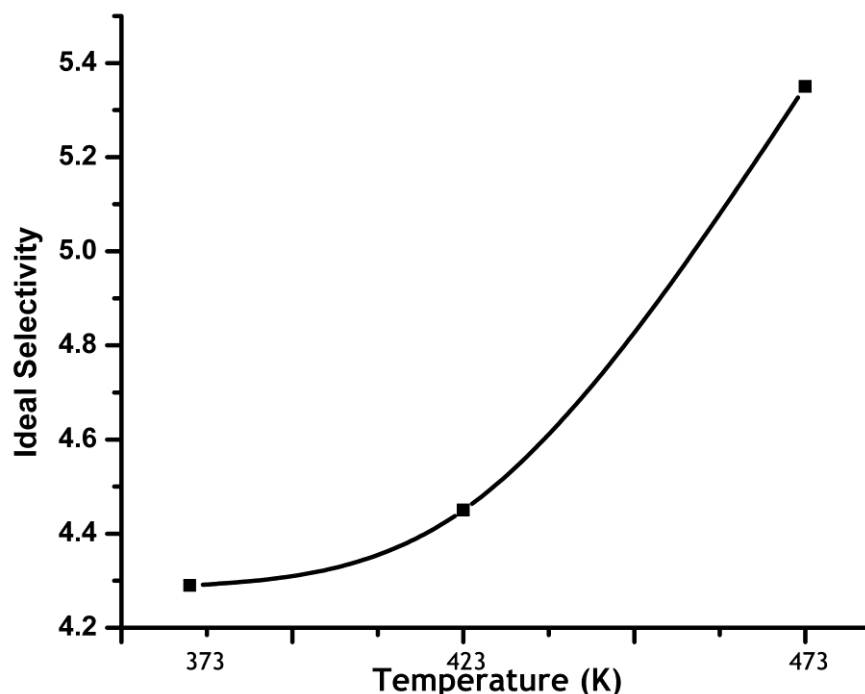


Figure 5.6: CO₂/H₂ ideal selectivity as a function of temperature (2-stage nanocomposite membrane).

5.4 Effects of pressure on separation performance of sodalite membrane

The effect of pressure was investigated using single gases and mixture gases (H₂ and CO₂) on the two-stage synthesized nanocomposite membrane. Figure 5.7 and Figure 5.8 depicts flux as a function of transmembrane pressure and permeance as a function of transmembrane pressure, respectively. As can be seen in Figure 5.8, the permeance of H₂ and CO₂ decreases with increases in the transmembrane pressure. The maximum permeance of H₂ and CO₂ obtained are $7.4 \times 10^{-8} \text{ mol.s}^{-1}.\text{m}^{-2}.\text{Pa}^{-1}$ and $3.5 \times 10^{-8} \text{ mol.s}^{-1}.\text{m}^{-2}.\text{Pa}^{-1}$, respectively. However, H₂ permeance decreases steadily from the maximum to $2.3 \times 10^{-8} \text{ mol.s}^{-1}.\text{m}^{-2}.\text{Pa}^{-1}$ at 304 kPa transmembrane pressure. This result could be attributed to strong adsorption experienced in zeolite membrane at higher pressures (Daramola et al., 2009a). In addition, the ideal selectivity was evaluated at these pressures and depicted in Figure 5.9. As the transmembrane pressure increased during the gas permeation through the sodalite/ceramic membrane, the gas flux increased, so also the gas concentration at the membrane surface

increased. High concentration of gas at the membrane surface would initiate the adsorption-diffusion process, the adsorption of non-adsorbing gas (H_2) is expected to be rapid and diffuse through the membrane at a relatively short time. However, adsorbing gas such as CO_2 would be relatively slower than H_2 , the slow adsorption-diffusion experienced in CO_2 permeation could be responsible for the plateau of Figure 5.8 between 2.0 and 3.0 Bar. Figure 5.9 depicts a decreasing permeance and Figure 5.10 depicts an increasing ideal selectivity. The permeance of H_2 and CO_2 through the sodalite membrane has been normalized by the transmembrane pressure (TMP) (i.e. ratio of membrane flux to TMP), so it is expected that the permeance will decrease with increasing pressure. In addition, the ideal selectivity witnessed a sharp increase after 2.0 bar transmembrane pressure mark, attributable to the reduced CO_2 permeation around 2.0 bar and 3.0 bar due to slow adsorption-diffusion of CO_2 in sodalite / ceramic membranes.

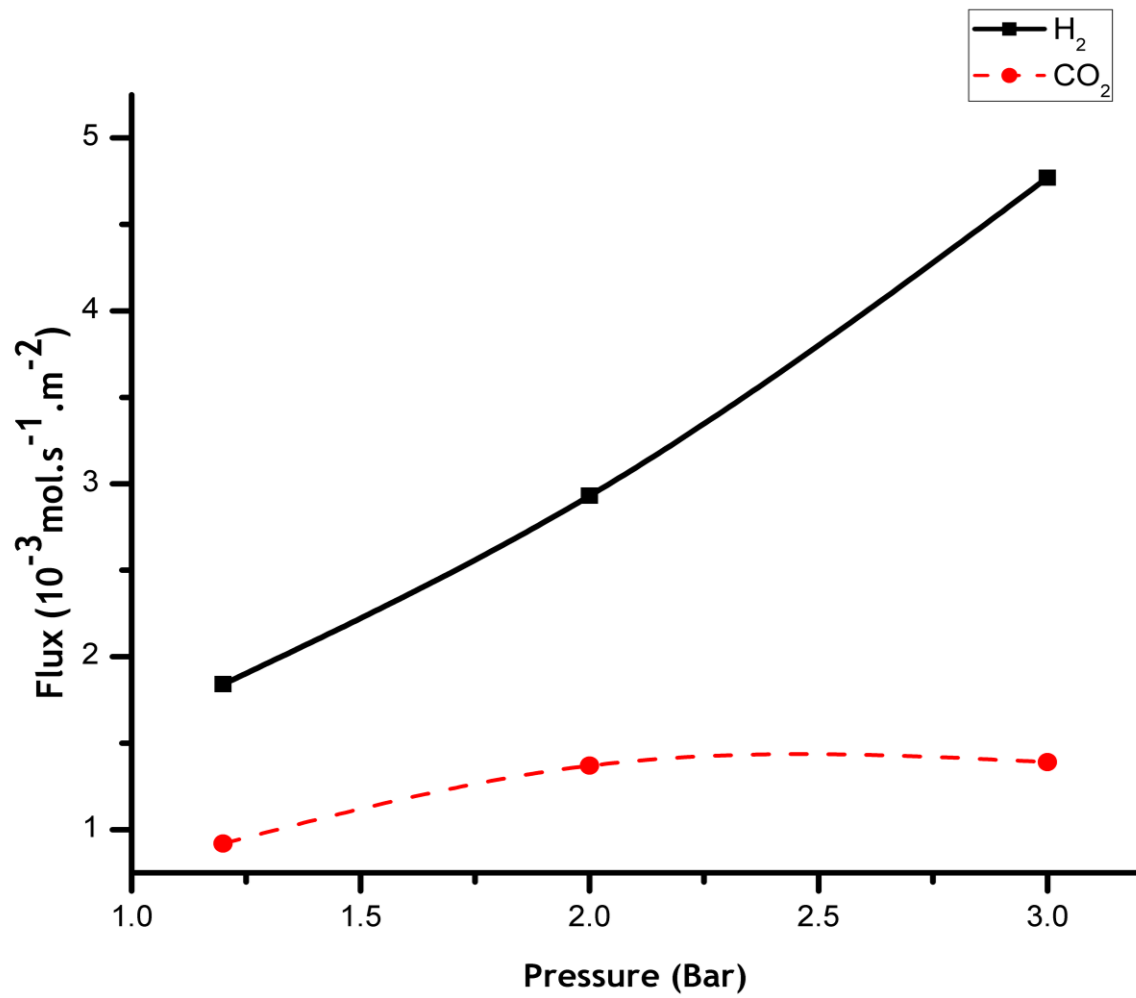


Figure 5.7: Flux as a function of pressure (2-stage nanocomposite membrane).

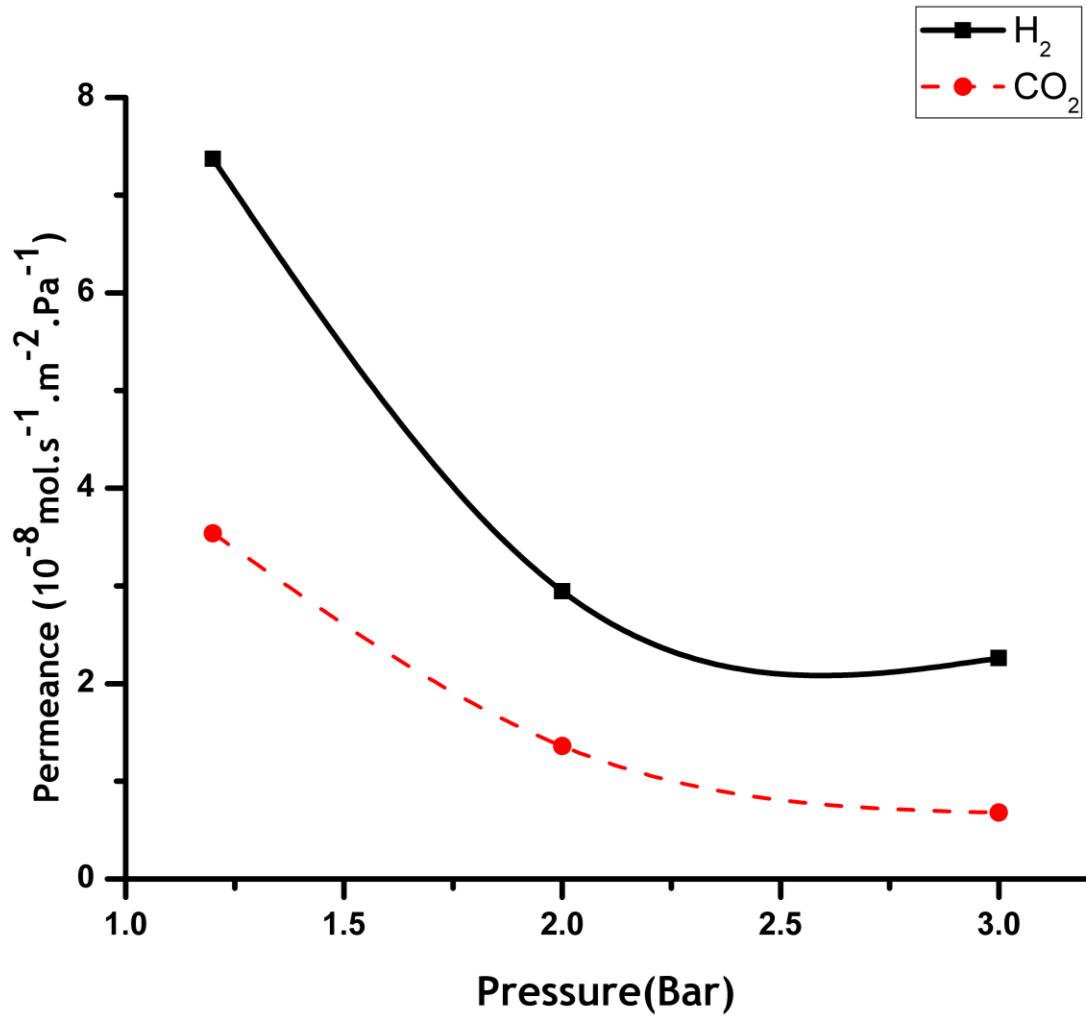


Figure 5.8: Permeance as a function of feed pressure (2-stage nanocomposite membrane).

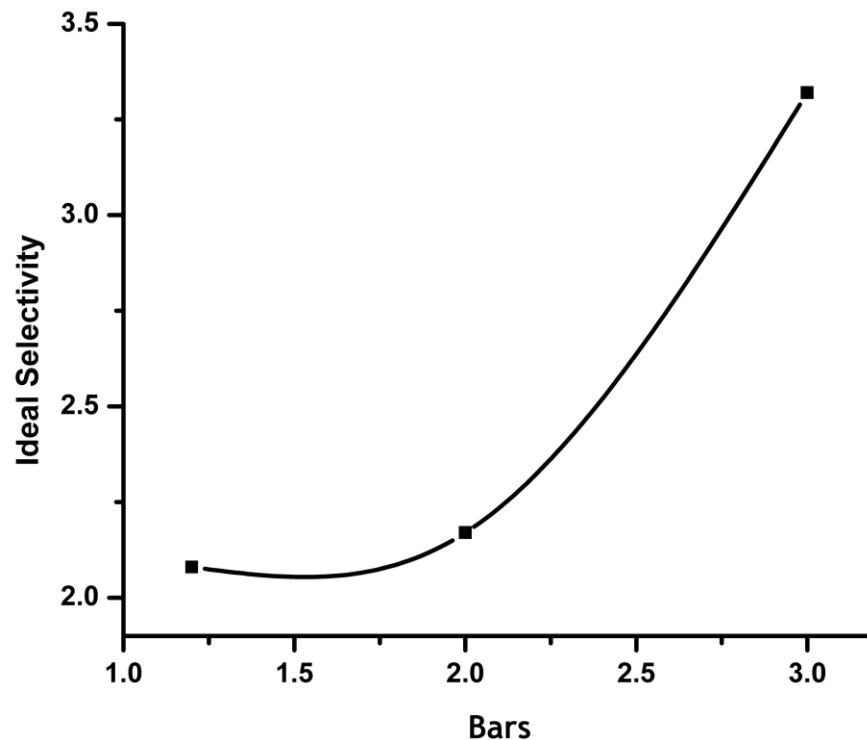


Figure 5.9: Ideal selectivity as a function of pressure (2-stage nanocomposite membrane).

5.5 Effects of feed flow rate on separation performance of sodalite membrane

The effect of feed flowrate was investigated on the membrane obtained by two-stage synthesis using H_2 and CO_2 . Figure 5.11 depicts the flux as a function of feed flowrate obtained at $10 \times 10^{-3} \text{ mol.s}^{-1}$, $25 \times 10^{-3} \text{ mol.s}^{-1}$ and $100 \times 10^{-3} \text{ mol.s}^{-1}$. Corresponding H_2 and CO_2 permeance for the feed flowrate under mentioned condition is plotted on Figure 5.12. The flux of H_2 and CO_2 increases with increasing feed gas flowrate, this translate into increase in permeance of H_2 and CO_2 and a decrease in ideal selectivity of the gases with increasing feed gas flowrate. The ratio of H_2 (kinetic diameter: 0.27 nm) flux through the sodalite membrane is much higher in comparison to CO_2 (kinetic diameter: 0.33 nm) flux, thus, the molecular sieving effect of sodalite (cage dimension: 0.27 nm) could be responsible for the difference in flux ratio between H_2 and CO_2 . In addition, as the feed gas flowrate increases, adsorption-diffusion mechanism could sufficiently characterize the gases (H_2 and

CO₂) behavior within the sodalite membrane during the gas permeation experiments. However, H₂ flux witnessed an anomaly at 10 x 10⁻³ mol.s⁻¹, this could be due to experimental error / system malfunctioning while obtaining the results (Figure 5.11). It is expected that H₂ permeance through sodalite / ceramic membrane will be higher due to smaller H₂ kinetic molecule diameter (0.27 nm) in comparison with 0.33 nm kinetic diameter of CO₂, also, the molecular sieving effect of sodalite, with a cage dimension of 0.26 nm should lead to higher permeance of H₂ than CO₂

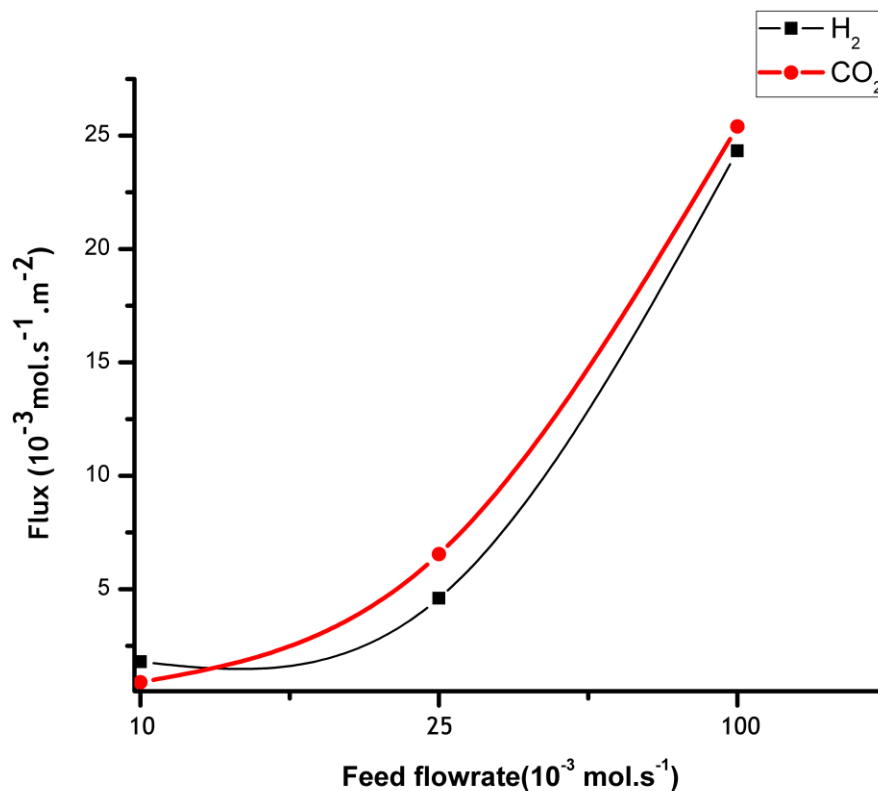


Figure 5.10: Flux as a function of feed flowrate on membrane obtained by the two-stage pore-plugging synthesis.

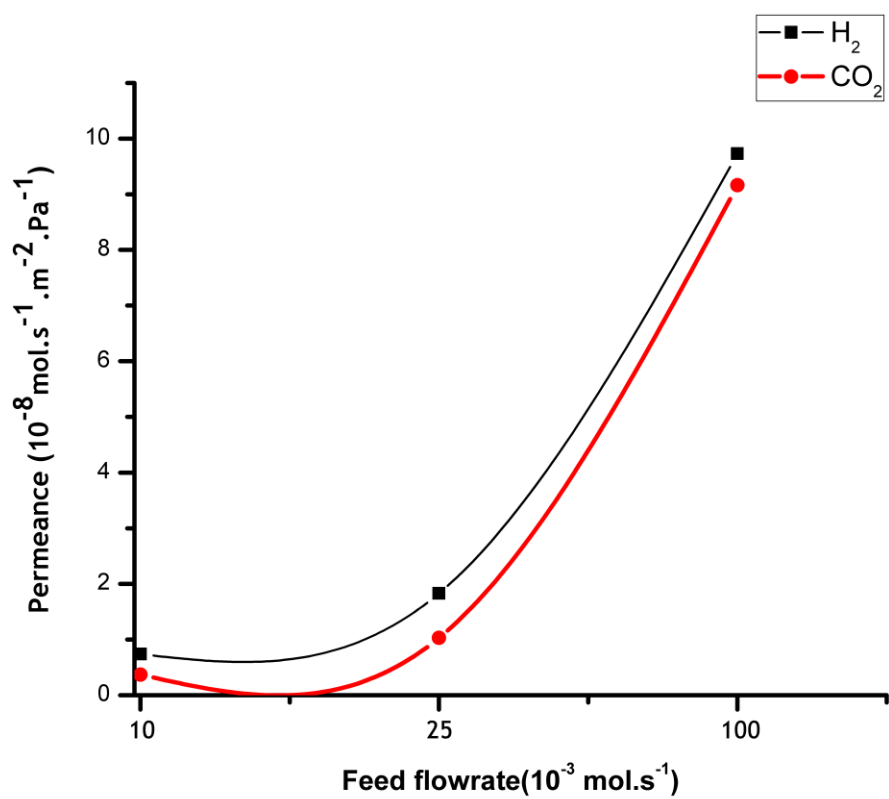


Figure 5.11: Permeance as a function of feed flowrate on the membrane obtained by two-stage pore-plugging synthesis.

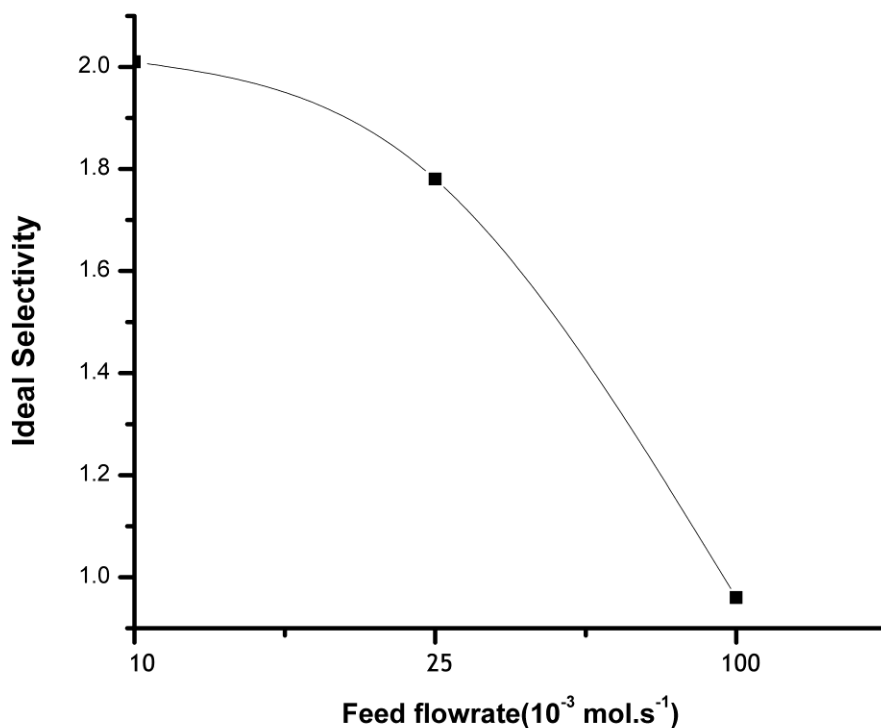


Figure 5.12: Ideal selectivity as a function of feed flowrate on the membrane obtained by two-stage pore-plugging synthesis.

5.6 Separation performance

In the present work, the nanocomposite sodalite / ceramic membranes obtained by two-stage synthesis were evaluated for H_2 and CO_2 gas separation. The membrane synthesized via two-stage shows tremendous improvement over one-stage synthesized membrane with improved selectivity but low permeance. However the two-stage synthesized nanocomposite sodalite / ceramic membrane, which is selective to hydrogen with ideal selectivity of 6.5, is not good enough for industrial application. Effects of operating variables such as feed flowrate, temperature and pressure were conducted. Further research should be conducted to evaluate the performance of the sodalite/ceramic membrane using a mixed gas mixture. In addition, separation of gas mixture (H_2/CO_2) should be conducted to evaluate the performance of the sodalite / ceramic membrane at pre-combustion carbon dioxide

capture conditions. Lastly, the effects of impurities such as H_2S and H_2O should be investigated to evaluate the operational stability of the nanocomposite sodalite ceramic membranes.

Chapter Six

Conclusions and Recommendations

6 Conclusions

Globally, energy demand and supply has increased exponentially as a result of increasing population and economic growth. Conventionally, fossil fuel (coal) is the main feed stock in energy generation and its combustion generate CO₂, a major GHG responsible for global warming that results in climate change. Recently, there is growing concern for the mitigation of anthropogenic CO₂ from reaching the atmosphere. Among the available technology for mitigating the effects of global warming includes absorption of the GHG. Absorption is energy inefficient with high operating cost. On this note, this work aimed to develop an alternative CO₂ capture technology via membrane technology. Membrane technology is a promising alternative to absorption system. According to the objective set out in Chapter 1 of this dissertation, the following under-listed conclusions could be drawn from this study:

1. Successful synthesis of nanocomposite sodalite supported on α -Al₂O₃ has been achieved with high degree of reproducibility. The membranes were successfully synthesized via one and two-stage synthesis. The multi-stage synthesis improved the quality of the membranes tremendously, showing a fully plugged porous substrate and improved separation performance.
2. The quality of the synthesized membranes were evaluated using static and dynamic characterization techniques such as SEM, XRD and BDQT. The SEM images confirmed the growth of sodalite crystals with the porous support both in the one and two-stage synthesis. The SEM image taken after the two-stage membrane shows that the three regions of the support were fully grown with sodalite crystals. XRD patterns obtained confirm that truly sodalite were synthesized. Dynamic characterization using the BDQT showed that the two-stage synthesized membrane has a better quality with fewer or no defects.
3. Gas separation measurement carried out using H₂ and CO₂, indicated that the membrane is highly selective towards H₂. The two-stage synthesized membrane with permeance of H₂ and CO₂ were $7.37 \times 10^{-8} \text{ mol.s}^{-1}.\text{m}^{-2}.\text{Pa}^{-1}$

and $1.14 \times 10^{-8} \text{ mol.s}^{-1}.\text{m}^{-2}.\text{Pa}^{-1}$, respectively and selectivity of 6.5. In addition, the activation energy of sodalite membrane reported in this work is in close agreement with reported activation energies for other zeolite membranes (NaA zeolite membrane). Moreover, the experimental results obtained from the gas separation experiment were well fitted and described by a deduced expression obtained from the Maxwell-Stefan model.

6.1 Recommendations

- The membrane synthesis should be optimized to improve on the membrane quality. Synthesis optimization could simplify the synthesis procedure, enhance the quality of the membrane and also reduce the synthesis time. Optimization of the composition of the precursor solution, the support pore size and interruption time during pore-plugging hydrothermal synthesis could improve the membrane quality.
- The separation performance of the nanocomposite sodalite membrane should be evaluated for gas mixture separation such as CO, CO₂, H₂ and H₂O (main gas components in pre-combustion carbon capture) during precombustion CO₂ capture and at pre-combustion CO₂ capture conditions. In addition, effects of impurities such as sulphur and particulate matters on the sodalite membrane, common impurities in pre-combustion capture, should be conducted.
- The operational long-term stability of nanocomposite sodalite membrane should be evaluated under real operating conditions such as pre-combustion carbon capture conditions and water-gas shift reaction. Sodalite membrane long-term thermal stability and operational stability are required for its industrial acceptance and application.
- It is recommended that the synthesis be carried out using hollow fibre as membrane support in order to increase the membrane flux. For example, MFI nanocomposite membrane prepared via pore-plugging hydrothermal synthesis has improved flux of about 30 % than the conventional thin-film MFI

membrane (Daramola et al., 2010). Moreover, the use of hollow fibre would enhance the surface-to-volume ratio. In addition, hollow fibres can be made into fibre bundles, which would result to reduction both in size and cost when implemented in industrial processes.

- Techno-economic feasibility and scale-up studies should be conducted. The studies are essential in other to unravel the competitive advantages of nanocomposite sodalite membranes over the conventional technologies. Today, most research on sodalite membranes are still within the laboratory scale; therefore, there is need for scale-up studies on nanocomposite sodalite membrane in gas separation applications in other to evaluate the competitiveness of the membrane with existing membrane technology and also fast-track commercialization of sodalite membrane in gas separation applications.

References

- Abas, N., Kalair, A., Khan, N., 2015. Review of fossil fuels and future energy technologies. *Futures* 69, 31–49.
- Akhtar, F., Sjöberg, E., Korelskiy, D., Rayson, M., Hedlund, J., Bergström, L., 2015. Preparation of graded silicalite-1 substrates for all-zeolite membranes with excellent CO₂/H₂ separation performance. *J. Membr. Sci.* 493, 206–211.
- Algieri, C., Bernardo, P., Golemme, G., Barbieri, G., Drioli, E., 2003. Permeation properties of a thin silicalite-1 (MFI) membrane. *J. Membr. Sci.* 222, 181–190.
- Alshebani, A., Pera-Titus, M., Landrison, E., Schiestel, T., Miachon, S., Dalmon, J.-A., 2008. Nanocomposite MFI – Ceramic hollow fibres: Prospects for CO₂ separation. *Microporous Mesoporous Mater.*, 4th International Zeolite Membrane Meeting 115, 197–205.
- Amponsah, N.Y., Troldborg, M., Kington, B., Aalders, I., Hough, R.L., 2014. Greenhouse gas emissions from renewable energy sources: A review of lifecycle considerations. *Renew. Sustain. Energy Rev.* 39, 461–475.
- An Overview of Our Changing Environment, 2005. , Geo Year Book. Interprint Ltd. Malta, Nairobi, Kenya.
- Aoki, K., Kusakabe, K., Morooka, S., 2000. Separation of gases with an A-type zeolite membrane. *Ind. Eng. Chem. Res.* 39, 2245–2251.
- Armor, J.N., 1998. Applications of catalytic inorganic membrane reactors to refinery products. *J. Membr. Sci.* 147, 217–233.
- Ashton, T.S., 1948. *The Industrial Revolution*. Oxford University, London, Great Britain.

- Bayati, B., Babaluo, A.A., Karimi, R., 2008. Hydrothermal synthesis of nanostructure NaA zeolite: The effect of synthesis parameters on zeolite seed size and crystallinity. *J. Eur. Ceram. Soc.* 28, 2653–2657.
- Bernardo, P., Drioli, E., Golemme, G., 2009. Membrane Gas Separation: A Review/State of the Art. *Ind. Eng. Chem. Res.* 48, 4638–4663.
- Bonilla, G., Vlachos, D.G., Tsapatsis, M., 2001. Simulations and experiments on the growth and microstructure of zeolite MFI films and membranes made by secondary growth. *Microporous Mesoporous Mater.* 42, 191–203.
- Bose, A., Das, N., Roy, S.N., Goswami, N., Kar, S., Bindal, R.C., Tewari, P.K., 2014. Synthesis, characterization and corrosion performance evaluation of DDR membrane for H₂ separation from HI decomposition reaction. *Int. J. Hydrog. Energy* 39, 12795–12803.
- Boudreau, L.C., Kuck, J.A., Tsapatsis, M., 1999. Deposition of oriented zeolite A films: in situ and secondary growth. *J. Membr. Sci.* 152, 41–59.
- Bounaceur, R., Lape, N., Roizard, D., Vallieres, C., Favre, E., 2006. Membrane processes for post-combustion carbon dioxide capture: A parametric study. *Energy* 31, 2556–2570.
- Bouzalakos, S., Maroto-Valer, M.M., 2010. 1 - Overview of carbon dioxide (CO₂) capture and storage technology, in: *Developments and Innovation in Carbon Dioxide (CO₂) Capture and Storage Technology*, Woodhead Publishing Series in Energy. Woodhead Publishing, pp. 1–24.
- Bragg, W.L., 1914. The Analysis of Crystals by the X-ray Spectrometer. *Proc. R. Soc. Lond. Math. Phys. Eng. Sci.* 89, 468–489.
- Broecks, K.P.F., van Egmond, S., van Rijnsoever, F.J., Verlinde-van den Berg, M., Hekkert, M.P., 2016. Persuasiveness, importance and novelty of arguments about Carbon Capture and Storage. *Environ. Sci. Policy* 59, 58–66.
- Bux, H., Liang, F., Li, Y., Cravillon, J., Wiebcke, M., Caro, J., 2009. Zeolitic Imidazolate Framework Membrane with Molecular Sieving Properties by Microwave-Assisted Solvothermal Synthesis. *J. Am. Chem. Soc.* 131, 16000–16001.

- Caro, J., Noack, M., 2008. Zeolite membranes – Recent developments and progress. *Microporous Mesoporous Mater.* 115, 215–233.
- Caro, J., Noack, M., Kölsch, P., Schäfer, R., 2000. Zeolite membranes – state of their development and perspective. *Microporous Mesoporous Mater.* 38, 3–24.
- Chau, C., Prevost, I., Dalmon, J.-A., Miachon, S., 2003. Process for preparing supported zeolitic membranes by temperature-controlled crystallisation. US6582495 B2.
- Chen, Qiao, Xie, Fan, Zhou, He, 2007. Self-Construction of Core–Shell and Hollow Zeolite Analcime Icositetrahedra: A Reversed Crystal Growth Process via Oriented Aggregation of Nanocrystallites and Recrystallization from Surface to Core. *J. Am. Chem. Soc.* 129, 13305–13312.
- Chiang, A.S.T., Chao, K., 2001. Membranes and films of zeolite and zeolite-like materials. *J. Phys. Chem. Solids* 62, 1899–1910.
- Chung, T.-S., Jiang, L.Y., Li, Y., Kulprathipanja, S., 2007. Mixed matrix membranes (MMMs) comprising organic polymers with dispersed inorganic fillers for gas separation. *Prog. Polym. Sci.* 32, 483–507.
- Colombo, U., 1984. A strategic view of the world energy problem. *Environ. Int.* 10, 347–358.
- Czaun, M., Goeppert, A., May, R.B., Peltier, D., Zhang, H., Prakash, G.K.S., Olah, G.A., 2013. Organoamines-grafted on nano-sized silica for carbon dioxide capture. *J. CO₂ Util.* 1, 1–7.
- Daramola, M., Aransiola, E., Ojumu, T., 2012. Potential Applications of Zeolite Membranes in Reaction Coupling Separation Processes. *Materials* 5, 2101–2136.
- Daramola, M.O., Burger, A.J., Pera-Titus, M., Giroir-Fendler, A., Lorenzen, L., Dalmon, J.-A., 2009a. Xylene Vapor Mixture Separation in Nanocomposite MFI-Alumina Tubular Membranes: Influence of Operating Variables. *Sep. Sci. Technol.* 45, 21–27.
- Daramola, M.O., Burger, A.J., Pera-Titus, M., Giroir-Fendler, A., Miachon, S., Lorenzen, L., Dalmon, J.-A., 2009b. Nanocomposite MFI–ceramic hollow

- fibre membranes via pore-plugging synthesis: Prospects for xylene isomer separation. *J. Membr. Sci.* 337, 106–112.
- Daramola, M.O., Dinat, A., Hasrod, S., 2015. Synthesis and characterization of nanocomposite hydroxy-sodalite/ceramic membrane via pore-plugging hydrothermal synthesis technique. *J. Membr. Sep. Technol.* 4, 1-7.
- Daramola, M.O., Oloye, O., Yaya, A., 2016. Nanocomposite sodalite/ceramic membrane for pre-combustion CO₂ capture: synthesis and morphological characterization. *Int. J. Coal Sci. Technol* 1-7.
- Das, J.K., Das, N., Bandyopadhyay, S., 2012. Highly selective SAPO 34 membrane on surface modified clay–alumina tubular support for H₂/CO₂ separation. *Int. J. Hydrog. Energy* 37, 10354–10364.
- Davis, S.P., Borgstedt, E.V.R., Suib, S.L., 1990. Growth of zeolite crystallites and coatings on metal surfaces. *Chem. Mater.* 2, 712–719.
- Deng, Z., Nicolas, C.-H., Daramola, M.O., Sublet, J., Schiestel, T., Burger, A.J., Guo, Y., Giroir-Fendler, A., Pera-Titus, M., 2010. Nanocomposite MFI-alumina hollow fibre membranes prepared via pore-plugging synthesis: Influence of the porous structure of hollow fibres on the gas/vapour separation performance. *J. Membr. Sci.* 364, 1–8.
- Ding, L., Yang, H., Rahimi, P., Omotoso, O., Friesen, W., Fairbridge, C., Shi, Y., Ng, S., 2010. Solid transformation of zeolite NaA to sodalite. *Microporous Mesoporous Mater.* 130, 303–308.
- Edenhofer, O., Pichs Madruga, R., Sokona, Y., United Nations Environment Programme, World Meteorological Organization, Intergovernmental Panel on Climate Change, Potsdam-Institut für Klimafolgenforschung (Eds.), 2012. Renewable energy sources and climate change mitigation: special report of the Intergovernmental Panel on Climate Change. Cambridge University Press, New York.
- EEA (Ed.), 2004. Impacts of Europe’s changing climate: an indicator-based assessment, EEA report. European Environment Agency; Office for Official

- Publications of the European Communities [distributor], Copenhagen, Denmark : Luxembourg.
- European Commission, 2007. , Limiting global climate change to 2 degrees Celsius—the way ahead for 2020 and beyond. Commission of the European Communities, Brussels.
- Gascon, J., Kapteijn, F., 2010. Metal-organic framework membranes--high potential, bright future? *Angew. Chem. Int. Ed Engl.* 49, 1530–1532.
- Gibbins, J., Chalmers, H., 2008. Carbon capture and storage. *Energy Policy, Foresight Sustainable Energy Management and the Built Environment Project* 36, 4317–4322.
- Giessler, S., Jordan, L., Diniz da Costa, J.C., Lu, G.Q. (Max., 2003. Performance of hydrophobic and hydrophilic silica membrane reactors for the water gas shift reaction. *Sep. Purif. Technol.* 32, 255–264.
- Gorgojo, P., de la Iglesia, Ó., Coronas, J., 2008. Preparation and Characterization of Zeolite Membranes, in: *Technology, B.-M.S. and (Ed.), Inorganic Membranes: Synthesis, Characterization and Applications.* Elsevier, pp. 135–175.
- Gouzinis, A., Tsapatsis, M., 1998. On the Preferred Orientation and Microstructural Manipulation of Molecular Sieve Films Prepared by Secondary Growth. *Chem. Mater.* 10, 2497–2504.
- Gu, X., Tang, Z., Dong, J., 2008. On-stream modification of MFI zeolite membranes for enhancing hydrogen separation at high temperature. *Microporous Mesoporous Mater.* 111, 441–448.
- Gu, Y., Hacıoğlu, P., Oyama, S.T., 2008. Hydrothermally stable silica–alumina composite membranes for hydrogen separation. *J. Membr. Sci.* 310, 28–37.
- Gu, Y., Ted Oyama, S., 2007. Ultrathin, hydrogen-selective silica membranes deposited on alumina-graded structures prepared from size-controlled boehmite sols. *J. Membr. Sci.* 306, 216–227.
- Guan, G., Kusakabe, K., Morooka, S., 2001. Gas Permeation Properties of Ion-Exchanged Lta-Type Zeolite Membranes. *Sep. Sci. Technol.* 36, 2233–2245.

- Guan, G., Tanaka, T., Kusakabe, K., Sotowa, K.-I., Morooka, S., 2003. Characterization of AlPO₄-type molecular sieving membranes formed on a porous α -alumina tube. *J. Membr. Sci.* 214, 191–198.
- Hammond, G.P., Spargo, J., 2014. The prospects for coal-fired power plants with carbon capture and storage: A UK perspective. *Energy Convers. Manag.* 86, 476–489.
- Hedlund, J., Sterte, J., Anthonis, M., Bons, A.-J., Carstensen, B., Corcoran, N., Cox, D., Deckman, H., De Gijnst, W., de Moor, P.-P., Lai, F., McHenry, J., Mortier, W., Reinoso, J., Peters, J., 2002. High-flux MFI membranes. *Microporous Mesoporous Mater.* 52, 179–189.
- Hong, M., Falconer, J.L., Noble, R.D., 2005. Modification of Zeolite Membranes for H₂ Separation by Catalytic Cracking of Methyl-diethoxysilane. *Ind. Eng. Chem. Res.* 44, 4035–4041.
- Hong, M., Li, S., Falconer, J.L., Noble, R.D., 2008. Hydrogen purification using a SAPO-34 membrane. *J. Membr. Sci.* 307, 277–283.
- Hosseini, S.S., Teoh, M.M., Chung, T.S., 2008. Hydrogen separation and purification in membranes of miscible polymer blends with interpenetration networks. *Polymer* 49, 1594–1603.
- Houghton, J.T., IPCC (Eds.), 2001. *Climate change 2001: the scientific basis: contribution of Working Group I to the third assessment report of the Intergovernmental Panel on Climate Change.* Cambridge University Press, Cambridge ; New York.
- Huang, A., Caro, J., 2011. Highly oriented, neutral and cation-free AlPO₄ LTA: From a seed crystal monolayer to a molecular sieve membrane. *Chem. Commun.* 47, 4201–4203.
- Huang, A., Liang, F., Steinbach, F., Gesing, T.M., Caro, J., 2010. Neutral and cation-free LTA-type aluminophosphate (AlPO₄) molecular sieve membrane with high hydrogen permselectivity. *J. Am. Chem. Soc.* 132, 2140–2141.
- Huang, A., Wang, N., Caro, J., 2012. Synthesis of multi-layer zeolite LTA membranes with enhanced gas separation performance by using 3-

- aminopropyltriethoxysilane as interlayer. *Microporous Mesoporous Mater.* 164, 294–301.
- IEA Statistics: Carbon dioxide emissions from fuel combustion (Highlights), 2015. . International Energy Agency, Paris.
- International Energy Agency; CO₂ Emissions from Fuel Combustion Highlights, 2013. . International Energy Agency, Paris, France.
- International Energy Outlook 2016 report, Energy Information Administration, Office of Energy Analysis. U.S Department of Energy, Washington, DC 20583, DOE / EIA - 0484, 2016; 290, 2016.
- IPCC, Edenhofer, O. (Eds.), 2014. Climate change 2014: mitigation of climate change: Working Group III contribution to the Fifth Assessment Report of the Intergovernmental Panel on Climate Change. Cambridge University Press, New York, NY.
- Irfan, M.F., Usman, M.R., Kusakabe, K., 2011. Coal gasification in CO₂ atmosphere and its kinetics since 1948: A brief review. *Energy* 36, 12–40.
- IZA (SOD), n.d. SOD [WWW Document]. URL http://izasc.ethz.ch/fmi/xsl/IZA-SC/ftc_fw.xml?-db=Atlas_main&-lay=fw&STC=SOD&-find (accessed 8.25.16).
- Jakobs, E., Koros, W.J., 1997. Ceramic membrane characterization via the bubble point technique. *J. Membr. Sci.* 124, 149–159.
- Jan, G., Andrew, G., Ernesta, S., 2012. Carbon Capture and Storage(CCS) : Towards a regulatory and legal regime in South Africa. Institute of Marine and Environmental Law (IMEL) and African Climate and Development Initiative (ACDI), University of Cape Town, Cape Town, Cape Town, South Africa.
- Jareman, F., Hedlund, J., Creaser, D., Sterte, J., 2004. Modelling of single gas permeation in real MFI membranes. *J. Membr. Sci.* 236, 81–89.
- Jian-Bin, H., Shao-Wu, W., Yong, L., Zong-Ci, Z., Xin-Yu, W., 2012. The Science of Global Warming. *Adv. Clim. Change Res.* 3, 174–178.

- Julbe, A., Motuzas, J., Cazevielle, F., Volle, G., Guizard, C., 2003. Synthesis of sodalite/ α -Al₂O₃ composite membranes by microwave heating. *Sep. Purif. Technol.* 32, 139–149.
- Kalantari, N., Vaezi, M.J., Yadollahi, M., Babaluo, A.A., Bayati, B., Kazemzadeh, A., 2015. Synthesis of nanostructure hydroxy sodalite composite membranes via hydrothermal method: support surface modification and synthesis method effects. *Asia-Pac. J. Chem. Eng.* 10, 45–55.
- Kanezashi, M., O'Brien-Abraham, J., Lin, Y.S., Suzuki, K., 2008. Gas permeation through DDR-type zeolite membranes at high temperatures. *AIChE J.* 54, 1478–1486.
- Kapteijn, F., Bakker, W.J.W., van de Graaf, J., Zheng, G., Poppe, J., Moulijn, J.A., 1995. Permeation and separation behaviour of a silicalite-1 membrane. *Catal. Today, Catalysis in Membrane Reactors* 25, 213–218.
- Karimi, S., Korelskiy, D., Mortazavi, Y., Khodadadi, A.A., Sardari, K., Esmaeili, M., Antzutkin, O.N., Shah, F.U., Hedlund, J., 2016. High flux acetate functionalized silica membranes based on in-situ co-condensation for CO₂/N₂ separation. *J. Membr. Sci.* 520, 574–582.
- Karimi, S., Korelskiy, D., Yu, L., Mouzon, J., Ali, K., Mortazavi, Y., Esmaeili, M., Hedlund, J., 2015. A simple method for blocking defects in zeolite membranes. *J. Membr. Sci.* 489, 270–274.
- Kazemimoghadam, M., Mohammadi, T., 2005. Separation of water/UDMH mixtures using hydroxysodalite zeolite membranes. *Desalination* 181, 1–7.
- Khajavi, S., Jansen, J.C., Kapteijn, F., 2010a. Production of ultra pure water by desalination of seawater using a hydroxy sodalite membrane. *J. Membr. Sci.* 356, 52–57.
- Khajavi, S., Jansen, J.C., Kapteijn, F., 2009. Application of hydroxy sodalite films as novel water selective membranes. *J. Membr. Sci.* 326, 153–160.
- Khajavi, S., Kapteijn, F., Jansen, J.C., 2007a. Synthesis of thin defect-free hydroxy sodalite membranes: New candidate for activated water permeation. *J. Membr. Sci.* 299, 63–72.

- Khajavi, S., Sartipi, S., Gascon, J., Jansen, J.C., Kapteijn, F., 2010b. Thermostability of hydroxy sodalite in view of membrane applications. *Microporous Mesoporous Mater.* 132, 510–517.
- Khatib, S.J., Oyama, S.T., de Souza, K.R., Noronha, F.B., 2011. Review of silica membranes for hydrogen separation prepared by chemical vapor deposition. *Membr Sci Tech* 14, 25.
- Kidd, S.W., 2013. Nuclear power – Economics and public acceptance. *Energy Strategy Rev., Nuclear Energy Today & Strategies for Tomorrow* 1, 277–281.
- Kosinov, N., Gascon, J., Kapteijn, F., Hensen, E.J.M., 2016. Recent developments in zeolite membranes for gas separation. *J. Membr. Sci.* 499, 65–79.
- Krewitt, W., Simon, S., Graus, W., Teske, S., Zervos, A., Schäfer, O., 2007. The 2°C scenario—A sustainable world energy perspective. *Energy Policy* 35, 4969–4980.
- Kundu, D., Dey, B., Naskar, M.K., Chatterjee, M., 2010. Emulsion-derived urchin-shaped hydroxy sodalite particles. *Mater. Lett.* 64, 1630–1633.
- Lassinantti, M., Hedlund, J., Sterte, J., 2000. Faujasite-type films synthesized by seeding. *Microporous Mesoporous Mater.* 38, 25–34.
- Le Page, M., 2007. News Review 2007: A dolphin dies out. *New Sci.* 196, 19.
- Lee, D., Oyama, S.T., 2002. Gas permeation characteristics of a hydrogen selective supported silica membrane. *J. Membr. Sci.* 210, 291–306.
- Lee, D.-J., Li, Q., Kim, H., Lee, K., 2012. Preparation of Ni-MOF-74 membrane for CO₂ separation by layer-by-layer seeding technique. *Microporous Mesoporous Mater.* 163, 169–177.
- Lee, S.-R., Son, Y.-H., Julbe, A., Choy, J.-H., 2006. Vacuum seeding and secondary growth route to sodalite membrane. *Thin Solid Films* 495, 92–96.
- Leung, D.Y.C., Caramanna, G., Maroto-Valer, M.M., 2014. An overview of current status of carbon dioxide capture and storage technologies. *Renew. Sustain. Energy Rev.* 39, 426–443.

- Li, Y., Liang, F., Bux, H., Yang, W., Caro, J., 2010. Zeolitic imidazolate framework ZIF-7 based molecular sieve membrane for hydrogen separation. *J. Membr. Sci.* 354, 48–54.
- Li, Y., Pera-Titus, M., Xiong, G., Yang, W., Landrison, E., Miachon, S., Dalmon, J.-A., 2008a. Nanocomposite MFI-alumina membranes via pore-plugging synthesis: Genesis of the zeolite material. *J. Membr. Sci.* 325, 973–981.
- L'Orange Seigo, S., Dohle, S., Siegrist, M., 2014. Public perception of carbon capture and storage (CCS): A review. *Renew. Sustain. Energy Rev.* 38, 848–863.
- Lovallo, M.C., Tsapatsis, M., 1996. Preferentially oriented submicron silicalite membranes. *AIChE J.* 42, 3020–3029.
- Luis, P., Van Gerven, T., Van der Bruggen, B., 2012. Recent developments in membrane-based technologies for CO₂ capture. *Prog. Energy Combust. Sci.* 38, 419–448.
- Maghsoudi, H., 2016. Defects of Zeolite Membranes: Characterization, Modification and Post-treatment Techniques. *Sep. Purif. Rev.* 45, 169–192.
- Mahajan, R., Koros, W.J., 2000. Factors Controlling Successful Formation of Mixed-Matrix Gas Separation Materials. *Ind. Eng. Chem. Res.* 39, 2692–2696.
- Manickam, S.S., Gelb, J., McCutcheon, J.R., 2014. Pore structure characterization of asymmetric membranes: Non-destructive characterization of porosity and tortuosity. *J. Membr. Sci.* 454, 549–554.
- Matsufuji, T., Nishiyama, N., Matsukata, M., Ueyama, K., 2000. Separation of butane and xylene isomers with MFI-type zeolitic membrane synthesized by a vapor-phase transport method. *J. Membr. Sci.* 178, 25–34.
- McCusker, L.B., Liebau, F., Engelhardt, G., 2001. Nomenclature of structural and compositional characteristics of ordered microporous and mesoporous materials with inorganic hosts(IUPAC Recommendations 2001). *Pure Appl. Chem.* 73, 381–394.
- McCusker, L.B., Olson, D.H., Baerlocher, C., 2007. Atlas of Zeolite Framework Types, *Atlas of Zeolite Framework Types*.
- McHale, J., 1969. World energy resources in the future. *Futures* 1, 4–13.

- McMullan, D., 1995. Scanning electron microscopy 1928–1965. *Scanning* 17, 175–185.
- Merkel, T.C., Lin, H., Wei, X., Baker, R., 2010. Power plant post-combustion carbon dioxide capture: An opportunity for membranes. *J. Membr. Sci.* 359, 126–139.
- Metz, B., IPCC (Eds.), 2005. IPCC special report on carbon dioxide capture and storage. Cambridge University Press, for the Intergovernmental Panel on Climate Change, Cambridge.
- Miachon, S., Ciavarella, P., Van Dyk, L., Kumakiri, I., Fiaty, K., Schuurman, Y., Dalmon, J.-A., 2007. Nanocomposite MFI-alumina membranes via pore-plugging synthesis: specific transport and separation properties. *J. Membr. Sci.* 298, 71–79.
- Miachon, S., Landrison, E., Aouine, M., Sun, Y., Kumakiri, I., Li, Y., Prokopová, O.P., Guilhaume, N., Giroir-Fendler, A., Mozzanega, H., Dalmon, J.-A., 2006. Nanocomposite MFI-alumina membranes via pore-plugging synthesis: Preparation and morphological characterisation. *J. Membr. Sci.* 281, 228–238.
- Michalkiewicz, B., Koren, Z.C., 2015. Zeolite membranes for hydrogen production from natural gas: state of the art. *J. Porous Mater.* 22, 635–646.
- Moon, J.-H., Bae, J.-H., Bae, Y.-S., Chung, J.-T., Lee, C.-H., 2008. Hydrogen separation from reforming gas using organic templating silica/alumina composite membrane. *J. Membr. Sci.* 318, 45–55.
- Morigami, Y., Kondo, M., Abe, J., Kita, H., Okamoto, K., 2001. The first large-scale pervaporation plant using tubular-type module with zeolite NaA membrane. *Sep. Purif. Technol.* 25, 251–260.
- Moteki, T., Chaikittisilp, W., Shimojima, A., Okubo, T., 2008. Silica Sodalite without Occluded Organic Matters by Topotactic Conversion of Lamellar Precursor. *J. Am. Chem. Soc.* 130, 15780–15781.
- Naskar, M.K., Kundu, D., Chatterjee, M., 2011. Coral-like hydroxy sodalite particles from rice husk ash as silica source. *Mater. Lett.* 65, 3408–3410.

- Olajire, A.A., 2010. CO₂ capture and separation technologies for end-of-pipe applications – A review. *Energy* 35, 2610–2628.
- Pachtova, O., 2003. Dynamic desorption of adsorbing species under cross membrane pressure difference: a new defect characterisation approach in zeolite membranes. *J. Membr. Sci.* 226, 101–110.
- Peinador, R.I., Calvo, J.I., Prádanos, P., Palacio, L., Hernández, A., 2010. Characterisation of polymeric UF membranes by liquid-liquid displacement porosimetry. *J. Membr. Sci.* 348, 238–244.
- Petrov, I., Michalev, T., 2012. Synthesis of Zeolite A: A Review.
- Pires, J.C.M., Martins, F.G., Alvim-Ferraz, M.C.M., Simões, M., 2011. Recent developments on carbon capture and storage: An overview. *Chem. Eng. Res. Des.* 89, 1446–1460.
- Poshusta, J.C., Noble, R.D., Falconer, J.L., 1999. Temperature and pressure effects on CO₂ and CH₄ permeation through MFI zeolite membranes. *J. Membr. Sci.* 160, 115–125.
- Rezakazemi, M., Shahidi, K., Mohammadi, T., 2012. Hydrogen separation and purification using crosslinkable PDMS/zeolite A nanoparticles mixed matrix membranes. *Int. J. Hydrog. Energy* 37, 14576–14589.
- Rogner, H.-H., 2013. World outlook for nuclear power. *Energy Strategy Rev., Nuclear Energy Today & Strategies for Tomorrow* 1, 291–295.
- Rohde, M.P., Schaub, G., Khajavi, S., Jansen, J.C., Kapteijn, F., 2008. Fischer–Tropsch synthesis with in situ H₂O removal – Directions of membrane development. *Microporous Mesoporous Mater., 4th International Zeolite Membrane Meeting* 115, 123–136.
- Saidi, K., Hammami, S., 2015. The impact of CO₂ emissions and economic growth on energy consumption in 58 countries. *Energy Rep.* 1, 62–70.
- Salame, C., Aillerie, M., Papageorgas, P., Mohtasham, J., 2015. The International Conference on Technologies and Materials for Renewable Energy, Environment and Sustainability –TMREES15Review Article-Renewable Energies. *Energy Procedia* 74, 1289–1297.

- Scholes, C.A., Smith, K.H., Kentish, S.E., Stevens, G.W., 2010. CO₂ capture from pre-combustion processes—Strategies for membrane gas separation. *Int. J. Greenh. Gas Control* 4, 739–755.
- Scott, D.S., 2013. Nuclear energy, climate, hydricity, radiation and foolish mythologies. *Energy Strategy Rev., Nuclear Energy Today & Strategies for Tomorrow* 1, 272–276.
- Suzuki, H., 1987. Composite membrane having a surface layer of an ultrathin film of cage-shaped zeolite and processes for production thereof. US4699892 A.
- Tomita, T., Nakayama, K., Sakai, H., 2004. Gas separation characteristics of DDR type zeolite membrane. *Microporous Mesoporous Mater.* 68, 71–75.
- Tsuru, T., Hino, T., Yoshioka, T., Asaeda, M., 2001. Permporometry characterization of microporous ceramic membranes. *J. Membr. Sci.* 186, 257–265.
- Tsuru, T., Takata, Y., Kondo, H., Hirano, F., Yoshioka, T., Asaeda, M., 2003. Characterization of sol–gel derived membranes and zeolite membranes by nanoporometry. *Sep. Purif. Technol., Seventh International Conference on Inorganic Membranes* 32, 23–27.
- Tuan, V.A., Li, S., Noble, R.D., Falconer, J.L., 2001. Preparation and pervaporation properties of a MEL-type zeolite membrane. *Chem. Commun.* 583–584.
- Varela-Gandía, F.J., Berenguer-Murcia, Á., Lozano-Castelló, D., Cazorla-Amorós, D., 2011. Zeolite A/carbon membranes for H₂ purification from a simulated gas reformer mixture. *J. Membr. Sci.* 378, 407–414.
- Varela-Gandía, F.J., Berenguer-Murcia, A., Lozano-Castelló, D., Cazorla-Amorós, D., 2010. Hydrogen purification for PEM fuel cells using membranes prepared by ion-exchange of Na-LTA/carbon membranes. *J. Membr. Sci.* 351, 123–130.
- Wang, H., Lin, Y.S., 2012. Synthesis and modification of ZSM-5/silicalite bilayer membrane with improved hydrogen separation performance. *J. Membr. Sci.* 396, 128–137.

- Wang, N., Liu, Y., Huang, A., Caro, J., 2015. Hydrophilic SOD and LTA membranes for membrane-supported methanol, dimethylether and dimethylcarbonate synthesis. *Microporous Mesoporous Mater.* 207, 33–38.
- Wang, N., Mundstock, A., Liu, Y., Huang, A., Caro, J., 2015. Amine-modified Mg-MOF-74/CPO-27-Mg membrane with enhanced H₂/CO₂ separation. *Chem. Eng. Sci., Metal-Organic Frameworks for Emerging Chemical Technologies* 124, 27–36.
- Wirawan, S.K., Creaser, D., Lindmark, J., Hedlund, J., Bendiyasa, I.M., Sediawan, W.B., 2011. H₂/CO₂ permeation through a silicalite-1 composite membrane. *J. Membr. Sci.* 375, 313–322.
- Xu, W., Dong, J., Li, J., Li, J., Wu, F., 1990. A novel method for the preparation of zeolite ZSM-5. *J. Chem. Soc. Chem. Commun.* 755–756.
- Xu, X., Bao, Y., Song, C., Yang, W., Liu, J., Lin, L., 2004. Microwave-assisted hydrothermal synthesis of hydroxy-sodalite zeolite membrane. *Microporous Mesoporous Mater.* 75, 173–181.
- Yang, H., Xu, Z., Fan, M., Gupta, R., Slimane, R.B., Bland, A.E., Wright, I., 2008. Progress in carbon dioxide separation and capture: A review. *J. Environ. Sci.* 20, 14–27.
- Yave, W., Car, A., Wind, J., Peinemann, K.-V., 2010. Nanometric thin film membranes manufactured on square meter scale: ultra-thin films for CO₂ capture. *Nanotechnology* 21, 395301.
- Zheng, Z., Gulians, V.V., Misture, S., 2008. Sodalites as ultramicroporous frameworks for hydrogen separation at elevated temperatures: thermal stability, template removal, and hydrogen accessibility. *J. Porous Mater.* 16, 343–347.

Appendix

Appendix A: Experimental equipment.



Figure A.0.1: Picture of EcoTherm® oven used for membrane synthesis (Picture not to scale).

Appendix B: XRD data conversion

For analysis XRD characterization was done using a cobalt XRD radiation with a wavelength of 1.78897 angstroms. Results obtained from this characterization had to be compared with that from literature. In literature, XRD characterization was done using copper radiation with a wavelength of 1.54056 angstroms. For the sake of comparison, a ratio was calculated in order to normalize the two different wavelengths. Calculations were done as follow:

Cobalt XRD \longrightarrow Copper XRD

Wavelength=1.78897 angstroms
angstroms

Wavelength=1.54056

Ratio of cobalt wavelength to copper wavelength

$$\text{Ratio} = \frac{1.78897 \text{ angstroms}}{1.54056 \text{ angstroms}} = 1.16124$$

This ratio was then used to normalize the wavelength of XRD cobalt data with copper wavelength by dividing cobalt raw XRD data by this ratio.

Appendix C: Procedures for operating the membrane gas separation system

Five stages are involved to successfully operate the membrane gas separation system, which are highlighted below.

Warming up of Mass Flow Meter (MFM) and Mass Flow Controller (MFC)

1. Close all forward pressure regulator (completely counter clockwise)
2. Open valves (V5, V6 & V8) connecting lines to the mixer
3. Set valve V9 to the back pressure regulator line
4. Set valve V10 to the feed line
5. Set valve V11 to the back pressure line
6. Close valve V12 and V13
7. Ensure that the two back pressure regulators are open
8. Turn the power on both 19" instrument racks to ON
9. Set the electro-pneumatic valves control to Manual
10. Set the electro-pneumatic valve selection switch to OFF.
11. Switch the power to the MFCs and MFM ON
12. Allow 10-15 minutes for the instruments to warm up and stabilize.

Setting the gas lines pressure and flow

1. Open laboratory main gas supplies and set to desired pressures
2. Open valves (V1, V2 & V4)
3. Adjust the individual gas inlet pressures to the desired pressure by adjusting the forward pressure regulators.
4. Adjust the mass flow control by turning carefully the right hand screw of the MFC.

Loading and preparing the membrane module

1. Carefully place the membrane in the module, ensuring the membrane aligns with the module
2. Fix the graphite O-ring at both ends of the membrane module
3. Carefully screw in both ends of the membrane to ensure it is gas-tight.
4. Position the membrane module in the oven and ensure that gas lines are leak proof.

Setting the gas lines back pressures and reactor / furnace temperature

1. Set valve V9 to the reactor
2. Set valve V10 to Retentate
3. Set valve V11 to Permeate
4. Adjust the pressure in the feed gas line by turning the GO back pressure regulator clockwise
5. Repeat the above for the sweep gas line.

Analyzing the gas mixtures by GC, with manual or NI DAC & LabVIEW Control

For the feed gas mixture

1. Switch valve V9 to the back pressure regulator
2. Switch valve V10 to the feed position
3. Switch the gas line selector switch to FEED/RETENTATE
4. Trap the gas from the GC line and analyze with the GC until statistically repeatable results are obtained.

For the permeate gas

1. Switch valve V9 to the reactor
2. Switch valve V10 to the retentate position
3. Switch the gas line selector switch to FEED/RETENTATE
4. Trap the gas from the GC line and analyze with the GC until statistically repeatable results are obtained.
5. Repeat the above till the desired results are obtained.

Appendix D: Procedures for running JAD X-tract Extreme Version 1.4.5

Double click JAD X-tract extreme to launch application

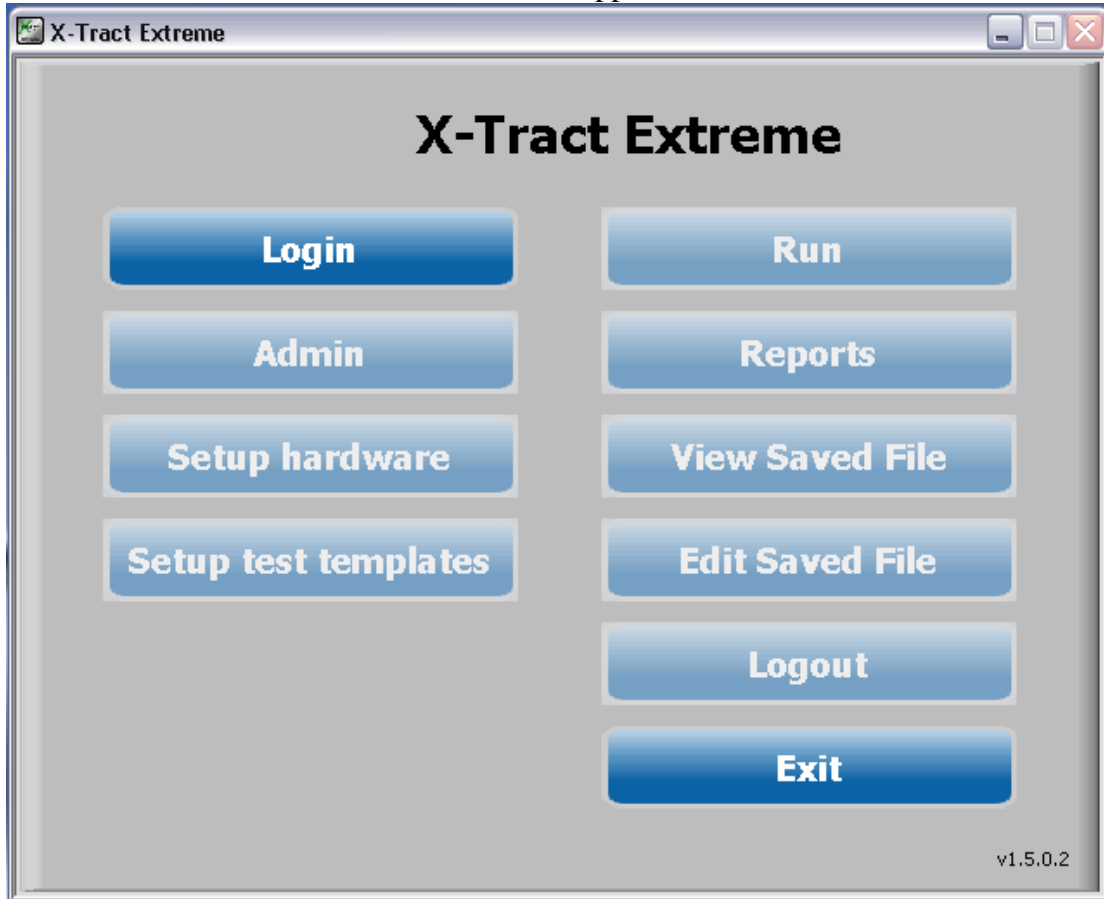


Figure D1: Login GUI for JAD X-tract extreme version 1.4.5

Select Login and provide the login credentials

Job information; experimental name and title are insert in next GUI

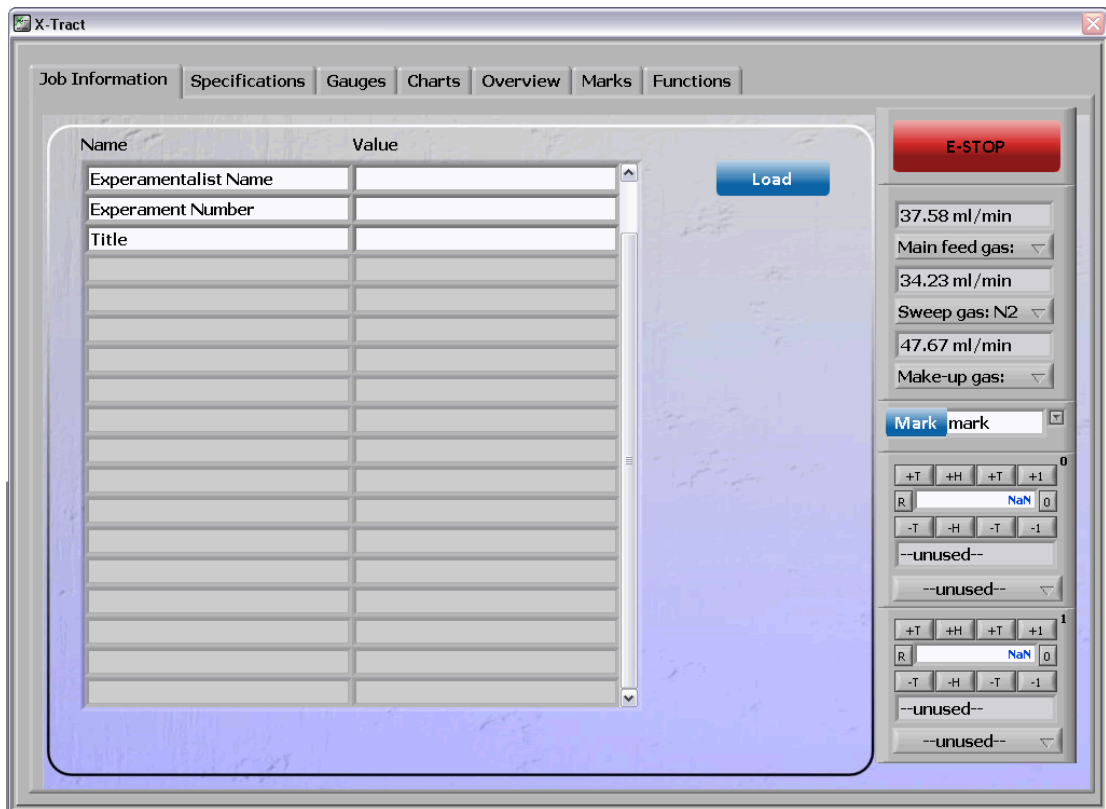


Figure D2: GUI for input of experimental name and title

Experimental number is generated by the system and is set to auto-increment.

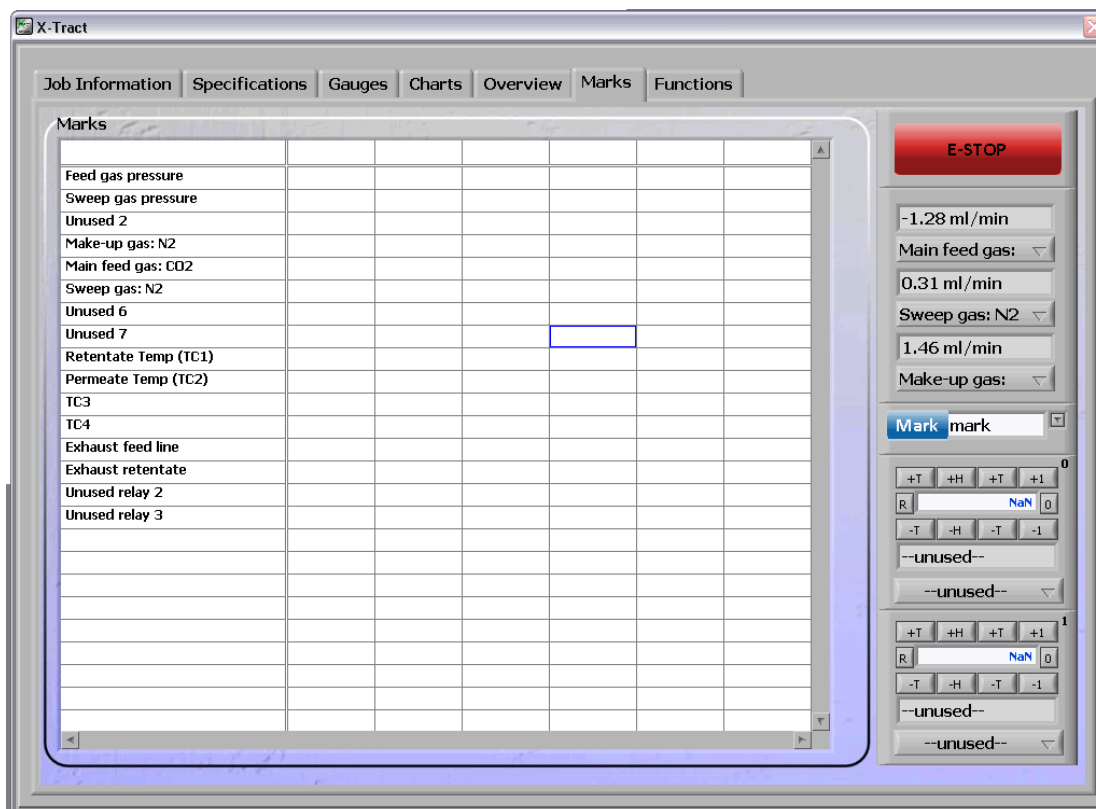


Figure D4: GUI displaying result obtained from National Instrument data acquisition

The GUI displayed all data collected via the NI data acquisition protocol. Sensors attached to the membrane gas separation system send signals to the NI. The sensors detect individual signals, the NI converts the signal to electrical signal which are sent to the JAD X-tract extreme via RJ 45 port. To mark data on the JAD X-tract extreme, the keyboard spacebar is hit.

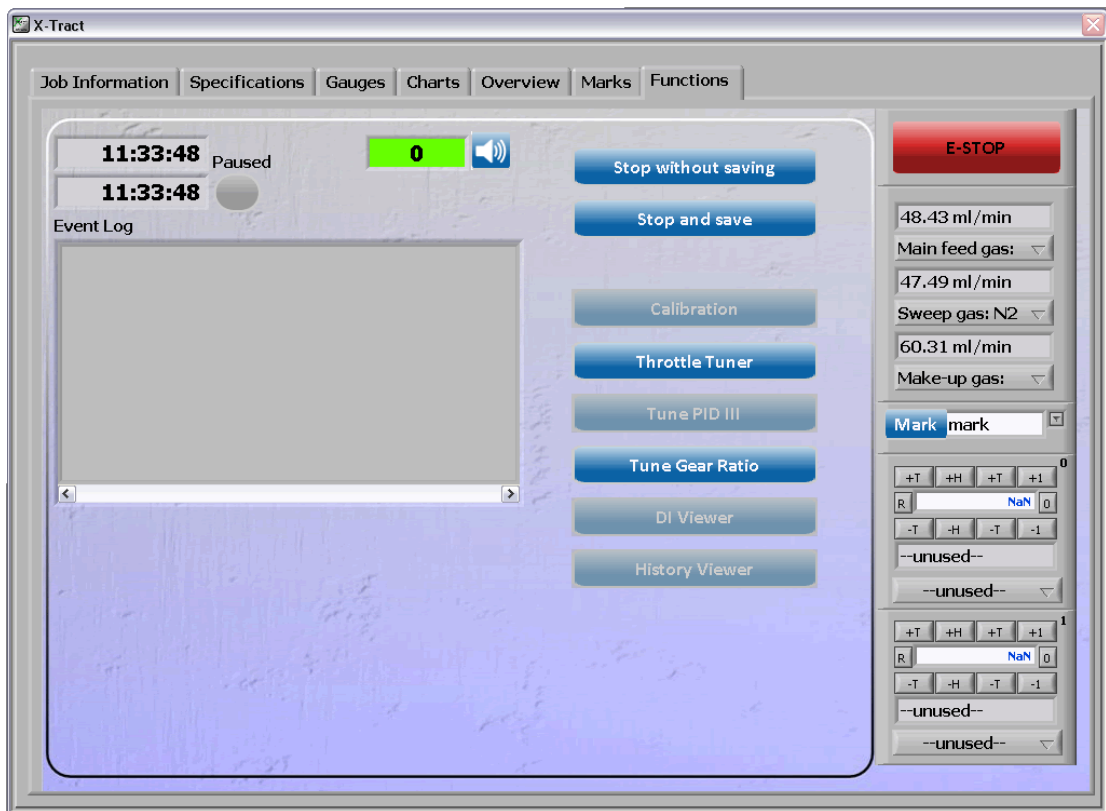


Figure D5: GUI showing stop and save icons.

After completion of data acquisition, the stop and save icon is used. The JAD X-tract extreme automatically creates a report file which could be converted to most readable file processing format.

Appendix E: Data obtained from JAD X-tract Extreme

Table E1: Hydrogen permeation at 373 K

Date	20/05/2014	Membrane Description	2 Layer PPH SOD Membrane	? ml/min
Experiment Number	3039802	Membrane Conditioning	Na	1 bar
Experimentalist Name	Temperature Variation @ 100	Feed Gas Mixture	6-7 mL/min	100 °C
Title				

Recorded Values

Time	Main feed gas: CO2 ml/min	Sweep gas: N2 ml/min	Make-up gas: N2 ml/min	Feed gas pressure kPa	Feed TC1 °C	Temp °C	Permeate TC2 °C	temp °C
9/6/2016 11:36	-1.5	0.8	0.4		2	26.1		24.9
9/6/2016 11:37	41	1.8	45.8		2	26.1		24.9
9/6/2016 11:38	-1.5	2.8	0.4		2	26.3		24.9
9/6/2016 11:39	-1.5	3.8	0.4		2	26.6		24.9
9/6/2016 11:40	41.2	4.8	46		2	26.8		25
9/6/2016 11:41	-1.5	5.8	0.1		2	27		25
9/6/2016 11:42	48.8	6.8	53.9		2	27.2		25.1
9/6/2016 11:43	-1.7	7.8	0.1		2	27.5		25.1
9/6/2016 11:44	-1.4	8.8	0.4		2	27.7		25.1
9/6/2016 11:45	-1.6	9.8	0.3		2	27.8		25.2
9/6/2016 11:46	46.8	10.8	51.5		2	28		25.1

Table E2: Hydrogen permeation at 423 K

Date	20/05/2014	Membrane Description	2 Layer PPH SOD Membrane	Temp Variation @ 200	Sweep Gas	? ml/min				
Experiment Number	3039802	Membrane Conditioning	Na	Sweep Gas Pressure	1 bar					
Experimentalist Name	Temperature Variation @ 150	Feed Gas Mixture	Na	Reactor Set Temperature	150 °C					
Title	Na									
Recorded Values	Main CO2	feed gas:	Sweep gas: N2	Make-up gas: N2	Feed gas pressure	Sweep pressure	gas	Retentate Temp TC1	Permeate TC2	temp
Time	ml/min		ml/min	ml/min	kPa	kPa		°C	°C	
9/6/2016 13:19		-1.5	0.8	0.7	2		1	31.9		25.9
9/6/2016 13:20		6.3	1.8	7.7	2		1	32.1		26
9/6/2016 13:21		-1.3	2.8	0.5	2		1	32.3		26
9/6/2016 13:22		-1.5	3.8	0.3	2		1	32.7		26
9/6/2016 13:23		-1.7	4.8	0.4	2		1	33		26
9/6/2016 13:24		-1.6	5.8	0.2	2		1	33.3		26.1
9/6/2016 13:24		14	6.8	13.8	2		1	33.4		26.1
9/6/2016 13:25		15.1	7.8	16.2	2		1	33.7		26.1
9/6/2016 13:26		-1.6	8.8	0.4	2		1	34		26.1
9/6/2016 13:27		40.2	9.8	42.8	2		1	34.4		26.1
9/6/2016 13:28		50.3	10.8	53.8	2		1	34.6		26.2

9/6/2016 13:29	-1.7	11.8	0.4	2	1	35	26.2
9/6/2016 13:30	-1.7	12.8	0.1	2	1	35.2	26.2

Table E3: Hydrogen permeation at 473 K

Date	20/05/2014	Membrane Description	2 Layer PPH SOD Membrane	Temp Variation	@	Sweep Gas	? ml/min
Experiment Number	3039802	Membrane Conditioning		Na		Sweep Gas Pressure	? bar
Experimentalist Name	Temperature Variation @ 200	Feed Gas Mixture		? mL/min		Reactor Set Temperature	200 °C
Title	Na						

Recorded Values

Time	Main feed gas: CO2 ml/min	Sweep gas: N2 ml/min	Make-up gas: N2 ml/min	Feed pressure kPa	gas	Sweep gas pressure kPa	Retentate TC1 °C	Temp	Permeate temp TC2 °C
9/6/2016 14:07	-1.5	0.8	0.4	2	1	48.6	27.4		
9/6/2016 14:08	47.9	1.8	49.2	2	1	48.8	27.4		
9/6/2016 14:09	-1.6	2.8	0.5	2	1	49.2	27.5		
9/6/2016 14:10	45.5	3.8	48.2	2	1	49.4	27.5		
9/6/2016 14:11	9.7	4.8	9.2	2	1	49.8	27.5		
9/6/2016 14:12	13.4	5.8	11.3	2	1	50	27.5		
9/6/2016 14:13	36.2	6.8	39.9	2	1	50.3	27.5		
9/6/2016 14:14	-1.4	7.8	0.4	2	1	50.6	27.5		
9/6/2016 14:15	-1.5	8.8	0.1	2	1	50.8	27.5		
9/6/2016 14:16	-1	9.8	0.5	2	1	51.2	27.5		
9/6/2016 14:17	-1.2	10.8	0.5	2	1	51.4	27.5		
9/6/2016 14:18	0	11.8	0.6	2	1	51.6	27.5		
9/6/2016 14:19	5.6	12.8	4	2	1	51.9	27.5		

9/6/2016 14:20	-1.5	0.3	0.4	2	1	52.1	27.5
9/6/2016 14:21	27.6	28.7	27.8	2	1	52.3	27.5
9/6/2016 14:22	-1.7	0.2	0	2	1	52.5	27.5
9/6/2016 14:23	-1.5	0.4	0.5	2	1	52.7	27.5

Table E4: Carbon Dioxide permeation at 373 K

Date	20/05/2014	Membrane Description	2 Layer PPH SOD Membrane	Sweep Gas	? ml/min
Experiment Number	3039802	Membrane Conditioning	Na	Sweep Gas Pressure	? bar
Experimentalist Name	CO2 Perm 100 C	Feed Gas Mixture	? mL/min	Reactor Temperature	Set 100 °C
Title	Na				

Recorded Values

Time	Main feed gas: CO2 ml/min	Sweep gas: N2 ml/min	Make-up gas: N2 ml/min	Feed gas pressure kPa	Sweep gas pressure kPa	Retentate Temp TC1 °C	Permeate temp TC2 °C
9/6/2016 19:24	50.9	0.8	47.7	2	0.8	38.6	27.4
9/6/2016 19:30	-1.5	1.8	0.4	2	0.8	38.8	27.4
9/6/2016 19:36	-1.5	2.8	0.5	2	0.8	38.8	27.5
9/6/2016 19:40	-1.5	3.8	0.3	2	0.8	38.8	27.5
9/6/2016 19:46	11.5	4.8	0.6	2	0.8	38.9	27.4

Table E5: Carbon Dioxide permeation at 423 K

Date	20/05/2014	Membrane Description	2 Layer PPH SOD Membrane	Sweep Gas	? ml/min
Experiment Number	3039802	Membrane Conditioning	Na	Sweep Gas Pressure	? bar
Experimentalist Name	Temperature Variation @ 150	Feed Gas Mixture	? mL/min	Reactor Set Temperature	150 °C
Title	Na				

Recorded Values

Time	Main feed gas: CO2 ml/min	Sweep gas: N2 ml/min	Make-up gas: N2 ml/min	Feed pressure kPa	gas	Sweep pressure kPa	gas	Retentate Temp TC1 °C	Temp	Permeate temp TC2 °C
9/6/2016 19:56	-1.6	0.8	0.2	2.3		0.9		39.1		27.5
9/6/2016 20:00	6.9	1.8	0.4	2.3		0.9		39.7		27.5
9/6/2016 20:04	-1.6	2.8	0.2	2.3		0.9		40.2		27.5

Table E6: Carbon Dioxide permeation at 473 K

Date	20/05/2014	Membrane Description	2 Layer PPH SOD Membrane	Sweep Gas	? ml/min
Experament Number	3039802	Membrane Conditioning	Na	Sweep Gas Pressure	? bar
Experamentalist Name	Variation @ 200	Feed Mixture	Gas	Reactor Temperature	Set 200 °C
Title	Na				

Recorded Values

Time	Main feed gas: CO2 ml/min	Sweep gas: N2 ml/min	Make-up gas: N2 ml/min	Feed gas pressure kPa	Sweep gas pressure kPa	Retentate Temp TC1 °C	Permeate temp TC2 °C
9/6/2016 20:49	-1.5	0.8	0.4	2.3	0.9	50.4	29.1
9/6/2016 20:55	38.6	1.8	37.1	2.3	0.9	51.1	29.2
9/6/2016 20:59	46.3	2.8	42.7	2.3	0.9	51.6	29.3

Table E7: Carbon dioxide permeation at 1.2 bar

Date	20/05/2014	Membrane Description	2 Layer PPH SOD Membrane	Sweep Gas	? ml/min
Experiment Number	3039802	Membrane Conditioning	1 Bar	Sweep Gas Pressure	? bar
Experimentalist Name	Variation @ 1.2 bar	Feed Mixture	Gas	Reactor Temperature	Set ? °C
Title	Na				

Recorded Values

Time	Main feed gas: CO2 ml/min	Sweep gas: N2 ml/min	Make-up gas: N2 ml/min	Feed pressure kPa	gas pressure kPa	Sweep gas pressure kPa	Retentate Temp TC1 °C	Permeate temp TC2 °C
9/6/2016 16:48	36.7	0.8	36.3		2.3	0.7	28.1	26.1
9/6/2016 16:50	32	1.8	27.1		2.3	0.7	28.1	26.1
9/6/2016 16:52	46.7	2.8	36.8		2.3	0.7	28.1	26.1
9/6/2016 16:54	38.3	3.8	33.4		2.3	0.7	28.1	26.1
9/6/2016 16:56	12.7	4.8	0.5		2.3	0.7	28.1	26.1
9/6/2016 16:58	39.2	5.8	34.3		2.3	0.7	28.1	26.1
9/6/2016 17:00	36.6	6.8	42		2.3	0.7	28.1	26.2

Table E8: Carbon dioxide permeation at 2 bar

Date	20/05/2014	Membrane Description	2 Layer PPH SOD Membrane	Sweep Gas	? ml/min
Experiment Number	3039802	Membrane Conditioning	Na	Sweep Gas Pressure	? bar
Experimentalist Name	Variation @ 2 bar	Feed Mixture	Gas	Reactor Temperature	Set ? °C
Title	Na				

Recorded Values

Time	Main gas: CO2 ml/min	feed	Sweep gas: N2 ml/min	Make-up gas: N2 ml/min	Feed gas pressure kPa	Sweep gas pressure kPa	Retentate Temp °C	TC1	Permeate temp °C	TC2
9/6/2016 17:05		-1.7	0.8	0.3	3.2	0.7	28		26.2	
9/6/2016 17:07		-1.7	1.8	0.3	3.2	0.7	28.1		26.2	
9/6/2016 17:09		34.8	2.8	23.3	3.2	0.7	28		26.2	
9/6/2016 17:11		57.3	3.8	46.5	3.2	0.7	28		26.2	
9/6/2016 17:13		52.8	4.8	42.1	3.2	0.7	28		26.2	
9/6/2016 17:15		-0.9	5.8	0.1	3.2	0.7	27.9		26.2	
9/6/2016 17:16		40.3	6.8	27.6	3.2	0.7	27.9		26.2	

Table E9: Carbon dioxide permeation at 3 bar

Date	20/05/2014	Membrane Description	2 Layer PPH SOD	Sweep Gas	? ml/min
Experiment Number	3039802	Membrane Conditioning	Na	Sweep Gas Pressure	? bar
Experimentalist Name	Variation @ 3 bar	Feed Mixture	Gas ? mL/min	Reactor Temperature	Set ? °C
Title	Na				

Recorded Values

Time	Main gas: CO2 ml/min	feed ml/min	Sweep gas: N2 ml/min	Make-up gas: N2 ml/min	Feed gas pressure kPa	Sweep gas pressure kPa	Retentate Temp TC1 °C	Permeate temp TC2 °C
9/6/2016 17:22		57.8	0.8	48.4	3.9	0.7	27.9	26.2
9/6/2016 17:24		63.2	1.8	48.4	3.9	0.7	27.9	26.2
9/6/2016 17:28		37	2.8	17.8	3.9	0.7	27.8	26.2
9/6/2016 17:29		-1.6	3.8	0.4	3.9	0.7	27.8	26.2
9/6/2016 17:31		19.9	4.8	0.6	3.9	0.7	27.7	26.2
9/6/2016 17:33		-1.5	5.8	0.4	3.9	0.7	27.7	26.2
9/6/2016 17:35		-1.7	6.8	0.2	3.9	0.7	27.7	26.2
9/6/2016 17:37		22.1	7.8	5	3.9	0.7	27.7	26.2

Appendix F: MATLAB Code used for MS model.

```
%%Start of Experimental Data Declaration%%

t = [298 375 423 473 523];
fluxH2 = [4.25e-6 2.98e-6 2.48e-6 2.2e-6 1.9e-6];
fluxCO2 = [2.38e-6 0.82e-6 0.74e-6 0.74e-6 0.74e-6];

%%End of Experimental Data Declaration%%

%%Start of Variable Declaration for Maxwell Stefan (MS) Model%%

R = 8.314; % Ideal gas constant in J/molK
Csat1 = 5.4; % Concentration of Hydrogen in SOD membrane in mol/Kg
Csat2 = 5.0; % Concentration of Carbon Dioxide in SOD membrane in
mol/Kg
rho = 1510; % Density of SOD in Kg/m3
E = 0.16; % Porosity of the SOD membrane
Di1 = 0.000000018; % Maxwell Stefan diffusivity @ zero coverage for
Hydrogen in m2/s
Di2 = 0.00000007; % Maxwell Stefan diffusivity @ zero coverage for
Carbon Dioxide in m2/s
tor = 1.2; % Tortuosity
l = 0.0095; %Equivalent SOD thickness in m, fitted parameters ;
%Pars1 = 1 ;
Temp = [298 375 423 473 523]; % Temperature is from 280 to 480K
Pr = 121590; % Retentate pressure in Pa
Pp = 101325; % Permeate pressure in Pa
Po = 101325; % Reference to atmospheric pressure (101325Pa)
SAE1 = -43; % Standard adsorption entropy for Hydrogen in J/molK
SAE2 = -58; % Standard adsorption entropy for Carbon Dioxide in
J/molK
DAE1 = 2000; % Diffusion activation energy for Hydrogen in J/mol
DAE2 = 9600; % Diffusion activation energy for Carbon Dioxide in
J/mol
SAD1 = -5900; % Standard adsorption enthalpy for Hydrogen in J/mol
SAD2 = -2410; % Standard adsorption enthalpy for Carbon Dioxide in
J/mol

%% End of Variable Declaration for MS Model%%

%% Expression for Maxwell Stefan Model for Hydrogen %%

term11 = Csat1*rho*E*Di1;
term12 = tor*l;
term1 = term11*term12.^-1;
term21 = (1 + (Pr*Po.^-1)*exp((SAE1- R)*R.^-1 - (SAD1*(R*Temp).^-
1)));
term22 = (1 + (Pp*Po.^-1)*exp((SAE1- R)*R.^-1 - (SAD1*(R*Temp).^-
1)));
term23 = term22.^-1 ;
term2 = log (term21.*term23);
term31 = -(DAE1)*(R*Temp).^-1 ;
```

```

term3 = exp(term31);
ffluxH2 = term1.*term2.*term3;
%end

%% Expression for Maxwell Stefan Model for Carbon Dioxide %%
termaa = Csat2*rho*E*Di2;
termab = tor*1;
terma = termaa*termab.^-1;
termbb = (1 + (Pr*Po.^-1)*exp((SAE2- R)*R.^-1 - (SAD2*(R*Temp).^-
1)));
termbc = (1 + (Pp*Po.^-1)*exp((SAE2- R)*R.^-1 - (SAD2*(R*Temp).^-
1)));
termbd = termbc.^-1 ;
termb = log (termbb.*termbd);
termcc = -(DAE2)*(R*Temp).^-1 ;
termc = exp(termcc);
ffluxCO2 = (terma).*termb.*termc;
%end

%% SECTION TITLE
% DESCRIPTIVE TEXT
%% Expression for Output : MS Model %%
plot (Temp,ffluxH2,'b-*', t,fluxH2,'r*', Temp,ffluxCO2,'g-*',
t,fluxCO2,'y*'), xlabel('Temperature, (K) '),ylabel('Flux(molm-2s-
1)')
grid on,
legend show

%plot (Temp,ffluxH2,'b-*', t,fluxH2,'r*'), xlabel('Temperature, (K)
'),ylabel('Flux(molm-2s-1)')
%grid on,
%legend show

```